

# **Network mechanisms underlying sharp-wave ripples and memory replay**

GABAergic modulation of sharp-wave ripples incidence

## **DISSERTATION**

zur Erlangung des akademischen Grades  
doctor rerum naturalium  
(Dr. rer. nat.)  
im Fach Biologie

eingereicht an der  
Lebenswissenschaftlichen Fakultät  
der Humboldt-Universität zu Berlin

von  
**M.Sc. Nikolay Aleksandrov Chenkov**

Präsidentin der Humboldt-Universität zu Berlin  
Prof. Dr.-Ing. Dr. Sabine Kunst

Dekan der Lebenswissenschaftlichen Fakultät  
Prof. Dr. Bernhard Grimm

Gutachter/innen:

1. Richard Kempter
2. Henning Sprekeler
3. Martin Both

Eingereicht am: 27.03.2017

Tag der mündlichen Prüfung: 21.06.2017



# Abstract

Complex patterns of neural activity appear during up-states in the neocortex and sharp-wave ripples (SWRs) in the hippocampus, including sequences that resemble those during prior behavioral experience. The mechanisms underlying this replay are not well understood. How can small synaptic footprints engraved by experience control large-scale network activity during memory retrieval and consolidation?

In the first part of this thesis, I hypothesise that sparse and weak synaptic connectivity between Hebbian assemblies are boosted by pre-existing recurrent connectivity within them. To investigate this idea, sequences of assemblies connected in a feedforward manner are embedded in random neural networks with a balance of excitation and inhibition. Simulations and analytical calculations show that recurrent connections within assemblies allow for a fast amplification of signals that indeed reduces the required number of inter-assembly connections. Replay can be evoked by small sensory-like cues or emerge spontaneously by activity fluctuations. Global—potentially neuromodulatory—alterations of neuronal excitability can switch between network states that favor retrieval and consolidation.

The second part of this thesis investigates the origin of the SWRs observed in *in-vitro* models. Recent studies have demonstrated that SWR-like events can be evoked after optogenetic stimulation of subpopulations of inhibitory neurons (Schlingloff et al., 2014; Kohus et al., 2016). To explain these results, a 3-population model is discussed as a hypothetical disinhibitory circuit that could generate the observed population bursts. The effects of pharmacological GABAergic modulators on the SWR incidence *in vitro* are analysed. The results are discussed in the light of the proposed disinhibitory circuit. In particular, how does gabazine, a GABA<sub>A</sub> receptor antagonist, suppress the generation of SWRs? Another explored question is whether the slow dynamics of GABA<sub>B</sub> receptors is modulating the time scale of the inter-event intervals.

# Zusammenfassung

Komplexe Muster neuronaler Aktivität entstehen während der Sharp-wave Ripples (SWRs) im Hippocampus und während der Up States im Neokortex (Zuständen mit hoher Aktivität). Sequenzen von Verhalten, die in der Vergangenheit erlebt wurden, werden während des komplexen Musters abgespielt. Die zugrunde liegenden Mechanismen sind nicht gründlich erforscht: Wie können kleine synaptische Veränderungen die großflächige Netzwerkaktivität während des Gedächtnisabrufes und der Gedächtniskonsolidierung kontrollieren?

Im ersten Teil dieser Abhandlung wird die Hypothese aufgestellt, dass eine schwache synaptische Konnektivität zwischen Hebb'schen Assemblies von der bereits vorhandenen rekurrenten Konnektivität gefördert wird. Diese Hypothese wird auf folgende Weise geprüft: die vorwärts gekoppelten Assembly-Sequenzen werden in neuronale Netzwerke eingebettet, mit einem Gleichgewicht zwischen exzitatorischer und inhibitorischer Aktivität. Simulationen und analytische Berechnungen haben gezeigt, dass rekurrente Verbindungen innerhalb der Assemblies zu einer schnelleren Signalverstärkung führen, was eine Reduktion der notwendigen Verbindungen zwischen den Assemblies zur Folge hat. Diese Aktivität kann entweder von kleinen sensorisch ähnlichen Inputs hervorgerufen werden oder entsteht spontan infolge von Aktivitätsschwankungen. Globale – möglicherweise neuromodulatorische – Änderungen der neuronalen Erregbarkeit können daher die Netzwerkzustände steuern, die Gedächtnisabruf und die Konsolidierung begünstigen.

Der zweite Teil der Arbeit geht der Herkunft der SWRs nach, die *in vitro* beobachtet wurden. Neueste Studien haben gezeigt, dass SWR-ähnliche Erscheinungen durch optogenetische Stimulation der Subpopulationen von inhibitorischen Neuronen hervorgerufen werden können (Schlingloff et al., 2014; Kohus et al., 2016). Um diese Ergebnisse zu erklären wird ein de-inhibierendes Schaltkreis-Modell diskutiert, das die beobachteten Populationsausbrüche generieren kann. Die Auswirkungen der pharmakologischen GABAergic Modulatoren auf die SWR-Häufigkeit werden *in vitro* untersucht. Die gewonnenen Ergebnisse wurden im Rahmen des Schaltkreis-Modells analysiert. Insbesondere wird den folgenden Fragen nachgegangen: Wie unterdrückt Gabazine, ein GABA<sub>A</sub>-Rezeptor-Antagonist, die Entwicklung von SWRs? Wird das Zeitintervall zwischen SWRs durch die Dynamik der GABA<sub>B</sub> Rezeptoren moduliert?

# Contents

<b>1</b>	<b>Introduction</b>	<b>1</b>
1.1	Sequences as a behavioural substrate: a historical overview . . . . .	1
1.2	Hebbian theory . . . . .	2
1.2.1	Hebbian learning: fire together, wire together <sup>1</sup> . . . . .	3
1.2.2	Hebbian assemblies . . . . .	6
1.2.3	Phase sequences . . . . .	8
1.3	Hippocampus: a brief survey . . . . .	9
1.3.1	Anatomy . . . . .	9
1.3.2	The role of the hippocampus in the human brain . . . . .	13
1.3.3	Neural correlates of behaviour . . . . .	14
1.3.4	Oscillations . . . . .	15
1.4	Sharp-wave ripples . . . . .	17
1.4.1	Behavioural correlates . . . . .	19
1.4.2	Generation mechanisms . . . . .	20
1.5	Scope . . . . .	21
<b>2</b>	<b>Memory replay in balanced recurrent networks</b>	<b>23</b>
2.1	Summary . . . . .	23
2.2	Introduction . . . . .	23
2.3	Results . . . . .	24
2.3.1	Sparse feedforward connectivity is sufficient for replay . . . . .	26
2.3.2	Recurrent connections are important for pattern completion . . . . .	29
2.3.3	Spontaneous replay . . . . .	29
2.3.4	Control of spontaneous and cued replay by external input . . . . .	33
2.3.5	Smaller assemblies require higher connectivity . . . . .	33
2.3.6	Stronger synapses are equivalent to more connections . . . . .	35
2.3.7	Forward and reverse replay in assembly sequences with symmetric connections . . . . .	37
2.4	Discussion . . . . .	39
2.4.1	Related models . . . . .	39
2.4.2	Relation between recurrent and feedforward connectivity . . . . .	41
2.4.3	Mechanisms for assembly-sequence formation . . . . .	42
2.4.4	Relations to hippocampal replay of behavioral sequences . . . . .	42
2.5	Materials and Methods . . . . .	43
2.5.1	Neuron model . . . . .	44
2.5.2	Network model . . . . .	45
2.5.3	Balancing the network . . . . .	45
2.5.4	Simulations and data analysis . . . . .	47

---

<sup>1</sup>A paraphrase from “neurons wire together if they fire together” (Lowel and Singer, 1992)

## Contents

2.5.5 Estimating response times of neurons and the network . . . . .	48
2.5.6 Estimating conditions for successful replay . . . . .	49
2.5.7 Calculating the slope $c$ . . . . .	50
2.5.8 Scaling the network size . . . . .	52
<b>3 Modulation of sharp-wave incidence</b>	<b>55</b>
3.1 Summary . . . . .	55
3.2 Introduction . . . . .	55
3.2.1 Inhibitory transmission in the hippocampus . . . . .	56
3.2.2 GABAergic modulation of sharp-wave ripple incidence <i>in vitro</i> . . . . .	58
3.2.3 Sharp-wave events driven by inhibition . . . . .	59
3.2.4 Hypothesis on the CA3 circuitry giving rise to sharp-wave ripples . . . . .	61
3.3 Results . . . . .	65
3.3.1 Serial correlations between peak amplitudes of SWRs and intervals between them . . . . .	65
3.3.2 Gabazine effects on sharp-wave ripples <i>in vitro</i> . . . . .	69
3.3.3 Gabazine effects on sharp-wave incidence <i>in silico</i> . . . . .	72
3.3.4 Involvement of GABA <sub>B</sub> receptors in sharp-wave ripples . . . . .	78
3.3.5 Role of postsynaptic GABA <sub>B</sub> receptors . . . . .	82
3.4 Discussion . . . . .	83
3.4.1 Hypotheses on how gabazine affects sharp-wave ripples . . . . .	84
3.4.2 Hypothesis on how GABA <sub>B</sub> receptors influence the sharp-wave incidence . . . . .	86
3.4.3 Overview . . . . .	88
3.5 Methods . . . . .	89
3.5.1 Data and data analysis . . . . .	89
3.5.2 Simulations . . . . .	91
<b>4 Outlook</b>	<b>93</b>
4.1 Bridging the assembly sequence model and the 3-population hypothesis . . . . .	93
4.2 Further implications of the disinhibitory circuit . . . . .	93
4.3 Why a hippocampal replay? . . . . .	94

# 1 Introduction

*There is a story that Simonides was dining at the house of a wealthy nobleman named Scopas at Crannon in Thessaly, and chanted a lyric poem which he had composed in honor of his host, in which he followed the custom of the poets by including for decorative purposes a long passage referring to Castor and Pollux; whereupon Scopas with excessive meanness told him he would pay him half the fee agreed on for the poem, and if he liked he might apply for the balance to his sons of Tyndaraus, as they had gone halves in the panegyric.*

*The story runs that a little later a message was brought to Simonides to go outside, as two young men were standing at the door who earnestly requested him to come out; so he rose from his seat and went out, and could not see anybody; but in the interval of his absence the roof of the hall where Scopas was giving the banquet fell in, crushing Scopas himself and his relations underneath the ruins and killing them; and when their friends wanted to bury them but were altogether unable to know them apart as they had been completely crushed, the story goes that Simonides was enabled by his recollection of the place in which each of them had been reclining at table to identify them for separate interment; and that this circumstance suggested to him the *discovery of the truth that the best aid to clearness of memory consists in orderly arrangement*.*

*He inferred that persons desiring to train this faculty must select localities and form mental images of the facts they wish to remember and store those images in the localities, with the result that the arrangement of the localities will preserve the order of the facts, and the images of the facts will designate the facts themselves, and we shall employ the localities and images respectively as a wax writing tablet and the letters written on it.<sup>1</sup>*

This thesis deals with sharp-wave ripples and the associated sequence replays. The introduction is intended to give the reader some insight about the relevance of these topics to our everyday life. It starts with a brief historical overview (Section 1.1) on mental sequences and their place in the understanding of memory and cognition over the centuries. Then, Section 1.2 dwells into fundamental concepts from Hebb's theory, such as synaptic plasticity, neural assemblies, and assembly sequences and their implications in theoretical neuroscience. The following Section 1.3 is dedicated to the description the hippocampus and its role in memory. Then, Section 1.4 describes the sharp-wave ripple phenomenon and the replay of behaviour sequences in greater detail.

## 1.1 Sequences as a behavioural substrate: a historical overview

Simonides of Ceos (556–468 BC) was both a celebrated and condemned lyric poet in Ancient Greek world. He is famed as the inventor of four letters of the Greek alphabet ( $\eta$ ,  $\psi$ ,  $\xi$ , and  $\omega$ )

---

<sup>1</sup>Cicero et al. (55BC), Book 2, 86.352–54.

## 1 Introduction

and is considered as the first commercial poet who created songs and odes for pay. Moreover, he is in the focus of the oldest reference (Unknown, 80BC) for a mnemonic technique called “Method of Loci” or “Memory palace” (see the legend above from Cicero et al. (55BC)). The method of loci has survived over the centuries as a technique to help orators, artists, clerks, and encyclopedists to remember information of virtually any quality and quantity (Yates, 1966). Nowadays, the method takes a central place in the training of every memory champion (Foer, 2011).

How does this mnemonic technique work? Can a naive person actually remember a large list of items consisting of tens or even hundreds of elements? In its essence, the method of loci is a mnemonic technique based on images and places. To deploy the method, one needs a predefined trajectory in some very well known spatial environment (e.g., a good starting point for beginners is imagining home). Then, to imprint the list, each item is sequentially placed in the virtual trajectory (e.g., entrance door, telephone cupboard, bookshelf, door to the living room, sofa, sofa table, etc.) and imagined as vividly as possible. It is suggested to recruit as many sensory modalities as possible when imagining the placed objects as this creates more hooks for later revoke of the items. For the following recall one needs only to do a virtual walk through the same trajectory and to recollect the items from their places (loci). A vivid imagination is always beneficial for these mental exercises.

Since ancient times it is known that memory can greatly benefit from predefined sequences. All known mnemonic techniques based on the method of loci or the story method (e.g., creating a story with the list items to be remembered) rely on the sequential storage and the recall of associated memories.

Sequences have been proposed also as a more general model for the occurrence and development of the mental processes. The oldest known references to the concept of association of thoughts and ideas can be tracked to Plato and Aristotle from the ancient world (Bostock, 1986; Bloch, 2007). Later, in the western world the thought sequence concept was further developed by early modern philosophers (Hobbes, 1650; Locke, 1690; Hume, 1739; Hume and Hendel, 1748; Stewart, 1855). David Hartley, a founder of the associationist school of psychology in the 18<sup>th</sup> century, proposed that even the most complex thought processes can be explained as sequential activations of clusters of elementary senses and representations. At the turn between the 19<sup>th</sup> and the 20<sup>th</sup> century, a lot of work devoted to associations was contributed in the field of psychology: The thought experiment about William James’ bear attempts to explain the physiological response of the body as a sequence of mental events after the sensory arousal of seeing a bear (James, 1884). Pavlov (1897) published his seminal work on the conditioned reflex, where he demonstrated the physiological effects of conditioning. Classical conditioning explains how conditioned stimuli (e.g., a bell) can be paired to unconditioned stimuli (e.g., food). Further work in experimental psychology conceived that sequences of experiences and their representations are in the base of motor action, cognition, and judgment (Watt, 1904; Titchener, 1905; Washburn, 1916).

Various disciplines have looked at the sequences of motor actions, thoughts, and memories as a basic behavioural substrate of the human nature. But how are such sequences represented in the brain, what is their neural basis?

## 1.2 Hebbian theory

In the 1940s, Donald Hebb, a Canadian psychologist and neurophysiologist, stated that the problem of understanding behaviour is the problem of understanding the total action of the

nervous system and vice versa. He was the first to apply the principles of the neuron doctrine (Ramón y Cajal, 1894) in a coherent framework attempting to explain the mechanisms behind the thought processes. In his seminal work, Hebb (1949) introduced three concepts that are widely used nowadays in the neuroscience community: a learning rule now known as “Hebbian learning”, “cell assemblies”, and “phase sequences”. Hebb suggested that if a neuron is participating in the firing of another neuron, then the corresponding synaptic efficacy is increased, or a new synapse is created (Figure 1.1). Thus, neurons that fire together form strong connections and organise into assemblies representing abstract mental concepts, today known as “Hebbian assemblies”, or simply assemblies. Once an assembly is activated, it can ignite associated concepts by activating the corresponding assemblies, thus forming a sequence of activation or a phase sequence.

These concepts led to the development of “connectionism” as a movement in neuroscience, cognitive sciences, and philosophy. Hebb’s theory had a huge influence on the early-day machine learning development, and in particular on the research in artificial neural networks. For example, the Hopfield network, a neural network model consisting of binary neurons as a content addressable memory model (Hopfield, 1982) uses Hebbian learning as a rule to adjust connection weights. Another technique based on the Hebbian theory is Oja’s rule for unsupervised learning, which can extract the main features (principal components) of datasets (Oja, 1982).

In the following paragraphs I briefly review literature that was triggered by Hebb’s theory. In particular, I focus on neurophysiological studies that shed light on the learning processes and the representation and detection of cell assemblies in the brain.

### 1.2.1 Hebbian learning: fire together, wire together <sup>2</sup>

It is an old idea that the formation of new memories does not require new neurons. Instead, already Ramón y Cajal (1894) suggested that for the creation or change of memories the brain might simply strengthen old synapses. This hypothesis stood the test of time and now is known as the synaptic plasticity and memory hypothesis (Martin et al., 2000; Takeuchi et al., 2014). Half a century after Ramón y Cajal, Hebb (1949) postulated that if neuron A takes part in the firing of neuron B, then the efficacy of the synapses from neuron A to B is increased, or that even new synaptic connections could be formed. Nowadays, this learning rule is known as “Hebbian learning”.

The first demonstration of the plastic nature of synapses was reported in anaesthetised rabbits by Lømo (1966) who found that a high-frequency stimulation to the presynaptic fibers in the perforant pathway increases the postsynaptic potentials (PSPs) measured in the dentate gyrus. Moreover, these changes in the synaptic efficacies lasted for hours. The idea that this synaptic facilitation might depend on the precise timing of the activation was proposed by Taylor (1973) who stated that a presynaptic spike shortly before the postsynaptic activity would facilitate the synaptic efficacy. In a computational model, Gerstner et al. (1996) showed that a sub-millisecond plasticity rule depending on the exact timing of pre- and postsynaptic firing can indeed lead to Hebbian learning. A year later, in experimental work, Markram et al. (1997) demonstrated that a synapse can be differentially up- or down-regulated depending on the precise time difference of the synaptic activation and the postsynaptic action potential. The spike-timing dependent plasticity (STDP) rule was described experimentally in greater detail by Bi and Poo (1998) who confirmed an asymmet-

---

<sup>2</sup>A paraphrase from “neurons wire together if they fire together” (Lowel and Singer, 1992)

## 1 Introduction

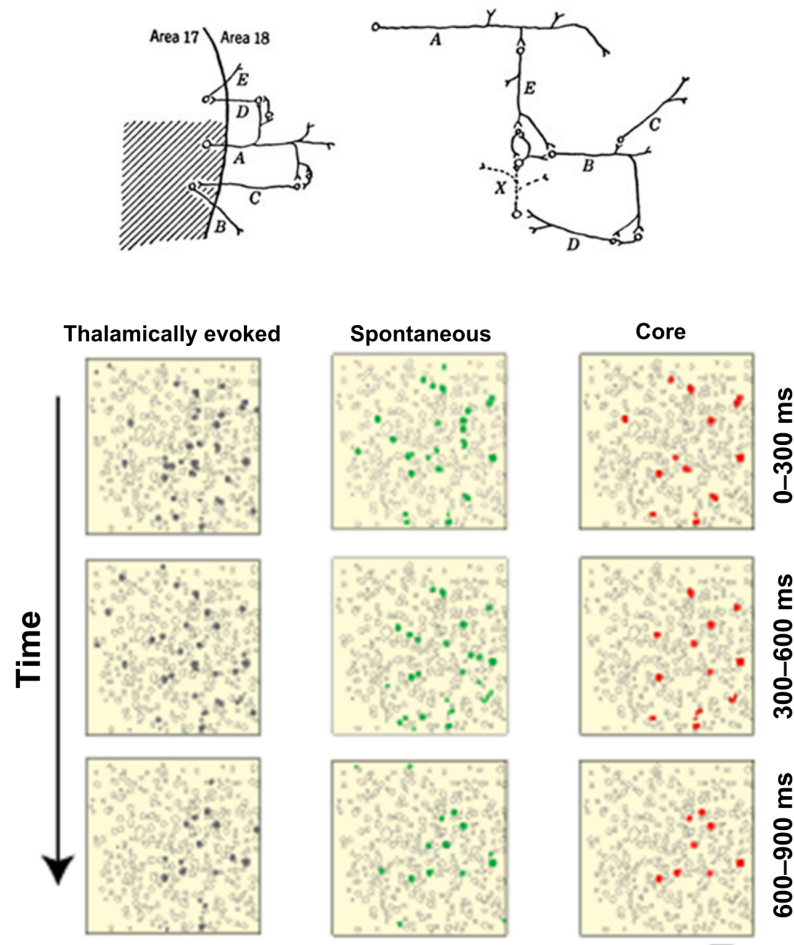


Figure 1.1: Cell assemblies. The top panel shows sketches from Hebb (1949). **top-left:** Cell A excites cell C, which excites cell B. The synaptic efficacy from A to B will be potentiated, or new synapses will be created after repetitive activation of cells A and C. **top-right:** Cells A, B, and C receive converging inputs (not shown). Cells D, E, and X among many other cells have connections with A, B, and C, and thus, contribute to the integration of their activity. **bottom:** Neural assemblies can be reliably evoked by thalamic inputs (left) or manifest themselves during spontaneous network activity (middle). Gray dots present neuronal cells, and colored dots show the cells activated during 3 consecutive 300 ms time windows. Assemblies (marked by the overlap of activated neurons; right hand-side) show reliable spatio-temporal activations where the sequential order of firing is preserved. The right panel shows the overlap of thalamic and spontaneous activations. Scale bar 50  $\mu\text{m}$  (Luczak and MacLean, 2012; adapted with permission).

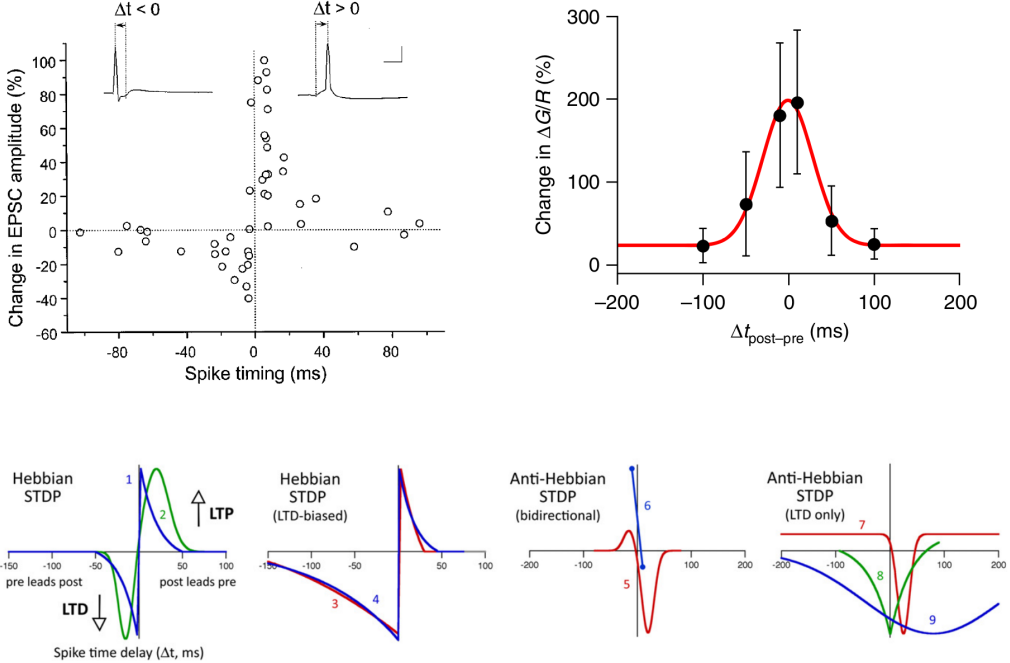


Figure 1.2: Spike-timing dependent plasticity relies on the precise time difference of pre- and post-synaptic activations. **top-left:** Critical window for induction of synaptic changes (Bi and Poo, 1998; adapted with permission). Positive time differences  $\Delta t > 0$  (first pre- and then post-synaptic activation) lead to synaptic potentiation, and negative time differences lead to depression 30 minutes after a repetitive pairing protocol. **top-right:** A symmetric STDP temporal window between CA3 pyramidal cells *in vitro* (Mishra et al., 2016). **bottom:** Various forms of STDP rules reported in the literature as summarised by Feldman (2012).

ric temporal window of plasticity between pyramidal neurons in hippocampal culture (see Figure 1.2, top-left panel). According to this rule, the order of spiking determines the sign and magnitude of synaptic change; a presynaptic spike followed closely by a postsynaptic one leads to long-term synaptic potentiation, while the reversed order leads to a long-term depression. The exact biological mechanism behind STDP remained elusive.

The classical asymmetric exponential temporal window has been confirmed by a number of studies (e.g., Debanne et al., 1998; Zhang et al., 1998). However, because of the used techniques, the results are met with some reservations. For example, Lisman and Spruston (2005) pointed out that in the aforementioned studies, the postsynaptic firing was induced by a current injection instead of more natural synaptic inputs. Spikes evoked by the postsynaptic potentials alone at low frequency do not lead to any synaptic potentiation (Wittenberg and Wang, 2006) suggesting that additional factors might be involved in the plasticity processes. The conventional STDP rule (i.e., Bi and Poo, 1998; Kempfer et al., 1999) is not universal for all synapses. Various STDP temporal windows (Figure 1.2, bottom panel) have been found in dependence upon the brain region, preparation, stimulation protocol, and the type of pre/post-synaptic neurons (Feldman, 2012; Vogels et al., 2013). Recently, Mishra et al. (2016) demonstrated that in hippocampal slices of mature rats, the potentiation of CA3-CA3 recurrent excitatory synapses is independent of the temporal order of stimulation, resulting

## 1 Introduction

in a symmetric STDP curve. The authors argue that the symmetric STDP curve (see Figure 1.2, top-right panel) allows for a reliable storage in the associative CA3 network. *In-vivo* experiments point out that the sign of synaptic changes might also depend on the exact phase of stimulation during the hippocampal theta oscillation (Hölscher et al., 1997).

Nowadays, the term “Hebbian learning” is widely used in the theoretical and physiological literature. While such a plasticity rule is shown to exist in various brain areas, it is not universal. Depending on the behaviour state, the local network oscillation phase, or on the type of synapse, various plasticity rules shape the connectivity matrix of the brain.

### 1.2.2 Hebbian assemblies

The idea that a memory, or an “engram”, is stored into a single cell or a group of neural cells was proposed by Semon (1904). According to Semon, engrams are representations of specific stimuli, and engram complexes are the basis of memory traces. Later, Hebb (1949) defined the assembly concept more specifically by postulating that, neurons that receive similar inputs, form strong connections among themselves, and organise into assemblies or engrams. Neurons in these assemblies are activated synchronously when the associated mental concept is revoked. While not strictly defined, the cell assembly has been a well-accepted conceptual tool that is widely used in theory and experiments.

The search of the assembly representation in the brain has proven to be a challenging task. Many questions are still open: What is the size of an assembly? How reliable is the participation of neurons from one activation to another? How stable are the assemblies during reactivation? Do assemblies overlap? Last but not least, is the assembly concept too general and thus too difficult to prove or disprove (Wallace and Kerr, 2010)? The most promising hints for the existence of assemblies come from the hippocampus and the early processing sensory brain areas where experimentators have better control over the inputs in comparison with other “higher brain areas”. Few lines of evidence, such as connectivity patterns between neurons and signatures of activity in the local circuits, suggest for the existence of neural assemblies.

When studying neural networks, an apparent problem is the complexity of the circuits. *In-vitro* experiments deal with minimal networks consisting of tens of thousands to hundreds of thousands neurons, and the number of possible connections scales as the square of the network size. Despite the rapid development of the current technologies, mapping such connectivity is not possible yet. Therefore, in their models, theoreticians often flavor the random networks as a tool to address complex network connectivities. However, the appearance of random and independent connections in biological neural networks is scarce. Clustered connectivity patterns have been reported in various cortical areas (Song et al., 2005; Ko et al., 2011; Perin et al., 2011; Shimono and Beggs, 2015) as well as in the hippocampus (Takahashi et al., 2010; Guzman et al., 2016). Moreover, neurons form bidirectional connections more often than expected by chance (Markram et al., 1997; Song et al., 2005; Takahashi et al., 2010; Ko et al., 2011; Perin et al., 2011). The distribution of synaptic weights is non-uniform. Local neocortical networks exhibit distributions of synaptic weights that are heavily skewed, and bidirectional connections are stronger than uni-directional connections (Markram et al., 1997; Song et al., 2005; Buzsáki and Mizuseki, 2014). Shimono and Beggs (2015) have shown that in neuronal culture, the microconnectome has different levels of clustering, from a few neurons up to hundreds of neurons. The authors suggested that the different levels of organisation lead to different levels of robustness, where larger clusters are more robust to be activated against noise such as errors in synaptic transmission or external noise.

How is this nonrandom connectivity related to the circuit activity? It has been shown that ongoing spontaneous activity in the cat visual cortex switches between different states, some of which correspond to the orientation maps of neurons (Kenet et al., 2003). These results suggest that a neuron's preferred tuning is not purely due to the sensory input but also reflects some intrinsic network structure. Comparison between spontaneous and evoked activity in the auditory and somatosensory cortices of rats showed that network dynamics is largely conserved between states, and that activity was drawn from a rather limited “vocabulary” (Luczak et al., 2009; Luczak and MacLean, 2012).

Although the direct link between connectivity and activity is rather sparse, there are some evidences that neurons in functional assemblies (groups of neurons that are co-activated simultaneously) are highly connected. Takahashi et al. (2010) has shown that in organotypic slices, neurons with highly correlated activity are connected with higher probability as compared to uncorrelated neurons. Moreover, connected neurons share common input and output neurons more than expected by chance. *In-vivo* work by Ko et al. (2011) in layer 2/3 of the mouse primary visual cortex revealed that cells with similar preference have bigger probability of uni- and bidirectional connections. Moreover, Cossell et al. (2015) showed that the synaptic strength between these neurons varies over two orders of magnitude, and the strongest connections are between neurons with very correlated responses, while weak synapses are between neurons with uncorrelated responses. And although hugely outnumbered, the strong inputs disproportionately control the response of neurons.

A number of studies point out that fine-scaled subnetworks (from tens up to hundreds of neurons) specialise in processing similar information where correlation in activity is correlated with connectivity. While the assemblies in the primary cortical areas (V1, A1, etc.) are constituted by neurons that are spatially close to each other, and thus, form “receptive maps” (e.g., Bathellier et al., 2012; Cossell et al., 2015), in the hippocampus the assemblies are spatially distributed (Guzman et al., 2016).

Another feature of Hebbian assemblies predicted by the theory is the discrete activation of neural populations as the network activity enters various attractor states (Hopfield, 1982). Attractors are defined as all-or-none states in the network activity, where states close to these points are attracted to them. Such attractor-like activity that exhibits reliably revolved spatio-temporal patterns has been observed in slices (e.g., Cossart et al., 2003; MacLean et al., 2005). More recently, Bathellier et al. (2012) have shown that sound stimuli evoke attractor-like dynamics in superficial layers of the auditory cortex with an abrupt switching between the different discrete modes. The discrete modes constitute of partially overlapping subpopulations where the same neurons can take part in multiple assemblies, and assemblies interact in a competitive fashion. Due to the complexity of stimuli representation, measures of assembly correlates are more challenging in the higher cortices. By projecting the measured neuronal activity in high-dimensional state space by kernel methods (PCA), Balaguer-Ballester et al. (2011) have shown that on-going activity in the higher cortices possesses attractor-like dynamics. Abrupt transitions between attractor states have been also reported in experiments where the external sensory cues were gradually changed. For example, continuously varying an odor results in abrupt changes in the odor representation in the olfactory bulb of zebrafish (Niessing and Friedrich, 2010), or gradually changing the environment evokes place cells to abruptly and simultaneously change representation (Wills et al., 2005). As shown in virtual teleportation experiments, one cycle of the theta oscillation is the temporal unit for expressing an attractor state in the hippocampus (Jezek et al., 2011). It is not known yet whether this discretization of activity is due to purely internal dynamics

## 1 Introduction

or if the inputs to the hippocampus are already discretised with theta-cycle resolution.

A lot of work has been devoted into capturing this “holy grail” in neuroscience called neural assemblies. Multiple experimental lines of evidence hint that the brain networks are indeed populated with clusters of neurons that share common representations. However, we do not have a clear picture of a more general syntax explaining how these subnetworks can interact, especially in higher-brain areas. Relaxing the definition of a cell assembly, Buzsáki (2010) suggests that hierarchical organization of cell assemblies may constitute syntactical rules that define first-order and higher-order relationship. Cell assemblies are then defined not by connectivity but by their synchronous activation during a concept representation. Pulvermüller (2010) argues that the assembly syntax might be tightly related to the linguistic syntax that we use. When introducing the assembly concept, Hebb (1949) also proposed that assemblies are organised in phase (or assembly) sequences, and these sequences themselves are evoked in a sequence of activations.

### 1.2.3 Phase sequences

The third, less known principle proposed by Hebb (1949) is about “phase sequences”: once an assembly is activated, i.e., the underlying neurons are firing, their activation would propagate and activate another assembly, thus mental concepts would ignite associated concepts. Hebb suggested that such sequential activation of assemblies of neurons underlies our most complex mental processes. Without going into detail, he suggested that phase sequences can interact with each other and organise more complex hierarchies and sequences.

Various brain areas reveal spatiotemporal activity patterns that repeat over time (e.g., Wilson et al., 1994; Kenet et al., 2003; Berkes et al., 2011). Therefore, it is common to find groups of neurons that fire reliably in a temporal order during the execution of the temporal patterns. Moreover, neurons do not always fire in a single burst but show more various patterns such as ramped activity, or more complex or chaotic firing. The microcircuits underlying such activity are largely unknown, and there is only scarce evidence pointing to a sequential activation of neural assemblies. An interesting idea by Goldman (2009) states that the decomposition of the connectivity matrix of a recurrent network in Schur modes allows to project the activity as a feedforward interaction between activity modes. Thus, with the appropriate projection, any recurrent network can be viewed as a “feedforward network in disguise”.

Some of the most striking examples of precise sequences of neural activity come from songbirds (Figure 1.3). Male songbirds such as the zebra finch perform complex stereotypical songs consisting of variable patterns on multiple timescales. The songs are learned from a tutor bird and are extensively rehearsed for around 60 days until deployed in practice upon reaching sexual maturity (George et al., 1995; Doupe et al., 2004). It is believed that song syllables and tempo motifs are stored in a forebrain nucleus called HVC (formerly, an abbreviation of the now invalidated region named Hyperstriatum Ventrale pars Caudalis; now HVC is a stand-alone name) where neurons fire selectively to sounds, syllables, or sequence of syllables (Albert and Margoliash, 1996). The HVC premotor neurons are shown to fire sparsely and very precisely in stereotypical sequences of bursts with very small jitter ( $< 1 \text{ ms}$ ) when aligned with the performed song (Hahnloser et al., 2002). The same sequences of activity are replayed offline during sleep, which is believed to support the memory consolidation of songs (Dave and Margoliash, 2000). While the connectivity within the HVC is mostly unknown (Hamaguchi and Mooney, 2012; Poole et al., 2012), most theoretical studies focus on models of feedforward networks for learning and performing songs (e.g., Li and Greenside, 2006;

Long et al., 2010; Hanuschkin et al., 2011). Experiments with lesions have supported the feedforward network model (Poole et al., 2012). Moreover, Kosche et al. (2015) have shown that the generation of song sequences not only relies on excitation, but also on patterned inhibition. However, the circuit generating these patterned sequences remains elusive.

For the assembly sequence hypothesis, it is important that the activity of one assembly synchronously drives the activity in another assembly. Such coding is compatible with the temporal code where the exact spike timing in relation to other neurons is crucial for the information transmission. Indeed, sequences of neural activity on fast, millisecond time scales have been reported in various neuronal circuits such as, just to name a few, insects (Fushiki et al., 2016), fishes (Romano et al., 2015), dragons (Shein-Idelson et al., 2016), in mammalian cortex (Euston et al., 2007) and hippocampus (Lee and Wilson, 2002), as well as *in-vitro* preparations (Mao et al., 2001; Segev et al., 2004; MacLean et al., 2005; Kruskal et al., 2013). Sequence replays depend on the behavioural state (Almeida-Filho et al., 2014), and reverberations are enhanced mostly in the desynchronised states (Contreras et al., 2013; Buzsáki et al., 1983) when the local circuit activity is intrinsically driven.

In the mammalian brain, the hippocampus exhibits a particularly rich repertoire of sequential activations of neurons. Firing patterns of behavioural sequences are replayed on various time scales, e.g., behaviour time scales up to minutes during REM sleep (Louie and Wilson, 2001), compressed sequences of tens of milliseconds in exploratory “theta sequences” (Skaggs and McNaughton, 1996; Dragoi and Buzsáki, 2006; Gupta et al., 2012; Feng et al., 2015), and few millisecond-precision of sequential firing during slow-wave sleep and resting (Lee and Wilson, 2002). Moreover, depending on the behavioural state, hippocampal replays can exhibit firing sequence in the same or reversed temporal order as experienced in the awake state (Foster and Wilson, 2006).

## 1.3 Hippocampus: a brief survey

Time is so intimate for us that it is difficult to imagine to live without it. We live in a dynamical system that constantly changes the environment that we perceive, and so we change as well. As our changes reflect past events, they can be generalised as memories. There are memories at various levels, such as physical, genetic, neurophysiological, etc. When we use the word “memory” in everyday talk, usually we particularly refer to the declarative memory that includes episodic (spatial and autobiographical experiences and events) and semantic (vocabulary, facts, concepts, etc.) types of memories. In humans and other mammals, the hippocampus is a vital brain structure for storing the past in the form of declarative memories and planning for the future.

The aim of this section is to give the reader a basic picture of the hippocampus. I start with a brief description of the hippocampal anatomy and then dive into its functional role.

### 1.3.1 Anatomy

The hippocampus was first described by Julius Caesar Aranzi in 1564 and was named due to its resemblance to the seahorse (from Greek *ιπποκαμπός*: seahorse, see Figure 1.4). The hippocampus is a subcortical structure, part of the limbic system. The hippocampal formation is remarkably preserved across mammalian species (Manns and Eichenbaum, 2006; Clark and Squire, 2013). Mammals have two hippocampi located bilaterally in the medial temporal lobes wrapped by the cerebral cortex (Figure 1.4). The hippocampus proper is

## 1 Introduction

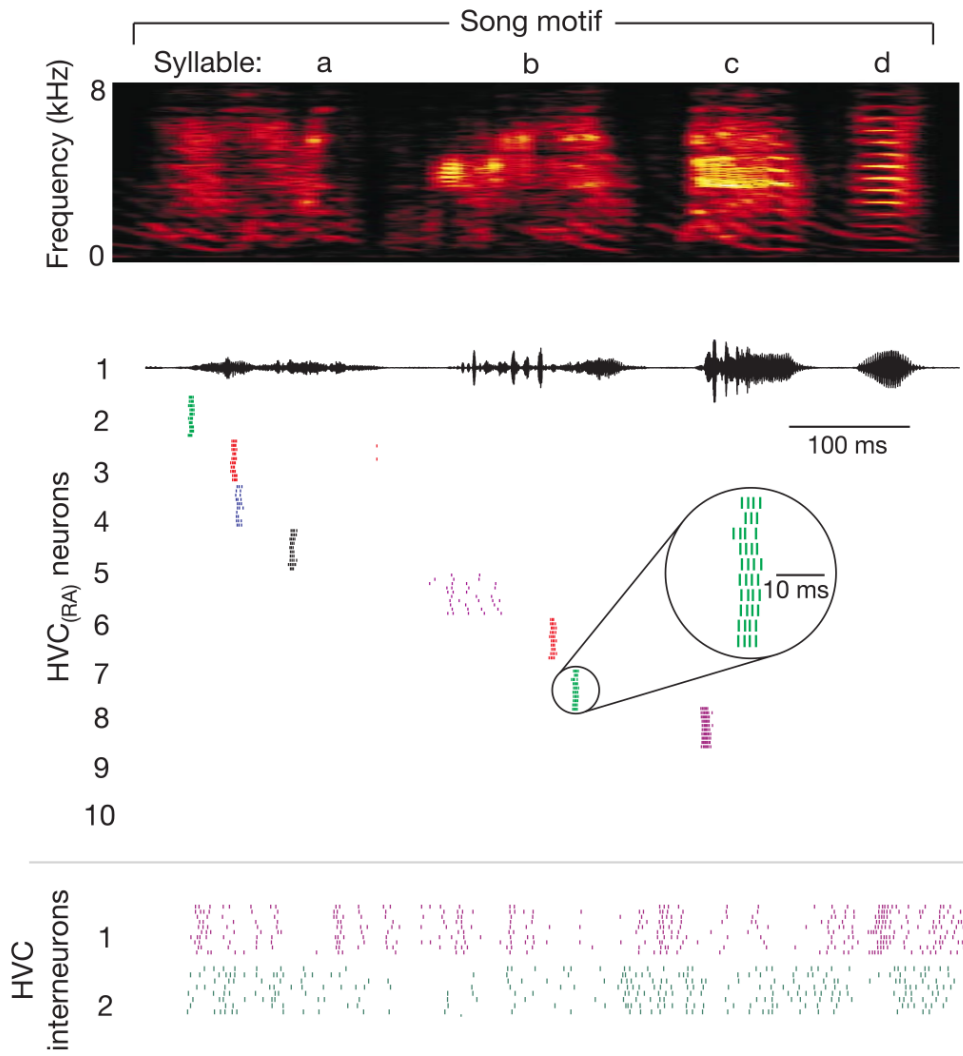


Figure 1.3: Firing sequences in songbirds. Spectrogram (top) and acoustic signal (the black curve below) of a song motif. Spike-raster plot of ten HVC neurons and two HVC interneurons recorded in one bird during singing (colored ticks). Each row of ticks marks spikes generated during one rendition of the song; roughly ten renditions are shown for each neuron. HVC neurons burst reliably at a single precise time in the song or call; however, interneurons spike or burst densely throughout the vocalizations (Hahnloser et al., 2002; adapted with permission).

one of the most extensively studied regions in the mammalian brain in terms of anatomy, electrophysiology, and behavioural function.

The hippocampal formation consists of the hippocampus itself, the subiculum proper, and the entorhinal cortex, which provides the major input and is the main output of the hippocampus. The hippocampus can be roughly divided into the dentate gyrus, and the *cornu ammonis* regions (namely, CA3, CA2, and CA1). The hippocampus gained popularity in neurophysiology partly because of the unidirectional transmission of information from dentate gyrus to the CA regions, which facilitates the study of the local microcircuits. The main input to the hippocampus is provided by the entorhinal cortex (EC). Activity from the superficial layers of the EC propagates through the entorhinal-hippocampal (or “trisynaptic”) loop and projects back to the deep layers of the EC (Figure 1.4, C and D). Much like the cortex, the hippocampal subregions are organised in well-defined laminar structures where different layers are populated by different cell types, and the different synaptic inputs are confined to specific layers.

**Dentate gyrus microcircuit.** The dentate gyrus (DG) consists of three neuronal layers: molecular, granular, and polymorphic. The principal excitatory cells, the granule cells, are located in the granular layer. The main input to the DG comes through the perforant path from layer II of the entorhinal cortex (Squire, 1992) while the output consist of unidirectional connections to the CA3 region through the mossy fiber (MF) synapses. Due to their extremely high efficacies where a single presynaptic spike can drive the postsynaptic neurons to fire, the MF synapses are also known as “detonators” (Bischofberger et al., 2006).

Another peculiar feature of the DG is the fact that granule cells are generated throughout the whole life in rodents as well as in humans. Due to this neurogenesis, the number of neurons in DG can vary, and subjects that use spatial navigation more extensively tend to have a larger number of granule cells. Moreover, the size of the DG correlates with spatial memory (Maguire et al., 2000; Spalding et al., 2013).

**CA3 microcircuit.** The CA3 hippocampal area is an important focus of this thesis. Like the rest of the hippocampal subregions, CA3 possesses a well-defined laminar structure that confines the localization of the different neuron types and inputs (see Figure 1.4). The deepest layer of the CA regions is the stratum lacunosum moleculare, followed by stratum radiatum, and the pyramidal cell layer. The most superficial layer is the stratum oriens. All layers are populated by inhibitory interneurons. There are over 20 types of interneurons that can be classified depending on the location, morphology, and genetic expression profile (Maccaferri and Lacaille, 2003; Klausberger and Somogyi, 2008). The principal cells, the pyramidal neurons are located in the pyramidal layer and comprise around 90% of all cells in that layer. Their number in rats is  $\sim 3 \cdot 10^5$  (Boss et al., 1985, 1987) in CA3, while the human hippocampus has  $\sim 2.7 \cdot 10^6$  neurons in CA3. Pyramidal neurons extend their basal dendritic trees into the superficial layers, while the apical branches are in the deep cell layers. The axons of pyramidal neurons can innervate around 70% of the dorsal-ventral axis of the hippocampus and project to other pyramids and interneurons in the stratum radiatum and stratum oriens (Sik et al., 1993; Li et al., 1994).

A major input to the CA3 comes through the MF synapses from the DG. The MF terminals form a (visually) distinguishable layer within the stratum radiatum, sometimes referred to as stratum lucidum. Two different major inputs come from the layer II of the entorhinal cortex: a direct projection from the axons of the EC layer II pyramidal neurons reach the CA3 region; and an indirect input from EC layer II stellate cells projecting to the DG through the perforant path, and then through the MF synapses to the CA3 (Tang et al.,

## 1 Introduction

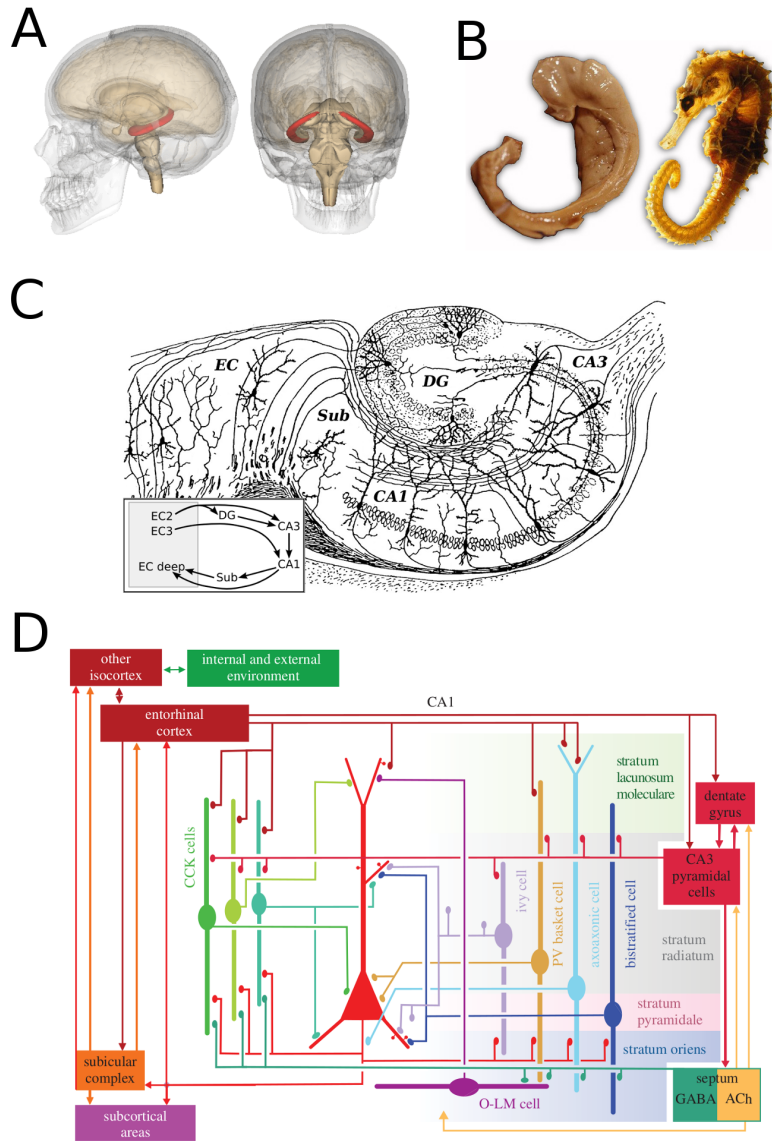


Figure 1.4: **A.** Location of the hippocampus (red color) in the human brain (transparent yellow) viewed from the side (left panel) and the back (right panel). **B.** A comparison between a human hippocampus and a seahorse. **C.** A drawing of the hippocampal formation of a rat after a horizontal cut (EC: entorhinal cortex; Sub: subiculum; DG: dentate gyrus). A few principal neurons for each region are sketched. The panel inset illustrates the major excitatory pathways. **D.** A schematic of the spatial relations between neurons within the CA1 region and major inputs/outputs from other areas. The pyramidal neurons and a few classes of interneurons are sketched according to their laminar location. The layers are color coded in the right-hand side of the panel. Attributions: A is adapted from lifesciedb.jp (Creative common licence). B and C are adapted from Wikipedia (Creative Commons licence). C is a modified after an original drawing of Ramón y Cajal and Azoulay (1911). D is adapted with permission from Somogyi et al. (2014).

2014).

The CA3 hippocampal area was considered to be densely connected ( $\sim 3\%$  in Miles and Wong, 1986) relative to the CA1, but more recent evidences show that the connectivity between principal cells is around 1% (Guzman et al., 2016). The major output of CA3 are the excitatory axonal projections to the ipsilateral and contralateral CA1 via the Schaffer collaterals (Finnerty and Jefferys, 1993). The reader is kindly referred to Le Duigou et al. (2014) for a more detailed description and analysis of the connectivity within the CA3 region.

**CA2 microcircuit.** Probably because of its smaller size, the hippocampal CA2 area has received a negligible amount of attention compared to its neighbors CA1 and CA3. The area gets projections from EC layer II pyramids through the perforant path, but no mossy fiber inputs. Interestingly, CA2 in mice is involved in sociocognitive memory processing (Hitti and Siegelbaum, 2014).

**CA1 microcircuit.** The CA1 hippocampal region has a similar laminar structure as CA3. However, the DG input is absent and the entorhinal input originates from EC, layer III. The principal neurons are more densely packed than in CA3, and there are around  $3.5 \cdot 10^5$  neurons in rats (West et al., 1991) and  $20.9 \cdot 10^6$  in humans (Šimić et al., 1997). For a more in-depth analysis of the recent findings on anatomy and connectivity of different cell types in the CA1 region, I kindly refer the reader to Bezaire and Soltesz (2013).

**Subiculum proper.** The region is subdivided into parasubiculum, presubiculum, post-subiculum, and prosubiculum. The subiculum is the major output of the hippocampus and receives projections from the CA1 region and EC layer III neurons.

**Entorhinal cortex.** The entorhinal cortex provides the major interface of other neocortical areas to the hippocampus. The EC is part of the neocortex with the typical 6-layered structure. Principal neurons are the stellate cells which populate layer II, and the pyramidal neurons, which populate layers II, III, and V. As mentioned above, principal cells from layer II of EC are projecting to the dentate gyrus and CA3, while layer III neurons are innervating the CA1 region and the subiculum. Inputs from the hippocampus are impinging on the deeper layer V of the EC.

### 1.3.2 The role of the hippocampus in the human brain

In the past, the hippocampus was assumed to be involved in various tasks. A dominant hypothesis until the end of 1930s suggested its involvement in olfactory processing (Andersen, 2007). Later hypotheses assigned roles in emotions and attention. Earlier results from Brown and Schäfer in 1888 and Bekhterev in 1900 hinted to the involvement of the hippocampus in memory (Andersen, 2007), but it was not a popular view until Scoville and Milner (1957) presented a study on the amnesic patient H.M.

Henry Gustav Molaison ( $\star 26.02.1926, \dagger 2.12.2008$ ), known as patient H.M. during most of his life, is probably the most influential patient in neuroscience. In an attempt to be cured from epileptic seizures, he underwent a brain surgery in 1953 in which most of his hippocampi, amygdalae and the surrounding entorhinal and parahippocampal cortices were removed. The operation was successful in its initial goal that he no longer suffered from seizures, however, at the price of some “side effects”. After the surgery H.M. was diagnosed with anterograde amnesia, i.e., the inability to form new (declarative) memories. Moreover, he suffered from temporally graded retrograde amnesia, i.e., he could not or had difficulties to recall events that took place shortly before the surgery while more distant memories from the past were intact. While subjected to numerous psychological experiments until his death in 2008, H.M. showed intact intellectual abilities and short-term memory. He revealed that

## 1 Introduction

the memory system is not a single entity but that there are multiple subsystems with possibly different neural origins. For instance, he could acquire new implicit memories when subjected to repetition priming (Corkin, 2002). Moreover, he showed intact motor learning skills in tasks that take multiple repetitions to be mastered. In a motor learning experiment, he could learn to draw seeing only a mirror reflection of his artistic piece, while not possessing any knowledge and memory that he is able to perform the task (Corkin, 1968). Studied for more than 50 years, H.M. pointed out the importance of the hippocampus for the formation of new episodic and semantic memories.

Work with other hippocampal amnesic patients has revealed some dissociation between the two types of declarative memories, i.e., episodic (or autobiographical) and semantic. While the overall recall of distant memories is intact in amnesic patients, the recall of the autobiographical memories is not as vivid and detailed as in control subjects. Moscovitch et al. (2005) suggested that the hippocampus is actively engaged during the recollection of episodic memories, and possibly during the recall of semantic memories that have autobiographical elements.

The dysfunction of the hippocampal formation not only causes impairment of remembering the past but also the inability to imagine the future. Work with amnesic patients with bilateral hippocampal damage suggested the involvement of the hippocampus in the process of planning and imagining new experiences (Klein et al., 2002; Hassabis et al., 2007). Overall, these results give the hippocampus a very peculiar function as a “time machine” in our cognition. Apart from simply storing experiences and semantic knowledge, the hippocampus also lets us mentally explore past or future experiences. Such a view naturally evokes the question whether H.M. or other amnesic patients ever experience mind-wandering.

### 1.3.3 Neural correlates of behaviour

After H.M. has sparked interest to the human hippocampus, numerous electrophysiological studies have been conducted in animals in the search of the neuronal basis of memory.

O’Keefe and Dostrovsky (1971) showed for the first time that some hippocampal pyramidal neurons in behaving rats are activated while the animal is at a specific location. As such cells code for the position in space, they were later named ‘place cells’. Following experiments showed that a subset of hippocampal and entorhinal neurons can code for head direction (Taube et al., 1990a,b), odors (Wood et al., 1999), environmental boundaries (Jeffery and Burgess, 2006), and particular objects (Manns and Eichenbaum, 2009). The discovery of cells in the entorhinal cortex that fire at multiple locations in an environment forming a particular hexagonal grid (Hafting et al., 2005) has attracted further attention. In a very recent report, Sarel et al. (2017) described hippocampal cells in bats that code for the vectorial representation of goal location, a firing pattern predicted previously by theory (Stemmler et al., 2015). So far, the rodent hippocampal formation has shown a remarkable repertoire of neural codes for spatial navigation that does not simply reflect the sensory input but reveals a more abstract representation of the environment.

There is evidence for the existence of place cells and grid cells also in humans exploring virtual environments (Ekstrom et al., 2003; Jacobs et al., 2013). Experiments with monkeys have revealed the existence of view-responsive neurons, that is, place-like and grid-like activity of neurons is evoked when the animal is looking at a particular location in the visual field (Rolls and Tovee, 1995; Killian et al., 2012). These data suggest that hippocampal activity during navigation does not only code the current position of the subject but can also encode virtual exploration of an environment.

Recordings from the hippocampal formation of epileptic patients have shown that some neurons fire very selectively to particular objects, landmarks or individuals (Quiroga et al., 2005). The firing of these cells is strikingly invariant as, for example, they are activated when various photos of Jennifer Aniston are presented, irrespective of the orientation and the angle of shooting. Moreover, the corresponding cells are even activated when only the written name is presented to the subject. Such cells are called “grandmother neurons” and are unofficially known as “Jennifer Aniston neurons”.

While the aforementioned studies show strong correlations between hippocampal activity and behaviour, what is the role of such representations for the cognition, and for the memory in particular? With the advance of neuroimaging techniques, and optogenetics specifically, now researchers are able to track the activity of large population of neurons (e.g., thousands of cells) and manipulate their behaviour during experiments. Tagging active cells during an association learning task, one can isolate the neural assembly that is activated during the learning. A following activation or inhibition of the assembly can evoke or suppress the learned response (Cowansage et al., 2014; Tanaka et al., 2014). These results provide evidence for the active role of the hippocampus in the neural representations during behaviour.

### 1.3.4 Oscillations

Rhythms are omnipresent in the brain. Oscillations with various frequencies can be detected using extracellular electrodes or electroencephalography (EEG) in any brain region. These oscillations reflect the underlying neuronal activity that is synchronised across large populations of cells and are often strongly correlated to specific behaviours that the subject is engaged in.

The hippocampus, particularly, shows some of the most striking rhythms in the mammalian brain. Electrophysiological recordings *in vivo* reveal a rich repertoire of rhythms in the local field potentials that are state dependent. For example, the theta oscillation ( $\sim 5 - 10$  Hz, see Figure 1.5), that is among the most regular rhythms, is associated with active behaviour such as walking and running, and also with the rapid-eye-movement (REM) phase of sleep (Jung and Kornmüller, 1938; Buzsáki, 2002). Moreover, the theta phase modulates the amplitude of the faster gamma oscillation ( $\sim 30 - 100$  Hz) that rides on top of it (Bragin et al., 1995; Buzsáki, 2002). Neuronal firing is largely modulated by the oscillation phase. While pyramidal cells are mostly firing at the trough of the theta cycle, various interneurons have different preferred phases (Klausberger and Somogyi, 2008; Klausberger, 2009). Moreover, neurons are differentially modulated by gamma oscillations.

As mentioned above, during exploration, pyramidal neurons are modulated by the current position of the animal, i.e., place cells. Interestingly, a place cell’s firing pattern shows peculiar modulations with respect to the local-field theta oscillation. When the animal enters the corresponding place field, the neuron starts to fire at a particular phase of the theta cycle, the so called entering phase. As the animal progresses within the field, the neuron fires at earlier phases in each subsequent theta cycle (Figure 1.5). The range of phases that a neuron precesses through does not exceed one theta cycle. This advance of firing phase with respect to the theta oscillation is known as “phase precession” (O’Keefe and Recce, 1993). Thus, in addition to the information coded in the firing rates of neurons (i.e., the rate code), there is additional information about the exact location of the animal carried in the exact spike timing in respect to the theta oscillation (i.e., the temporal code).

Phase precession has been in the focus of research due to its assumed role in learning, and particularly, it has been hypothesised to be a mechanism for bridging the temporal gap

## 1 Introduction

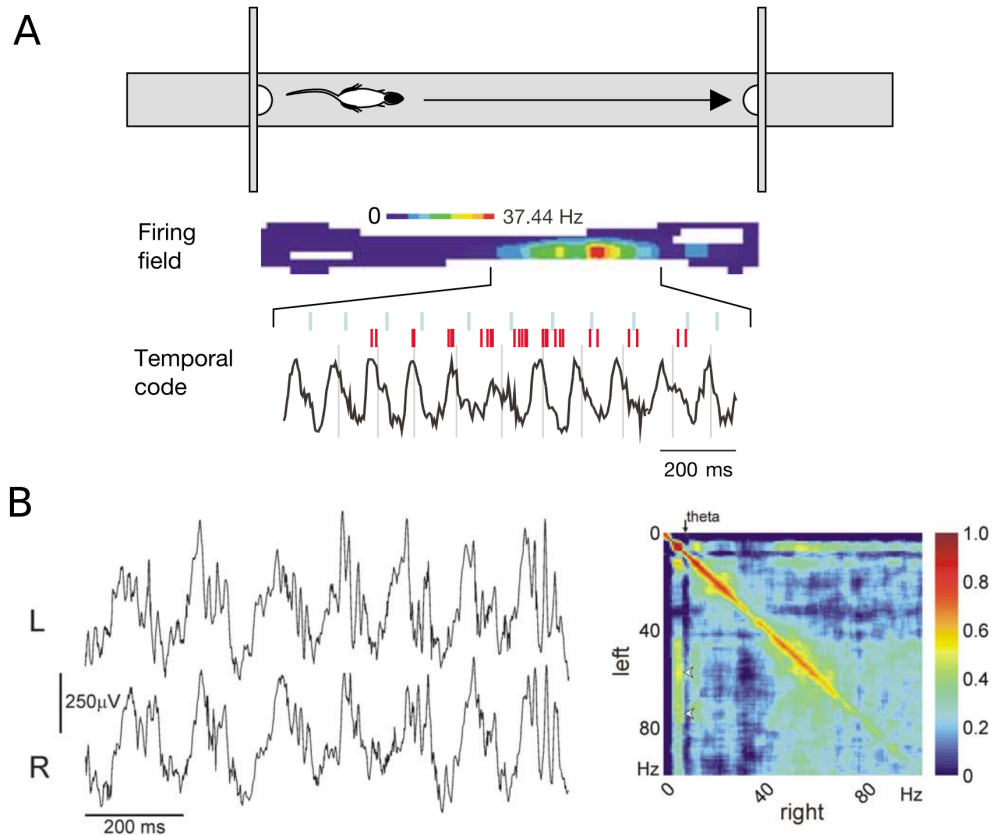


Figure 1.5: **A.** An illustration of a rat traversing a linear track (top panel). The place-field firing of a pyramidal neuron is color coded (middle panel) with red denoting the location of maximum firing rate. Activity from a single run is shown in the bottom panel. The EEG activity (black curve) is dominated by the theta oscillation. The place cell is firing in bursts of spikes (red vertical bars) at a rate higher than theta frequency, causing each successive burst to occur at an earlier theta phase (Huxter et al., 2003; adapted with permission). **B.** Bilateral coherence of theta and gamma oscillations (Buzsáki et al., 2003; adapted with permission). Extracellular recordings from the pyramidal-cell layer in the left (L) and right (R) hippocampi show local-field potentials modulated by theta and gamma. Co-modulation of frequency power in the two hemispheres (right panel). Theta power in one hemisphere is co-modulated with gamma power of the other hemisphere (yellow band at 9 Hz and 50–100 Hz, white arrowheads).

between the behavioural time scales (in the order of seconds) to the physiological time scales at which synaptic plasticity operates (order of milliseconds to tens of milliseconds; e.g., Bi and Poo, 1998). For example, disruption of phase precession through a systemic administration of a cannabinoid-receptor agonist leaves the spatial selectivity of hippocampal neurons intact but impairs the performance of rats in memory tasks (Robbe and Buzsáki, 2009).

When the animal traverses partially overlapping place fields, the corresponding place cells are sequentially activated. Moreover, as place cells show phase precession, the sequential spike order is preserved in the firing-phase difference on a fine time scale (Figure 1.5). Interestingly, the sequential spiking of neurons is more reliable than the spiking phase of single neurons (Dragoi and Buzsáki, 2006). Such firing sequences within a theta cycle are called “theta sequences”. The temporal compression of sequences within a theta cycle is assumed to be a crucial mechanism for the formation of memories (Skaggs and McNaughton, 1996), and in particular of single-trial learning (Rutishauser et al., 2006).

What is the relation between phase precession and the theta sequence? Are they two sides of the same phenomenon? Feng et al. (2015) observed phase precession in neurons during the first exposure of animals in a novel environment but reported the absence of theta sequences. From the second trial on, stable and reliable theta sequences were present. These results suggest that a single-trial experience is needed to form the sequence in the memory. Theta sequences, however, do not cover uniformly the whole environment, but are segmented in their representations. Gupta et al. (2012) showed that different theta sequences reliably represent chunks of the environment, frequently bounded by the space between landmarks.

Sequence replay is observed also during other prominent hippocampal oscillations, the sharp-wave ripples. Due to the central place of this phenomenon in this thesis, the following Section 1.4 is dedicated to their more detailed description.

## 1.4 Sharp-wave ripples

Sharp-wave ripples (SWRs) are hippocampal population bursts during which large numbers of neurons are orchestrated in precise firing. The sharp waves are reflected in brief (50–100 ms) and large ( $> 1$  mV) amplitude deflections observed in the local-field in the stratum radiatum of the CA regions (see Figure 1.6). The incidence of SWRs ranges from 0.01 up to 3 events/sec. The accompanying phenomenon of the sharp wave, the ripples, is fast (120–200 Hz) and short-lasting ( $\sim 50$  ms) oscillation that is most prominent in the pyramidal cell layer of the CA1 region. SWRs play an important role in memory processes such as learning, retrieval, consolidation, as well as planning.

The sharp-wave phenomenon was first described in the rabbit hippocampus (Stumpf, 1965). Later reports come from dogs (Yoshii et al., 1966), monkeys (Freemon et al., 1969), humans (Freemon and Walter, 1970), and the first classification used the term “large irregular activity” (Vanderwolf, 1969). Buzsáki and Wise (1992) first analysed and named the fast oscillation component, the ripple. Afterwards, sharp-wave ripples have been detected in every tested mammalian species.

In what follows, I am going to describe the sharp-wave ripples and some of their main properties. For the curious reader looking for more in-depth information concerning SWRs, I highly recommend the recent *opus magnum* by Buzsáki (2015).

## 1 Introduction

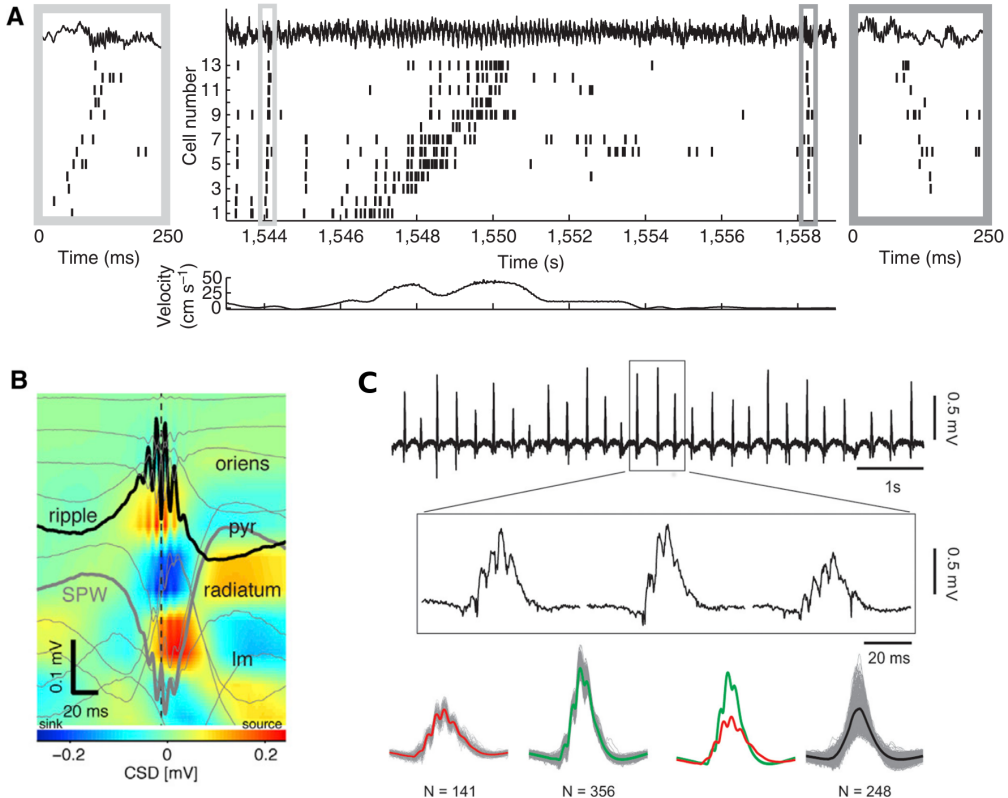


Figure 1.6: Sharp-wave ripples. **A.** Forward and reverse replay of a place-cell sequence. The big central panel shows the local field potential (top), a raster plot of 13 neurons where spike times are denoted with bars (middle), and the velocity of the rat in time (lower panel). Two 250 ms time windows magnify sequence replay during SWRs at the beginning and at the end of the lap (Diba and Buzsáki, 2007; reproduced with permission). **B.** Local activation of PCs *in vivo* evokes reliably SWRs with conserved waveforms (Stark et al., 2014; reproduced with permission). Depth profile of SWRs measure with multi-shank probes in a freely moving mouse (average from  $n = 961$  events; vertical site separation: 100  $\mu$ m). Voltage traces (light gray) are superimposed on current-source density map. The black trace is from the site of maximum amplitude ripple (pyr: stratum radiatum); and thick gray trace is from the site of maximum amplitude of sharp wave (radiatum). oriens: stratum oriens, lm: stratum lacunosum moleculare. **C.** *In-vitro* SWRs can show regular occurrence (Reichinnek et al., 2010; reproduced with permission). SWRs are stable over the recording, as the same waveforms occur over hour-long intervals. Waveforms can be sorted according to their electrographic characteristics. Averaged waveforms show a congruent appearance (red and green) compared with averaged randomly chosen SWRs (black).

### 1.4.1 Behavioural correlates

*In-vivo* sharp-wave ripples (SWRs) can be observed during sleep and wakefulness. In the awake state, SWRs occur predominantly during “off-line” resting behaviours such as drinking, feeding, grooming, whisking, or being still; but can also be seen during the “exploratory” theta-dominated states (O’Neill et al., 2006). During sleep, SWRs are observed in the non-rapid-eye-movement phase of the sleep, the slow-wave sleep (SWS). The SWR events are associated with a massive population burst of activity where large numbers of cells are synchronously active. The fraction of engaged cells can vary from 1% to 40% but a typical number is 10% (Mizuseki and Buzsáki, 2013). SWRs co-occur with the thalamo-cortical spindles. It is hypothesised that this co-activation facilitates the communication between the hippocampus and the neocortex (Sirota et al., 2003).

While the exact functions and mechanisms for the generation of SWRs are still elusive, it is known that they are involved in the formation and consolidation of new memories. According to the dominant theory in the field, i.e., the two-stage memory hypothesis (Buzsáki, 1989), SWRs perform information transfer of memory traces that are temporally stored in the hippocampus to the distributed neocortical network. This hypothesis is supported by multiple lines of experimental observations. On the one hand, higher incidence of spindles and SWRs is observed after learning (Eschenko et al., 2006, 2008; Girardeau et al., 2014), and the number of successfully recalled items in a learning task is correlated to the incidence of SWRs measured in the rhinal cortex (Axmacher et al., 2008). Moreover, boosting slow-wave oscillations through transcranial stimulation during sleep potentiates memory performance in humans (Marshall et al., 2006), and presenting odor cues during SWS, but not during REM sleep or wakefulness enhance declarative memories that were formed during the odor exposure (Rasch et al., 2007). On the other hand, disruption of SWRs during sleep or wakefulness impairs the performance of rats on hippocampus-dependent spatial tasks, presumably deteriorating the memory consolidation process (Girardeau et al., 2009) and the planning of future actions (Jadhav et al., 2012).

Another line of observation supporting the hypothesis that the hippocampus acts as a temporal storage of memory traces is the replay of behavioural sequences that takes place during SWRs. Wilson et al. (1994) showed in rats that hippocampal neurons with overlapping place fields that were coactive in the awake state showed strong activity correlations during SWRs. Later, Lee and Wilson (2002) demonstrated that the sequence of experienced events is preserved during the SWR replay, but temporally compressed ~20-fold. More recent experiments reveal that the hippocampal SWR replay is coordinated with grid-cell replay of sequences in the entorhinal cortex (Ólafsdóttir et al., 2016). However, O’Neill et al. (2017) demonstrated that replay of behaviour trajectories in superficial layers of the EC can also occur independently of the hippocampal SWRs.

An amazing amount of data supports the memory-consolidation hypothesis of sharp-wave ripples but some experimental results have challenged the model. Foster and Wilson (2006) showed that immediately after a spatial experience, the most recent spatial episodes are replayed in a temporally reversed order. While such reverse replay is assumed to consolidate the most recent experiences, its appearance questions the relevance the classical spike-timing dependent plasticity (STDP) rule with an asymmetric window (Bi and Poo, 1998) as a mechanism for sequence storage. A somewhat bigger challenge to the classical model have been the reports of preplay of behaviour sequences. Dragoi and Tonegawa (2011) measured the hippocampal neuronal activity during SWRs prior to an animal’s exposure to a novel environment and reported replay of place-cell sequences representing the not-yet ex-

## 1 Introduction

posed environment. Such results suggest that sequences are not rapidly stored in the CA3 region, but that they might be precoded. An estimation based on multiunit activity recordings predicts that the rat hippocampus might store sequences of about 15 different novel environments (Dragoi and Tonegawa, 2013).

### 1.4.2 Generation mechanisms

Sharp-waves ripples(SWRs) can be observed in the whole hippocampal region. They are most prominent in the CA regions revealing a stereotypical laminar profile signature in the local-field potential (LFP). A current-source density analysis shows that sharp waves are associated with a large negative deflection of the LFP (sink) in the stratum radiatum (see Figure 1.6B), which reflects the excitatory input impinging on the apical dendrites of the pyramidal neurons. The ripple component is most prominent in the stratum pyramidale where the local potential shows a fast oscillation ( $\sim 200$  Hz) riding on top of a positive deflection.

The temporal order of local population activations suggests that the origin of the SW burst is in the CA3 region, presumably initiated by a build-up of recurrent activity (de la Prida et al., 2006; Ellender et al., 2010; Schlingloff et al., 2014; Hulse et al., 2016), and then the activity propagates to the CA1 region through the Schaffer collateral projections (Csicsvari et al., 2000). The propagation of activity from CA3 to CA1 is important for memory formation. Blocking the excitatory CA3-CA1 projections impairs the formation of hippocampus-dependent memories in mice (Nakashiba et al., 2008). Interestingly, SWRs were still observable in the CA1 region, although with a lower incidence, ripple frequency, and number of ripples per event (Nakashiba et al., 2009). This result suggests that the CA1 region is also able to generate sharp waves independently of CA3, when integrating inputs from cortical and subcortical areas.

The ripple oscillation is among the most synchronous activity patterns in the mammalian brain. A few classes of models have aimed to explain the origin of these fast oscillations. One model class relies on the electrical coupling between axons of pyramidal cells in the CA3/CA1 regions (Draguhn et al., 1998; Schmitz et al., 2001; Traub et al., 2012; Vladimirov et al., 2013). In another model class the supralinear amplification of precisely synchronised inputs (Memmesheimer, 2010; Jahnke et al., 2015) leads to discrete waves of activity that generate ripple oscillations while propagating. The third proposed mechanism relies on networks of inhibitory neurons. According to this model, sparsely connected networks of fast inhibitory neurons can enter a sparsely synchronous regime, where the population oscillation can reach frequencies of  $\sim 200$  Hz (Brunel and Wang, 2003). While the proposed mechanisms are not mutually exclusive, experimental results are in favour of the inhibition-generated ripples (Buhl and Buzsáki, 2005; Schlingloff et al., 2014; Donoso et al., 2017).

*In-vivo* data has suggested that SWRs are local hippocampal events. For example, decoupling the hippocampus from the rest of the brain by removing the main inputs leads to spontaneous dynamics largely dominated by SWRs (Buzsáki et al., 1983), pointing out that SWRs might be a “default” network state for the hippocampus. *In-vitro* slice models have been developed to facilitate the study of SWRs (e.g., Maier et al., 2002, 2003; Kubota et al., 2003; Colgin et al., 2004). Horizontal slices of a thickness around 300–600  $\mu\text{m}$  from the ventral hippocampus are typically used for *in-vitro* studies. The slice models offer clear advantages in investigating the synaptic, the cellular, and the network properties of the neuronal circuit by giving more control to the experimenters. SWRs *in vitro* show preserved main characteristics such as spontaneously generated events, propagation pathway, laminar

profile of the LFP, ripple oscillations, neuron participation, and synaptic inputs. Moreover, SWRs can occur with conserved waveforms over long periods of time (in the order of hours), and single PC firing is coupled to certain waveforms but not to others (Reichinnek et al., 2010). There are, however, also some differences: SWRs *in vitro* tend to be shorter and have a slightly higher ripple frequency (150–180 Hz *in vivo*;  $\sim 200$  Hz *in vitro*). It is worth mentioning that even *in-vivo* SWRs show slightly different properties depending on the behavioural state and even on the location of the animal (Buzsáki, 2015).

Regardless of being in the focus of many research groups, the mechanisms behind the SWR initiation are still not well understood. As SWRs are large population events, traditionally it is assumed that they originate from the build-up of excitatory activity mainly in the CA3 region (Ellender et al., 2010; Schlingloff et al., 2014; Hulse et al., 2016). For example, the excitation of a large number of cells in the local circuit by an external stimulation can lead to SWRs events (Maier et al., 2003; Behrens et al., 2005; Nimmrich et al., 2005; Both et al., 2008). Recent evidences, however, point to the involvement of the interneuron network in the initial phases of the events (Sasaki et al., 2014; Bazelet et al., 2016). Schlingloff et al. (2014) and Kohus et al. (2016) have shown that activation of parvalbumin-positive basket cells in slices can lead to SWR events within milliseconds. SWRs can also be induced by a single action potential of a CA3 pyramidal neuron. Bazelet et al. (2016) show that the induced spike of a PC was followed by putative-interneuron firing after a small delay  $< 3$  ms indicating the relevance of the interneurons in SW generation.

Other open questions are what terminates the SWR event, and what mechanisms control the incidence of their occurrence. Chapter 3 of this thesis tackles these problems. There, I provide some further literature overview on how SWR incidence is controlled in experimental settings through pharmacology and other means, and propose a phenomenological model about SWR generation based on the latest experimental results from the literature.

## 1.5 Scope

The focus of this thesis is on the mechanisms of SWR generation and the associated sequence replay in the hippocampus. In Chapter 2 is presented a computational model of assembly sequences that aims to explain the replay during SWRs. There are explored the conditions in which assembly sequences can be replayed by external inputs, or manifest themselves as activity patterns that emerge spontaneously. In Chapter 3, I review experimental findings hinting at the origins of the sharp-wave complexes, analyse data from *in-vitro* recordings, and test hypotheses in analytical and *in-silico* models. There, I discuss in detail a minimal hypothetical model that could explain the sharp waves observed *in vitro*.



## 2 Memory replay in balanced recurrent networks

### 2.1 Summary

<sup>1</sup> Synaptic plasticity is the basis for learning and memory, and many experiments indicate that memories are imprinted in synaptic connections. However, basic mechanisms of how such memories are retrieved and consolidated remain unclear. In particular, how can one-shot learning of a sequence of events achieve a sufficiently strong synaptic footprint to retrieve or replay this sequence? Using both numerical simulations of spiking neural networks and an analytic approach, we provide a biologically plausible model for understanding how minute synaptic changes in a recurrent network can nevertheless be retrieved by small cues or even manifest themselves as activity patterns that emerge spontaneously. We show how the retrieval of exceedingly small changes in the connections across assemblies is robustly facilitated by recurrent connectivity within assemblies. This interaction between recurrent amplification within an assembly and the feed-forward propagation of activity across the network establishes a basis for the retrieval of memories.

### 2.2 Introduction

The idea of sequential activation of mental concepts and neural populations has deep roots in the history of the cognitive sciences (Titchener, 1909; Brown, 1914; Washburn, 1916) as well as its share of criticism (Lashley, 1951). In one of the most influential works in neuroscience, Donald Hebb extended this concept by suggesting that neurons that fire simultaneously should be connected to each other, thus forming a cell assembly that represents an abstract mental concept (Hebb, 1949). He also suggested that such assemblies could be connected amongst each other, forming a network of associations in which one mental concept can ignite associated concepts by activating the corresponding assemblies. Hebb referred to the resulting sequential activation as well as the underlying circuitry as “phase sequence”. We will refer to such connectivity patterns as “assembly sequences”.

The notion of Hebbian assemblies has triggered a huge number of experimental studies (reviewed by Wallace and Kerr, 2010), but relatively few experiments have been dedicated to the idea of assembly sequences (Kruskal et al., 2013; Almeida-Filho et al., 2014). Many theoretical studies focused on feedforward networks, also known as synfire chains (Abeles, 1991; Diesmann et al., 1999; Aviel et al., 2002; Jahnke et al., 2013). Synfire chains are characterized by a convergent-divergent feedforward connectivity between groups of neurons, where pulse packets of synchronous firing can propagate through the network. Few works were also dedicated on synfire chains embedded in recurrent networks (Aviel et al., 2003;

---

<sup>1</sup>The work presented in this chapter is published as a manuscript in PLoS Computational Biology, titled “Memory replay in balanced recurrent networks” (Chenkov et al., 2017). This project was a collaboration with Henning Sprekeler and Richard Kempter.

## 2 Memory replay in balanced recurrent networks

Kumar et al., 2008; Trengove et al., 2013), however, without explicitly considering recurrent connectivity within groups.

In this study, we combine the concept of feedforward synfire chains with the notion of recurrently connected Hebbian assemblies to form an assembly sequence. Using numerical simulations of spiking neural networks, we form assemblies consisting of recurrently connected excitatory and inhibitory neurons. The networks are tuned to operate in a balanced regime where large fluctuations of the mean excitatory and inhibitory input currents cancel each other. In this case, distinct assemblies that are sparsely connected in a feedforward fashion can reliably propagate transient activity. This replay can be triggered by external cues for sparse connectivities, but also can be evoked by background activity fluctuations for larger connectivities. Modulating the population excitability can shift the network state between cued-replay and spontaneous-replay regimes. Such spontaneous events may be the basis of the reverberating activity observed in the neocortex (Kenet et al., 2003; Luczak et al., 2009; Contreras et al., 2013) or in the hippocampus (Lee and Wilson, 2002; Dragoi and Tonegawa, 2013; Stark et al., 2015). Finally, we show that assembly sequences can also be replayed in a reversed direction (i.e., reverse replay) as observed during replay of behavior sequences (Foster and Wilson, 2006; Diba and Buzsáki, 2007).

### 2.3 Results

To test Hebb’s hypothesis on activity propagation within a recurrent network, we use a network model of excitatory and inhibitory conductance-based integrate-and-fire neurons. The network has a sparse random background connectivity  $p_{\text{rand}} = 0.01$  (Guzman et al., 2016). We form a neural assembly (Figure 2.1A) by picking  $M$  excitatory ( $M = 500$  if not stated otherwise) and  $M/4$  inhibitory neurons and connecting them randomly with probability  $p_{\text{rc}}$ , resulting in a mutually coupled excitatory and inhibitory population. The new connections are created independently and in addition to the background connections. To embed an assembly sequence in the network, we first form 10 non-overlapping assemblies. The assemblies are then connected in a feedforward manner where an excitatory neuron from one group projects to an excitatory neuron in the subsequent group with probability  $p_{\text{ff}}$  (Figure 2.1B). Thus, by varying the feedforward and the recurrent connectivities, we can set the network structure anywhere in the spectrum between the limiting cases of synfire chains ( $p_{\text{ff}} > 0, p_{\text{rc}} = 0$ ) and uncoupled Hebbian assemblies ( $p_{\text{ff}} = 0, p_{\text{rc}} > 0$ ), as depicted in Figure 2.1C.

To ensure that the spontaneous activity of the network is close to an *in-vivo* condition, we use Hebbian plasticity of inhibitory connections (Vogels et al., 2011), which has been shown to generate a balance of excitatory and inhibitory currents in individual neurons (Figure 2.2A). As a consequence, spikes are caused by current fluctuations (Figure 2.2B), and the network settles into a state of asynchronous irregular (AI) firing (Figure 2.2C).

To simulate a one-shot sequence learning paradigm, we initially embed assemblies that have recurrent connectivity  $p_{\text{rc}}$  only and are not connected via feedforward connections (Figure 2.2, left-hand side). A stimulation of the first assembly does not evoke a replay. Then, in a sham learning event, new feedforward connections are created between subsequent assemblies followed by a short phase ( $\sim 5$  seconds) with inhibitory plasticity turned on in order to properly balance the network. If we then stimulate the first group in the embedded assembly sequence (Figure 2.2C, right-hand side), the network responds with a wave of activity that traverses the whole sequence, as hypothesised by Hebb (1949). We refer to such a

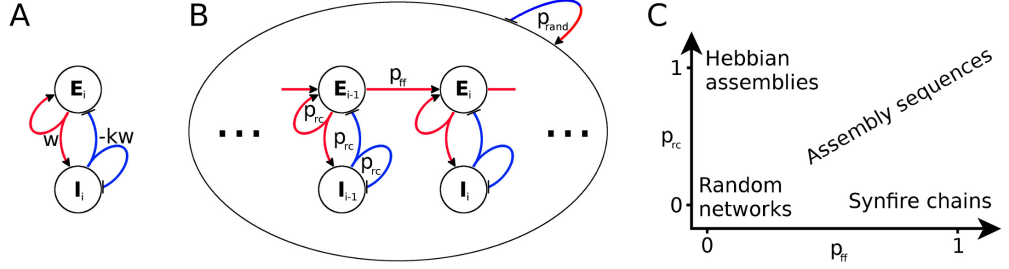
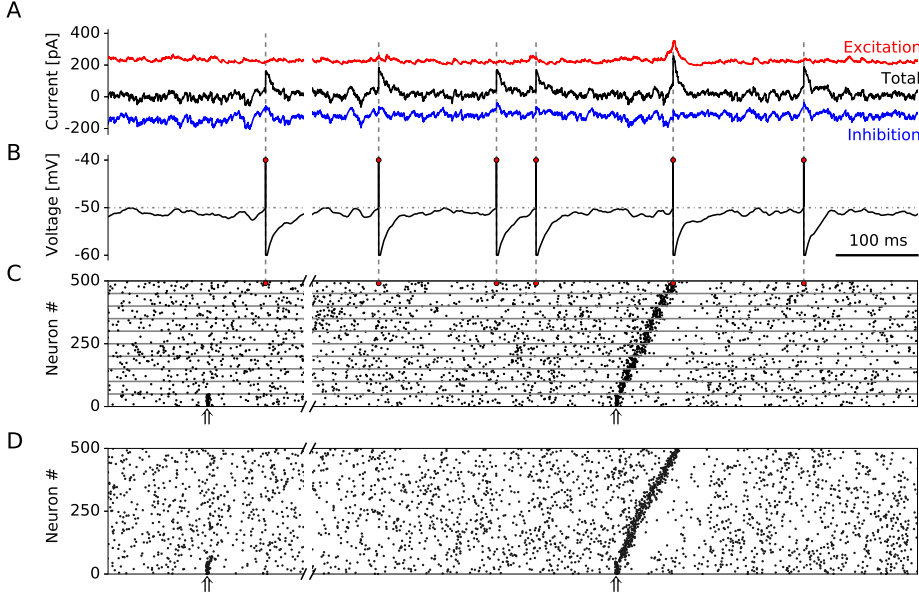


Figure 2.1: **Network connectivity.** **A:** Schematic of an assembly  $i$  consisting of an excitatory ( $E_i$ ) and an inhibitory ( $I_i$ ) population. Red and blue lines indicate excitatory and inhibitory connections, respectively. The symbols  $w$  and  $-kw$  denote total synaptic couplings between populations. **B:** Sketch of network connectivity. The inhomogeneous network is randomly connected with connection probability  $p_{\text{rand}}$ . A feedforward structure consisting of 10 assemblies (only  $i-1$  and  $i$  shown) is embedded into the network. Each assembly is formed by recurrently connecting its neurons with probability  $p_{\text{rc}}$ . Subsequent assemblies are connected with feedforward probability  $p_{\text{ff}}$  between their excitatory neurons. **C:** Embedded structure as a function of connectivities.

propagation of activity wave as replay. As excitatory and inhibitory neurons are part of the assemblies, they both have elevated firing rates during group activation. Despite the high population transient firing rates ( $\sim 100$  spikes/sec for excitatory, and  $\sim 60$  spikes/sec for inhibitory neurons when using a Gaussian smoothing window with width  $\sigma = 2$  ms) single neurons are firing at most one spike during assembly activation. Because excitatory neurons in an assembly transiently increase their population firing rate from 5 to 100 spikes/sec, a replay can be inferred from the large change in activity, which resembles replay in hippocampal CA networks (Lee and Wilson, 2002). On the other hand, interneurons have higher background firing rates of  $\sim 20$  spikes/sec and smaller maximum firing rates of  $\sim 60$  spikes/sec during replay. As a result, interneurons have a much lower ratio of peak to background activity than excitatory neurons in our model, in line with the reported lower selectivity of interneurons (Wilson and McNaughton, 1993).

We chose the particular wiring scheme of discrete assemblies partly due to the resemblance of the discrete windows of activity defined by the fast oscillations during hippocampal replay: ripples during sharp-wave ripples (SWRs) and gamma cycles during theta sequences. Additionally, our approach facilitates the model description and gives a leverage for an analytical treatment. Accordingly, in Figure 2.2A-C, we modeled discrete assemblies of size  $M = 500$ , which have a distinct recurrent connectivity  $p_{\text{rc}} = 0.1$  within each assembly, and a feedforward connectivity  $p_{\text{ff}} = 0.04$  between two assemblies in the sequence. However, in biological networks, assemblies could potentially overlap, making a clear-cut distinction between feedforward and recurrent connectivities difficult. To study assembly sequences in a more continuously wired sequence, we use an extreme case where no assemblies are defined at all. All neurons are arranged in a linear sequence, and every neuron is connected to its  $M = 500$  neighbouring excitatory cells ( $M/2$  preceding and  $M/2$  succeeding) with probability  $p_{\text{rc}}$ . Recurrent connections to and from inhibitory neurons are embedded analogously in a continuous manner. To imitate the connectivity pattern from the discrete model, every excitatory neuron is connected to the  $M$  following neurons without overlapping with the recurrent connections (i.e., the range from  $\frac{1}{2}M$  to  $\frac{3}{2}M$ ) with probability  $p_{\text{ff}}$ . After stimulating the first  $M$  neurons with a transient input, the whole sequence is replayed (Figure 2.2D). Compared to the discrete assembly sequence (Figure 2.2C) where the same connection prob-

## 2 Memory replay in balanced recurrent networks



**Figure 2.2: Example of 1 second network activity.** The first 250ms depict the dynamics of a network with random and recurrent connections only ( $p_{rc} = 0.1$ ). The same network after embedding feedforward connectivity ( $p_{ff} = 0.04$ ) is shown in the last 750ms. **A:** Input currents experienced by an example neuron. The excitatory and inhibitory inputs are denoted by the red and blue traces, respectively. The sum of all currents (synaptic, injected, and leak currents) is shown in black. **B:** Membrane potential of the same neuron. Red dots denote the time of firing. **C:** Raster plot of spike times of 500 neurons (50 neurons per group are shown). The red dots correspond to the firing of the example neuron in A and B. The stimulation times of the first assembly are denoted with upward arrows. **D:** Raster plot of a continuous sequence. Each neuron is connected to its  $M$  neighbours (in the range  $[-\frac{1}{2}M, \frac{1}{2}M]$ ) with probability  $p_{rc}$  (left-hand side); and afterwards (right-hand side), a feedforward connectivity  $p_{ff}$  to the following  $M$  neurons (in the range  $[\frac{1}{2}M, \frac{3}{2}M]$ ) is introduced.

abilities were used, the replay is continuous and qualitatively similar. In what follows, however, we return to the discrete assemblies because this description facilitates a connection of simulations with an analytical treatment.

### 2.3.1 Sparse feedforward connectivity is sufficient for replay

Whether an assembly sequence is replayed is largely determined by the connectivities within and between assemblies. Therefore, we first study how the quality of replay depends on the recurrent ( $p_{rc}$ ) and the feedforward ( $p_{ff}$ ) connectivities. The network dynamics can be roughly assigned to regimes where the connectivity is too weak, strong enough, or too strong for a successful replay. We use a quality measure of replay, which determines whether activity propagates through the sequence without evoking a “pathological” burst of activity (Figure 2.3). In such “pathological” cases the spatiotemporal structure of replay is often preserved while the background activity deviates from the AI state, or the whole network is involved in the events. To disregard such events, the quality measure punishes replays that

### 2.3 Results

(1) evoke bursting of neurons within assemblies during activation or (2) activate the whole network (for details, see Section 2.5.4).

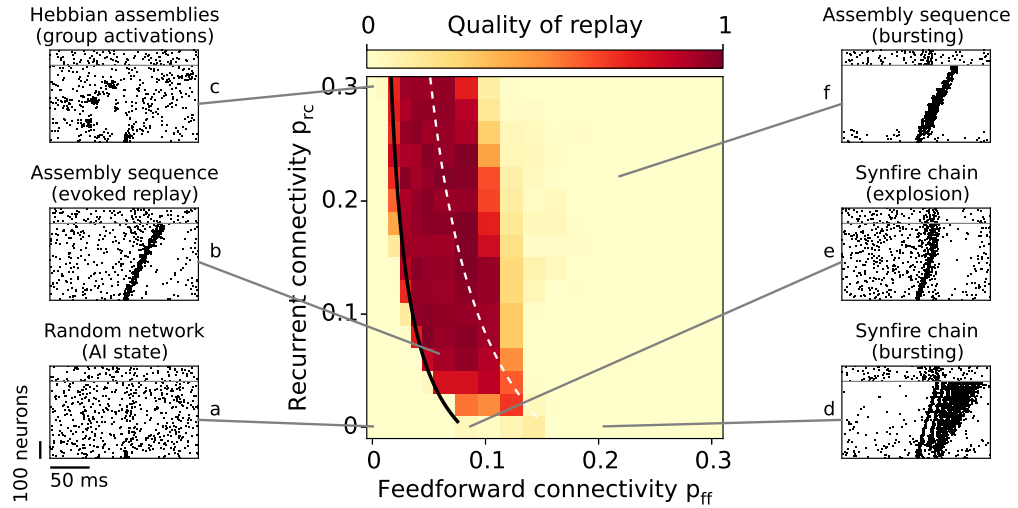


**Figure 2.3: Evoked replay.** Assembly-sequence activation as a function of the feedforward  $p_{ff}$  and the recurrent  $p_{rc}$  connectivities. The color code denotes the quality of replay, that is, the number of subsequent groups firing without bursting (see Materials and Methods, Section 2.5.4). The black curve corresponds to the critical connectivity required for a replay where the slope  $c$  of the transfer function (see Section 2.5.7 and Equation 2.1) is matched manually to fit the simulation results for connectivities  $p_{rc} = 0.08$  and  $p_{ff} = 0.04$ . The slope  $c$  is also estimated analytically (dashed white line). The raster plots (a-f) illustrate the dynamic regimes observed for different connectivity values; neurons above the gray line belong to the background neurons.

Naturally, for a random network ( $p_{ff} = 0$ ,  $p_{rc} = 0$ , Figure 2.3a) the replay fails because the random connections are not sufficient to drive the succeeding groups. In the case of uncoupled Hebbian assemblies (e.g.,  $p_{ff} = 0$ ,  $p_{rc} = 0.30$ ), groups of neurons get activated spontaneously (Figure 2.3c), which is reminiscent to the previously reported cluster activation (Litwin-Kumar and Doiron, 2012) but on a faster time scale. Already for sparse connectivity (e.g.,  $p_{ff} = p_{rc} = 0.06$ ) the assembly-sequence replay is successful (Figure 2.3b). In the case of denser recurrence ( $p_{rc} \approx 0.10$ ), a pulse packet propagates for even lower feedforward connectivity ( $p_{ff} \approx 0.03$ ). The feedforward connectivity that is required for a successful propagation decreases with increasing recurrent connectivity because assemblies of excitatory and inhibitory neurons can increase small fluctuations of the input through “balanced amplification” (Murphy and Miller, 2009; Hennequin et al., 2012) as summarized in Materials and Methods, Section 2.5.3.

For high feedforward ( $p_{ff} \gtrsim 0.10$ ) but low recurrent ( $p_{rc} \lesssim 0.10$ ) connectivity, the replay has low quality. In this case, excitatory neurons receive small recurrent inhibitory input compared to the large feedforward excitation, because the recurrent connection probability is lower than the feedforward one. Due to the lack of sufficiently strong inhibitory feedback within the assembly (compared to the strong feedforward excitation), the propagating activity either leads to run-away excitation (Figure 2.3e), also called synfire explosion (Mehring et al., 2003; Aviel et al., 2004), or to epileptiform bursting (Figure 2.3d). When both recurrent and feedforward connectivities are high, the inhibition is able to keep the propagating activity transient (Figure 2.3f). However, because of the strong input each neuron is firing

## 2 Memory replay in balanced recurrent networks

multiple times within a small time window. The fact that neurons in each group (except the first) are firing multiple times during a replay alters the spatio-temporal structure of the sequence. While activity propagates from one group to another, neurons do not necessarily spike in order due to the many emitted spikes. Another reason to assign low quality to such replays is the fact that the network dynamics is deviating from the AI background state because neurons that are part of the sequence tend to fire almost exclusively during replays but not outside replays.

To get an analytical understanding of the network, we use a linear approximation of the network dynamics to derive conditions under which replay is successful. The key determinant for replay is an amplification factor  $\kappa(p_{\text{ff}}, p_{\text{rc}}) = \frac{r_{i+1}}{r_i}$ , which measures how large is the rate  $r_{i+1}$  in group  $i + 1$  in relation to the rate in the previous group  $i$ .

In the case where the amplification factor is smaller than one ( $r_{i+1} < r_i$ ), the activity propagating through the assembly sequence will decrease at each step and eventually vanish, while for amplification larger than one ( $r_{i+1} > r_i$ ) one would expect propagating activity that increases at each step in the sequence. An amplification factor  $\kappa(p_{\text{ff}}, p_{\text{rc}}) = 1$  represents the critical value of connectivity for which the replay is marginally stable, and the magnitude of activations is similar across groups. In the Materials and Methods we show that a linear model can approximate the amplification factor by

$$\kappa = cM p_{\text{ff}} g^E (1 + cM p_{\text{rc}} g^E) \quad (2.1)$$

where  $c = 0.25 \text{ nS}^{-1}$  is a constant that fits the model to the data (see Materials and Methods). We can interpret  $\kappa$  as an “effective feedforward connectivity” because the recurrent connectivity ( $p_{\text{rc}}$ ) effectively scales up the feedforward connectivity  $p_{\text{ff}}$ . We can match the analytical results for critical connectivities to the numerical simulation, and show a qualitative fit between the approaches (black line in Figure 2.3).

We note that the number of excitatory synapses that is needed for an association,  $M^2(p_{\text{rc}} + p_{\text{ff}})$ , weakly depends on the position on the line  $\kappa = 1$ . By solving

$$\underset{p_{\text{rc}}, p_{\text{ff}} \in \kappa=1}{\operatorname{argmin}} M^2(p_{\text{rc}} + p_{\text{ff}})$$

we find that the minimum number of new connections required for a replay is obtained for  $p_{\text{rc}} = 0$  because lines for which  $p_{\text{rc}} + p_{\text{ff}} = \text{const}$  have slope of  $-1$  in Figure 2.3, and the slope of the line defined by  $\kappa = 1$  is more negative. For example, when  $p_{\text{rc}} = 0.0$ , we need 40 new synapses; for  $p_{\text{rc}} = 0.05$ , we need 50 new synapses; and for  $p_{\text{rc}} = 0.2$ , 111 synapses are required for a new association. However, as feedforward connections might be created/facilitated on demand in one-shot learning, it is advantageous to keep their number low at the cost of higher recurrent connectivity, which has more time to develop *prior* to the learning. We extend this arguments further in the Discussion, Section 2.4.

In summary, the recurrent connections within an assembly play a crucial role in integrating and amplifying the input to the assembly. This facilitation of replay is predominantly due to the excitatory-to-excitatory (E-E) recurrent connections, and not due to the excitatory-to-inhibitory (E-I) connections, a connectivity also known as “shadow pools” (Aviel et al., 2004). We tested that embedding shadow pools and omitting the E-E connectivity within assemblies has no beneficial effect on the quality of replay.

### 2.3.2 Recurrent connections are important for pattern completion

Neural systems have to deal with obscure or incomplete sensory cues. A widely adopted solution is pattern completion, that is, reconstruction of patterns from partial input. We examine how the network activity evolves in time for a partial or asynchronous activation of the first assembly.

To determine the capability of our network to complete patterns, we quantify the replay when only a fraction of the first group is stimulated by external input. If 60 % of the neurons in the first group (strong cue) are synchronously activated (Figure 2.4A, left panel), the quality of replay is virtually the same as in the case of full stimulation (100% activated) in Figure 2.3. However, when only 20 % of the neurons (weak cue) are simultaneously activated (Figure 2.4A, middle panel), we see a deterioration of replay mostly for low recurrent connectivities. The effect of the recurrent connections is illustrated in the right-most panel in Figure 2.4A where quality of replay is shown as a function of  $p_{rc}$  while the feedforward connectivity was kept constant ( $p_{ff} = 0.05$ ).

Small input cues lead to a weak activation of the corresponding assembly. In the case of stronger connectivity (e.g.,  $p_{rc}$ ) this weak activity can build up and result in a replay as shown in the example from Figure 2.4B. The top and bottom rows of raster plots correspond to two assembly sequences with different recurrent connectivities, as highlighted by the rectangles in Figure 2.4A, while left and right columns show the activity during strong and weak cues, respectively. In the case of  $p_{ff} = 0.05$  and  $p_{rc} = 0.10$  (Figure 2.4B, top-right), the weak cue triggers a wide pulse packet with large temporal jitter in the first groups, which gradually shapes into a synchronous pulse packet as it propagates through the network. On the other hand, for a smaller recurrent connectivity ( $p_{rc} = 0.06$ ), the 20% partial activation triggers a rather weak response that does not result in replay (Figure 2.4B, bottom-right).

The quality of replay depends not only on the number of neurons that are activated but also on the temporal dispersion of the pulse packet. Here, we adopt a quantification method that represents the activity evolution in a state-space portrait (Diesmann et al., 1999). Figure 2.4C shows the time course of the fraction  $\alpha$  of cells that participate in the pulse packet and the temporal dispersion  $\sigma$  of the packet as the pulse propagates through the network. The state-space representation of two assembly sequences with equal feedforward ( $p_{ff} = 0.05$ ) but different recurrent connectivity are shown in Figure 2.4C (top:  $p_{rc} = 0.10$ , bottom:  $p_{rc} = 0.06$ ). For each assembly sequence we repeatedly stimulated the first group with varying cue size  $\alpha$  and time dispersion  $\sigma$ , depicted by the black dots. Depending on the strength and dispersion of the initial stimulation, the dynamics of a network can enter one of two attractor points. For high  $\alpha$  and low  $\sigma$  the pulse packet propagates, entering the so-called synfire attractor (white background). On the other hand, for low  $\alpha$  and high  $\sigma$  the pulse packet dies out resulting in low asynchronous firing (gray background). The black-arrow traces in Figure 2.4C are example trajectories that describe the propagating pulse packets from Figure 2.4B in the  $(\alpha - \sigma)$  space.

To summarize, increasing both the recurrent and feedforward connectivity facilitates the replay triggered by weak and dispersed inputs. Recurrent connectivity is particularly important for pattern completion.

### 2.3.3 Spontaneous replay

An interesting feature of assembly sequences is the potential emergence of spontaneous activations, that is, a replay when no specific input is given to the network. Random fluctuations

## 2 Memory replay in balanced recurrent networks

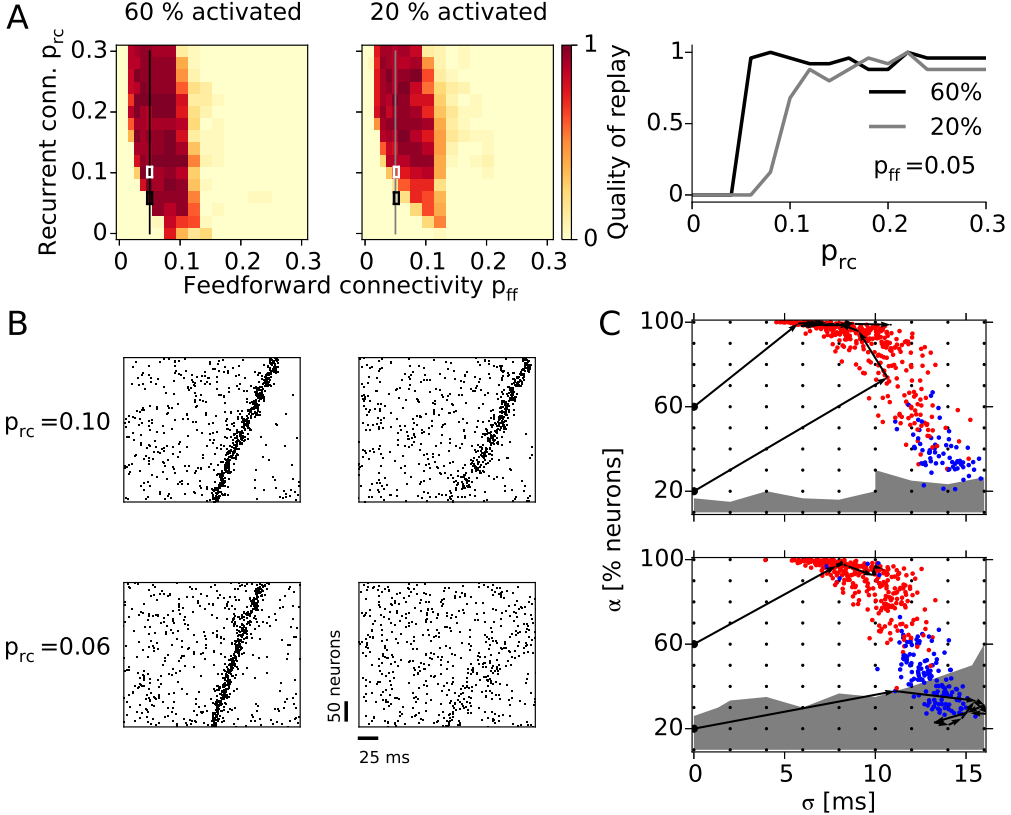


**Figure 2.4: Pattern completion.** **A:** Quality of replay after partial activation of the first group for cue size 60% (left panel) and 20% (middle) as a function of feedforward and recurrent connectivity. The right-most panel shows the quality replay after a cue activation (20% and 60%) as a function of the recurrent connectivity ( $p_{rc}$ ) while the feedforward connectivity is constant ( $p_{ff} = 0.05$ ). **B:** Examples of network activity during 60% (left) and 20% (right) cue activation. The top and bottom raster plots correspond to assembly sequences with higher ( $p_{rc} = 0.10$ , top) and lower ( $p_{rc} = 0.06$ , bottom) recurrent connectivity, highlighted in A with white and black rectangles, respectively. **C:** State-space portraits representing the pulse-packet propagation. The activity in each group is quantified by the fraction of firing excitatory neurons ( $\alpha$ ) and the standard deviation of their spike times ( $\sigma$ ). The initial stimulations are denoted with small black dots while the colored dots denote the response of the first group to the stimulations; red dot if the whole sequence is activated, and blue otherwise. Stimulations in the region with white background result in replays, while stimulating in the gray region results in no replay. The black arrows illustrate the evolution of pulse packets during the replays in B. Top:  $p_{rc} = 0.10$ ; bottom:  $p_{rc} = 0.06$ .

in the network can be amplified by the feedforward structure and give rise to a spontaneous wave of propagation.

We find that spontaneous and evoked replay share various features such as sequential group activation on the background of AI network activity (Figure 2.5A, rasters a and b). As in the case of evoked replay, for exceedingly large connectivities the network dynamics can be dominated by epileptiform bursting activity (Figure 2.5A, rasters c and d).

To assess spontaneous replay, we quantify the number of replay events per time taking into account their quality, i.e., huge bursts of propagating activity are disregarded as replay.

### 2.3 Results

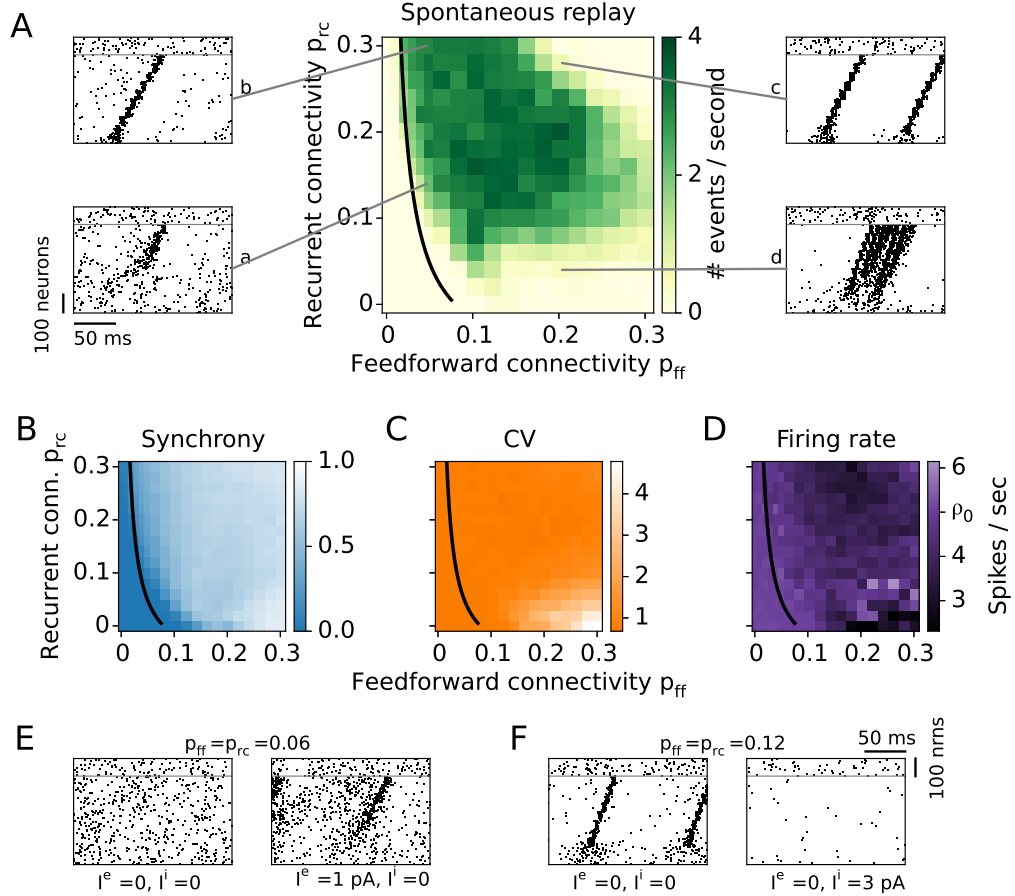


**Figure 2.5: Spontaneous network activity.** **A:** The rate of spontaneous sequence activation is measured in the unperturbed network. The black curve is the analytical result for the lower bound of successful propagation from Figure 2.3. Examples of spontaneous replays for different connectivities are shown in the raster plots **a-d**. Synchrony (**B**), coefficient of variation (**C**), and firing rate (**D**) are averaged over the neurons in the last group of the sequence. **E:** Spontaneous events modulated by an external input. For low enough connectivities no spontaneous events occur (left). A small additional constant current input to the whole excitatory population ( $I^e = 1 \text{ pA}$ ) generates spontaneous replays (right). **F:** A densely connected network shows replays (left). Once the inhibitory population receives an additional constant current input ( $I^i = 3 \text{ pA}$ ), the firing rate decreases and no spontaneous events occur (right).

The rate of spontaneous activation increases as a function of both the feedforward ( $p_{ff}$ ) and the recurrent ( $p_{rc}$ ) connectivity (Figure 2.5A). For large connectivities ( $p_{ff}, p_{rc} > 0.20$ ) the quality of the spontaneous events is again poor and mostly dominated by strong bursts (Figure 2.5A, raster c). The dynamics of networks with large feedforward and low recurrent connections is dominated by long-lasting bursts of activity consisting of multiple sequence replays within each burst (Figure 2.5A, raster d). The maximum rate of activations does not exceed 4 events per second because the inhibitory synaptic plasticity adjusts the inhibition

## 2 Memory replay in balanced recurrent networks

such that the excitatory firing rate is close to 5 spikes/sec.

The starting position of spontaneous replays largely depends on the network connectivity. Sequences with low  $p_{rc}$  are seldom initiated in the first group(s), while for high  $p_{rc}$  spontaneous replays occur predominantly at the beginning of the embedded sequence. Spontaneous replays for sequences with low  $p_{rc}$  arise from noise fluctuations that are amplified mainly by the underlying feedforward connections. Fluctuations propagate through a few groups until they result in a full-blown replay. On the other hand, to explain the preference of starting position at the beginning of the sequence for high  $p_{rc}$ , we refer to the case of disconnected Hebbian assemblies (Figure 2.3A, panel c) that get activated by the noise fluctuations. In case of weak feedforward connectivity (e.g.,  $p_{ff} < 0.02$ ), these fluctuations do not always activate the following assemblies due to insufficient feedforward drive. On the other hand, for  $p_{ff} > 0.03$  even a weak activation of an assembly will lead to a replay of the rest of the sequence. If replays were to start at random locations in the sequence, neurons in the later section of the sequence would participate in more replays than those earlier in the sequence, increasing the firing rate in these neurons. The inhibitory plasticity, which homeostatically regulates the rate, will hence increase the amount of inhibition in these later assemblies, with the effect of reducing the background activity. Because this in turn suppresses the fluctuations that trigger replays, spontaneous replays are less likely to be initiated in later assemblies.

To better characterize spontaneous dynamics, we refer to more extensive measures of the network dynamics. First, to account for deviations from the AI network state, we measure the synchrony of firing among neurons within the assemblies. To this end, we calculate the average pairwise correlation coefficient of spike trains of neurons within the same group. A low synchrony (value  $\sim 0$ ) means that neurons are uncorrelated, while a high synchrony (value  $\sim 1$ ) reveals that neurons fire preferentially together and seldom (or not at all) outside of an assembly activation. Because the synchrony builds up while activity propagates from one group to the next, a synchronization is most pronounced in the latter groups of the sequence. Therefore, we use correlations within the last group of the sequence as a measure of network synchrony (Figure 2.5B). The average synchrony is low ( $\sim 0$ ) for low connectivities ( $p_{ff}, p_{rc} < 0.10$ ) and increases as a function of both  $p_{ff}$  and  $p_{rc}$ . In the case of high  $p_{rc}$ , neurons participating in one assembly excite each other, and hence tend to fire together. On the other hand, for high  $p_{ff}$ , neurons within an assembly receive very similar input from the preceding group, so they fire together. This attachment of single neurons to group activity has two major consequences: first, it alters the AI state of the network, and second, it alters the stochastic behavior of the neurons, leading to more deterministic firing and bursting.

The network exhibits frequent epileptiform bursting in the case of high feedforward and low recurrent connectivities (raster plot examples in Figure 2.3, panel d, and Figure 2.5A, panel d). To assess this tendency of neurons to fire in bursts, we calculate the coefficient of variation (CV) for individual neurons' spike trains. The average CV of neurons in the last group of the sequence exhibits Poisson-like irregular firing (CV value  $\sim 1$ ) for a large range of parameters (Figure 2.5C). However, for high  $p_{ff}$  ( $\geq 0.10$ ) and low  $p_{rc}$  ( $\leq 0.10$ ), the CV value exceeds 1, in line with irregular and bursting firing. In this parameter region, small fluctuations of activity in the first groups of the sequence are strongly amplified by the underlying feedforward connectivity, leading to ever increasing activity in the following groups (Figure 2.5A, panel d). Because of the variable shapes and sizes of these bursts, they are not always classified as spontaneous activations in Figure 2.5A. Highly bursty firing (CV  $> 3$ ) and high synchrony ( $\sim 1$ ) suggest that the network cannot be properly balanced.

To test whether the inhibitory plasticity can balance the network activity when assembly sequences are embedded, we measure the average firing rate in the last group of the sequence (Figure 2.5D). The firing rate deviates from the target rate of 5 spikes/sec mostly for high feedforward connectivity ( $p_{ff} \gtrsim 0.15$ ). This inability of inhibition to keep the firing rate at the target value can be explained by the frequent replays that shape a stronger inhibitory input during the balancing of the network. Once the inhibition gets too strong, neurons can fire only when they receive excessive amount of excitation. Thus, in the case of high clustering, e.g., strong assembly connectivity, the inhibitory plasticity prevents the neurons from reaching high firing rates, but is unable to sustain an AI state of the network.

### 2.3.4 Control of spontaneous and cued replay by external input

Further, we investigate how spontaneous and cued replay are related. The black line in Figure 2.5A refers to the analytical approximation for connectivities that enable evoked replay. Compared to the connectivity region of successfully evoked replays in Figure 2.3, the region for spontaneous replays in Figure 2.5 is slightly shifted to the top and to the right. Therefore, in only a narrow area of the parameter space, sequences can be replayed by external input but do not get spontaneously activated. This finding suggests that to embed a sequence with high signal-to-noise ratio of propagation, the connectivities should be chosen appropriately, in line with previous reports (Kumar et al., 2010). In what follows we show that the size of this region can be controlled by external input to the network.

We demonstrate how a small amount of global input current to all excitatory or all inhibitory neurons can modulate the network and shift it between AI and spontaneous-replay regimes (Figure 2.5E and F). In the first example, the connectivities are relatively low ( $p_{ff} = p_{rc} = 0.06$ ) such that replay can be evoked (Figure 2.3) but no spontaneous activations are present (Figure 2.5A and Figure 2.5E, left). After injecting a small additional current of only 1 pA into the whole excitatory population, the network becomes more excitable, i.e., the firing rate rises from 5 to 12 spikes/sec and spontaneous replays do arise (Figure 2.5E, right).

On the other hand, in a network with high connectivities ( $p_{ff} = p_{rc} = 0.12$ ), replay can be reliably evoked (Figures 2.3 and 2.4A) and also occurs spontaneously (Figure 2.5A). An additional input current of 3 pA to the inhibitory population decreases the firing rate of the excitatory population from 5 to 0.33 spikes/sec and shifts the network from a regime showing frequent spontaneous replays to a no-replay, AI regime (Figure 2.5F, left and right, respectively). Nevertheless, replays can still be evoked as in Figure 2.3. Hence, the spontaneous-replay regime and the average firing rate in the AI state can be controlled by global or unspecific external current.

In summary, the balanced AI network state and successfully evoked replay of assembly sequences can coexist for a range of connectivities. For higher connectivities, the underlying network structure amplifies random fluctuations, leading to spontaneous propagations of activity between assemblies. A dynamical control of the rate of spontaneous events is possible through external input, which modulates the network activity and excitability. In the brain, such a switching between regimes could be achieved via neuromodulators, in particular via the cholinergic or adrenergic systems (Hasselmo et al., 1995; Thomas, 2015).

### 2.3.5 Smaller assemblies require higher connectivity

So far, we have shown basic properties of sequences at fixed assembly size  $M = 500$ . To determine the role of this group size in replay, we vary  $M$  and the connectivity while keeping

## 2 Memory replay in balanced recurrent networks

the size of the network fixed. As we have already explored how recurrent and feedforward connections determine replay individually, we now consider the case where they are equal, i.e.,  $p_{ff} = p_{rc} = p$ .

Assembly sequences can be successfully replayed after stimulation for various assembly sizes (Figure 2.6A). Smaller assemblies require denser connectivity (e.g.,  $p = 0.25$  for  $M = 100$ ), while larger assemblies allow sparser connectivity (e.g.,  $p = 0.05$  for  $M = 500$ ). Moreover, assemblies as small as 20 neurons are sufficient to organize a sequence given the condition of all-to-all connectivity within and between assemblies. The analytically derived critical value of effective connectivity  $\kappa = 1$  is in agreement with the numerical simulations (black line in Figure 2.6A).

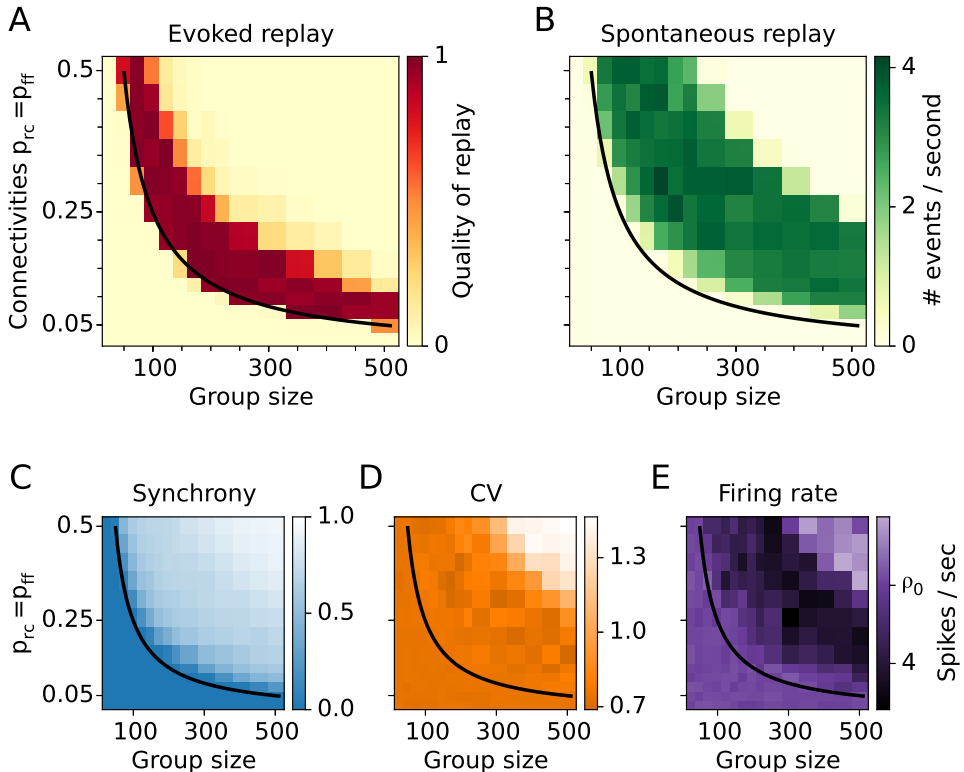


**Figure 2.6: Assembly-sequence activation for various group sizes and connectivities.** **A:** Simulation results for the quality of replay. **B:** Rate of spontaneous replay. **C:** Synchrony. **D:** Coefficient of variation **E:** Firing rate.  $\rho_0 = 5$  spikes/sec is the target firing rate. In C, D, and E quantities are averaged over the neurons in the last group of the sequence. The black line is an analytical estimate for the evoked replay as in Figures 2.3 and 2.5.

To further characterize the network dynamics for varying group size, we measure the rate of spontaneous activations of assembly sequences in undisturbed networks driven solely by constant input. As indicated in Figure 2.6B, spontaneous replays occur for a limited set of parameters resembling a banana-shaped region in the  $(M, p)$  plane. The parameter region for spontaneous replays partly overlaps with that of evoked replay. Again, there is a narrow range of parameters to the right of the black line in Figure 2.6B for which sequences can be evoked by external input while not being replayed spontaneously. As shown above, the size of this region can be controlled by external input to the whole network (Figure 2.5E, F).

To further assess the spontaneous dynamics, we measure the firing synchrony of neurons within the last group. The synchrony grows as function of both connectivity and group size (Figure 2.6C). The fact that the synchrony approaches the value one for higher connectivity and group size indicates that the network dynamics gets dominated by spontaneous reactivations. The simulation results reveal that neurons always fire rather irregular with coefficient of variation (CV) between 0.7 and 1.4 (Figure 2.6D). Because the recurrent and the feedforward connectivities are equal ( $p_{\text{ff}} = p_{\text{rc}} = p$ ), the inhibition is always strong enough and does not allow epileptiform bursting activity. This behavior is reflected in a rather low maximal value of the ( $\text{CV} < 1.4$ ) compared to the results from Figure 2.5, where the CV could exceed values of 4 for low  $p_{\text{rc}}$ . The measured firing rates in the last assembly are at the target firing rate of  $\rho_0 = 5$  spikes/sec for parameter values around and below the critical value  $\kappa = 1$  (Figure 2.6E). However, for increasing connectivity  $p$  and increasing group size  $M$ , the firing rate deviates from the target, indicating that the inhibitory plasticity cannot keep the network fully balanced.

To conclude, the assembly size  $M$  plays an important role in the network activity. The critical values of connectivity and group size for successful propagation are inversely proportional. Thus, the analytics predicts that larger assemblies of several thousands neurons require only a fraction of a percent connectivity in order to propagate synchronous activity. However, for this to happen, the group size  $M$  must be much smaller than the network size  $N^E$ . Here  $N^E$  was fixed to 20,000 neurons for easier comparison of scenarios, but results are also valid for larger networks (see Materials and Methods, Section 2.5.8). The good agreement between the mean-field theory and the numerical results suggests that the crucial parameter for assembly-sequence replay is the total input one neuron is receiving, e.g., the number of input synapses.

### 2.3.6 Stronger synapses are equivalent to more connections

Up to this point, all excitatory synaptic connections in our model had constant and equal strengths. By encoding an assembly sequence we implicitly altered the structural connectivity by creating new synaptic connections. This case of structural plasticity can also occur when silent synapses are turned into functionally active connections upon learning (Atwood and Wojtowicz, 1999; Hanse et al., 2013). However, learning new associations might also be possible through a change of synaptic strength of individual connections (Bliss and Lømo, 1973; Malenka and Bear, 2004). If a sequence is to be learned through synaptic plasticity, then instead of increasing the connectivity between groups of neurons, the synaptic conductances could be increased as well. To test whether these two types of plasticity are equivalent in our approach, we embed assembly sequences with various feedforward connectivities  $p_{\text{ff}}$  and various feedforward conductances  $g_{\text{ff}}^E$ , while keeping the recurrent connectivity ( $p_{\text{rc}} = 0.06$ ) and recurrent conductances ( $g^E = 0.1$  nS) constant.

Numerical results show that feedforward connectivity and feedforward conductance have identical roles in the replay of a sequence. That is, the sparser the connections, the stronger synapses are required for the propagation of activity. The analytical estimate (Figure 2.7A, black line corresponds to  $\kappa \sim p_{\text{ff}} g_{\text{ff}}^E = \text{const.}$ ) predicts that the product of  $p_{\text{ff}}$  and  $g_{\text{ff}}^E$  is the essential parameter for replay.

That this analytical prediction is fulfilled in the numerical simulations becomes clearer when we show the replay quality as a function of the feedforward connectivity and the total feedforward input  $p_{\text{ff}} g_{\text{ff}}^E / g^E$  a neuron is receiving (Figure 2.7B). It is irrelevant whether the number of connections are changed or their strength, what matters is their product. This rule

## 2 Memory replay in balanced recurrent networks

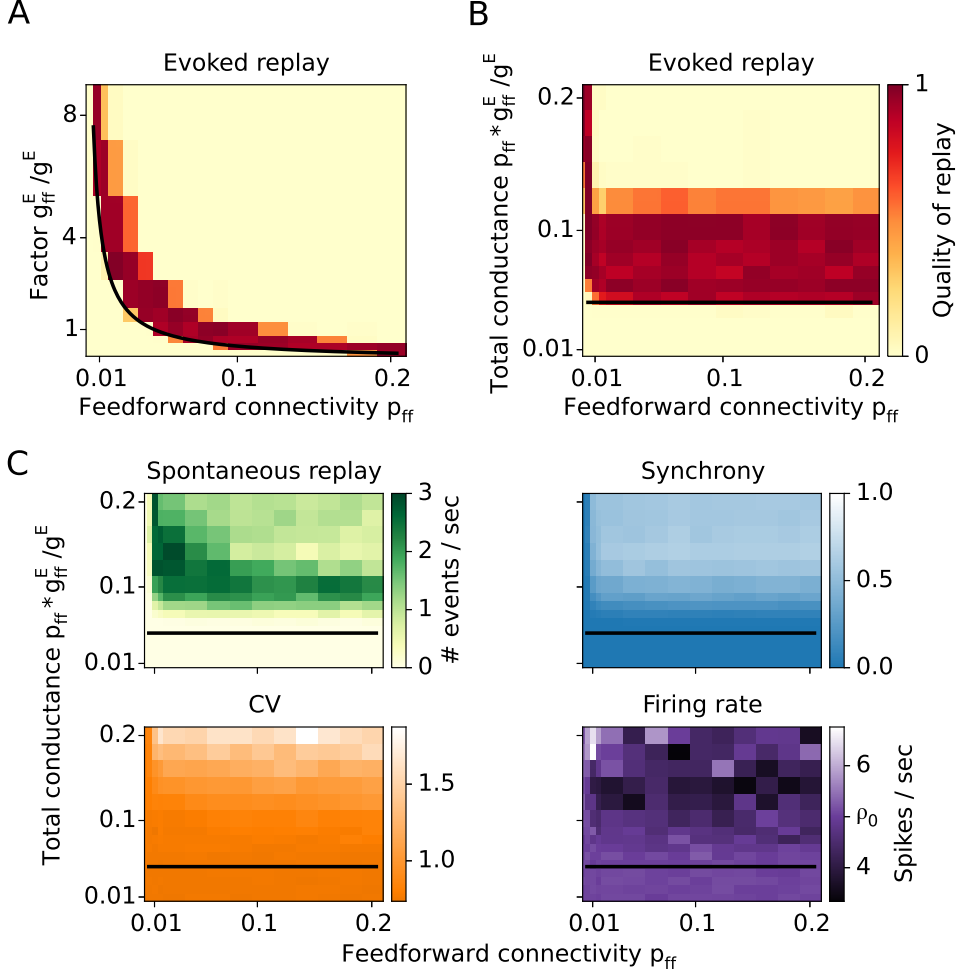


**Figure 2.7: Feedforward conductance versus feedforward connectivity.** **A:** Quality of replay as a function of connectivity and synaptic strength. **B:** The replay as a function of connectivity and total feedforward conductance input shows that the propagation is independent of connectivity as long as the total feed-forward input is kept constant. **C:** Spontaneous network dynamics described by the rate of spontaneous replay, synchrony, CV, and firing rate.

breaks only for sparse connectivities ( $p_{ff} < 0.01$ ), i.e. when the mean number of feedforward connections between two groups is low (< 5). Therefore, the number of relevant connections cannot be reduced to very low numbers.

Consistent with earlier findings, the quality of replay is high above a certain strength of the total feedforward conductance ( $\gtrsim 0.05$  in Figure 2.5B) and for  $p_{ff} \geq 0.01$ . However, for sufficiently large feedforward input ( $p_{ff} g_{ff}^E/g^E > 0.12$ ), the replay of sequences is severely impaired as the network is in a state of highly synchronous bursting activity (Figure 2.7B), which is similar to the results shown in Figures 2.5 and 2.6.

We also examined sequences that are formed by increasing existing background connections between the assemblies by a factor  $p_{ff}/p_{rand}$ , rather than by adding additional connections. Replays are possible also in this condition and they are indistinguishable from

networks with increased feedforward connectivities.

The rule that the total input  $p_{ff} g_{ff}^E$  determines the network behavior also holds for spontaneous activity. Spontaneous replay rate, CV, synchrony, and firing rate all vary as a function of the total input (Figure 2.7C), and only weakly as a function of the connectivity or the conductance alone. Similar to the previous results in Figures 2.5 and 2.6, for  $0.05 \leq p_{ff} g_{ff}^E / g^E < 0.10$  it is possible to evoke a replay while preserving the AI state of the network. Increasing the total input beyond this value drives the network into a state of spontaneous replay with increased synchrony.

### 2.3.7 Forward and reverse replay in assembly sequences with symmetric connections

The assembly-sequence model discussed until now contains asymmetric connections, i.e., neurons from one group project extensively within the same and the subsequent group but not to the previous group. We showed that such feedforward assembly sequences are capable of propagating activity, which we call replay. Thus, the proposed model may give an insight on the replay of behavioral sequences that have been observed in the hippocampus (Lee and Wilson, 2002). However, further experiments revealed that sequences are also replayed in the inverse temporal order than during behavior, so-called reverse replay (Foster and Wilson, 2006; Diba and Buzsáki, 2007). The direction of this replay also depended on the context, i.e., when the animal was at the beginning of the path, forward replays prevailed; while after traversing the path, more reverse replays were detected (but see Karlsson and Frank, 2009). This suggests that the replay activity might be cued by the sensory input experienced at the current location of the animal.

As the feedforward structure adopted in the network model is largely asymmetric, the assembly sequence is incapable of reverse replay in its current form. To be able to activate a sequence in both directions, we modify the network and add symmetric connectivity between assemblies (Litwin-Kumar and Doiron, 2014; Sadeh et al., 2015). The symmetric STDP window that has been reported recently in the hippocampal CA3 area *in vivo* (Mishra et al., 2016) would allow for strong bidirectional connections. In such a model, an assembly of neurons does not project only to the subsequent assembly but also to the preceding, and both projections are random with probability  $p_{ff}$  (Figure 2.8A). While this connectivity pattern decreases the group clustering and makes the sequence more continuous, it does not lead to full merge of the assemblies because the inhibition remains local for each group.

Interpreting this network as a model for hippocampal activity during spatial navigation of a virtual rat on a linear track (Figure 2.8B, top), we test the idea that external input can switch the network between a spontaneous-replay state during rest and a non-replay, spatial-representation state during locomotion. During immobility at the beginning of the track, a context-dependent input cue is mimicked by a constant current  $I^e = 2\text{ pA}$  injected into the excitatory neurons of the first assembly (Figure 2.8B, red bar from 0 to 500 ms). The elevated firing rate of the first assembly results in a spontaneous forward replay, similar to the experimental findings during resting states at the beginning of a linear track (Foster and Wilson, 2006; Diba and Buzsáki, 2007).

After the initial 500 ms resting period, an external global current of  $-10\text{ pA}$  is injected into the whole excitatory population to decrease network excitability and to mimic a state in which the rat explores the environment. In addition, to model place-specific sensory input that is locked to theta oscillations, we apply a strong and brief conductance input (as in Figure 2.2) every 100 ms to the assembly that represents the current location. In this

## 2 Memory replay in balanced recurrent networks

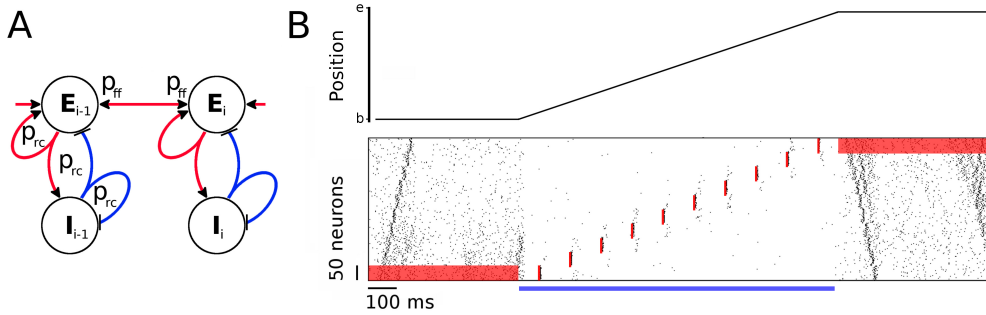


**Figure 2.8: Symmetric assembly sequence.** **A:** Schematic of an assembly sequence with symmetric connections between groups. **B:** Virtual rat position on a linear track (top) and the corresponding neuronal activity (bottom) as a function of time for 2 seconds. The rat rests at position “b” for half a second, then moves from “b” to “e” with constant speed for one second, where it rests for another 500 ms. While the rat is immobile at both ends of the track, a positive current input  $I^e = 2 \text{ pA}$  is applied to the excitatory population of the first and last assembly as shown by the red background in the raster plot. Spontaneous replays start from the cued assemblies. During exploration, however, the network activity is decreased by a current  $I^e = -10 \text{ pA}$  injected to the whole excitatory population, denoted with a blue horizontal bar. Strong sensory input during traversal activates the location-specific assemblies but does not result in any replay. The timing and location of the stimulations is denoted with red vertical bars in the raster plot. Recurrent and feedforward connectivities are  $p_{rc} = 0.15$  and  $p_{ff} = 0.03$ , respectively.

situation, the assemblies fire at their corresponding locations only. There is, however, a weak activation of the neighboring assemblies that does not result in a replay. An extension of the model including lateral inhibition and short-term plasticity would possibly enable theta sequences that span in one direction only (Romani and Tsodyks, 2015). Such an extension is, however, beyond the scope of the current project.

At the end of the track, we retract the global external current to return to the virtual resting state for the last 500 ms of the simulation, and the network switches back to higher mean firing rates. A context-dependent sensory cue to the last group ( $I^e = 2 \text{ pA}$  current injected continuously) then leads to a spontaneous reverse replay, similar to experimental findings at the end of a linear track (Foster and Wilson, 2006; Diba and Buzsáki, 2007).

In the absence of a context-dependent current injection during virtual resting state, spontaneous replays start at around the middle of the sequence (as in Figure 2.5) and propagate in forward or reverse direction. As noise fluctuations are gradually amplified while propagating between assemblies, it is rare to find a spontaneous event that is simultaneously replayed in both directions. In our simulations (Figure 2.8), we assumed that the starting position of replay is cued by the sensory input from the current location. However, it has been shown that replays during theta sequences are rather segmented and represent the environment in discrete “chunks” (Gupta et al., 2012). These segments are not uniformly distributed but tend to cover the space between physical landmarks, noteworthy positions in the environment. The finding of Gupta et al. (2012) suggests that there might be other mechanisms controlling the starting position of replay other than the sensory input. Currently, it is an open question whether SWR replays represent the environment also in a segmented manner from a landmark to a landmark.

In summary, we show that given symmetric connectivity between assemblies, transient activity can propagate in both directions. Large negative external currents injected into all

excitatory neurons can decrease network excitability and thus block the replay of sequences. On the other hand, spontaneous replay can be cued by a small increase in the firing rate of a particular assembly. Interestingly, once a replay is initiated, it does not change direction, in spite of the symmetric connectivity. An active assembly receives feedback inhibition from its inhibitory subpopulation, which prevents immediate further activations and hence a reversal of the direction of propagation.

## 2.4 Discussion

We revived Hebb's idea on assembly sequences (or "phase sequences") where activity in a recurrent neural network propagates through assemblies (Hebb, 1949), a dynamics that could underlie the recall and consolidation of memories. An important question in this context is how learning of a series of events can achieve a strong enough synaptic footprint to replay this sequence later. Using both numerical simulations of recurrent spiking neural networks and an analytical approach, we provided a biologically plausible model for understanding how minute synaptic changes can nevertheless be uncovered by small cues or even manifest themselves as activity patterns that emerge spontaneously. We showed how the impact of small changes in the connections between assemblies is boosted by recurrent connectivity within assemblies. This interaction between recurrent amplification within an assembly and the feedforward propagation of activity establishes a possible basis for the retrieval of memories. Our theory thus provides a unifying framework that combines the fields of Hebbian assemblies and assembly sequences (Hebb, 1949), synfire chains (Abeles, 1991; Diesmann et al., 1999), and fast amplification in balanced recurrent networks that are in an asynchronous-irregular state (Murphy and Miller, 2009; Vogels et al., 2011).

Main conclusions from our work are that the effective coupling between assemblies is a function of both feedforward and recurrent connectivities, and that the network can express three main types of behavior: 1. When the coupling is weak enough, assembly sequences are virtually indistinguishable from the background random connections, and no replays take place. 2. For sufficiently strong coupling, a transient input to some assembly propagates through the sequence, resulting in a replay. 3. For even stronger coupling, noise fluctuations get amplified by the underlying structure, resulting in spontaneous replays. Each of these three regimes has a certain advantage in performing a particular task. Weak coupling is appropriate for imprinting new sequences if the network dynamics is driven by external inputs rather than controlled by the intrinsically generated activity. Intermediate coupling is suitable for recollection of saved memories; sequences remain concealed and are replayed only by specific input cues; otherwise, the network is in the asynchronous-irregular, spontaneous state. For strong coupling, spontaneous replays might be useful for offline recollection of stored sequences when there are no external input cues. Importantly, the network behaviour and the rate of spontaneous events depends not only on the coupling but can be controlled by modulating the network excitability through external input. Neuromodulator systems, for example the cholinergic and the adrenergic systems (Hasselmo et al., 1995; Thomas, 2015) might therefore mediate the retrieval process.

### 2.4.1 Related models

Assembly sequences are tightly related to synfire chains, which were proposed (Abeles, 1991) as a model for the propagation of synchronous activity between groups of neurons. Diesmann

## 2 Memory replay in balanced recurrent networks

et al. (1999) showed for the first time that synfire chains in a noisy network of spiking neurons can indeed support a temporal code. It has been shown, however, that the embedding of synfire chains in recurrent networks is fragile (Aviel et al., 2003; Mehring et al., 2003), because on the one hand, synfire chains require a minimal connectivity to allow propagation, while on the other hand, a dense connectivity between groups of neurons can generate unstable network dynamics. Therefore, Aviel et al. (2004) introduced “shadow pools” of inhibitory neurons that stabilize the network dynamics for high connectivity. The network fragility can also be mitigated by reducing the required feedforward connectivity: inputs from the previous assembly are boosted by recurrent connections within the assembly. This approach was followed by Kumar et al. (2008), who examined synfire chains embedded in random networks with local connectivity, thus, implicitly adopting some recurrent connectivity within assemblies as proposed by the assembly-sequence hypothesis; nevertheless, their assemblies were fully connected in a feedforward manner. Recently, it was shown that replay of synfire chains can be facilitated by adding feedback connections to preceding groups (Moldakarimov et al., 2015). However, this Hebbian amplification significantly increased the duration of the spike volleys and thus decreased the speed of replay. Our model circumvents this slowing effect by combining the recurrent excitation with local feedback inhibition, effectively replacing Hebbian amplification by a transient “balanced amplification” (Murphy and Miller, 2009).

Other analytical studies have used the Fokker-Planck approach to describe the propagation of pulse packets in synfire chains (Câteau and Fukai, 2001; Gerstner and Kistler, 2002). In particular, Monasson and Rosay (2014) have used diffusion analysis to explore the interplay between different environments encoded in the network and their effects on the activity propagation during replay. To store sequences, further classes of models were proposed, e.g., “winner-takes-all” (Klampfl and Maass, 2013; Kappel et al., 2014; Mostafa and Indiveri, 2014) and “communication through resonance” (Hahn et al., 2014). However, the activity propagation in these models has an order of magnitude slower time scales than the synfire chain or the assembly sequence, and thus, are not suitable for rapid transient replays.

The spontaneous replay in our network bears some resemblance with the population bursts that occur in a model with supralinear amplification of precisely synchronised inputs (Memmesheimer, 2010; Jahnke et al., 2015). Adding such nonlinearities to the conductances in our model might decrease even further the connectivity required for the assembly-sequence replay. Another model class, which relies on lognormal conductance distributions, has been proposed as a burst generator for sharp-wave ripples (SWRs) (Omura et al., 2015). The model accounts for spontaneously generated stereotypical activity that propagates through neurons that are connected with strong synapses.

Other computational models have focused more on different aspects of the SWR events. Taxidis et al. (2012), for example, proposed a hippocampal model where a CA3 network rhythmically generates bursts of activity, which propagate to a predominantly inhibitory CA1 network that generates fast ripple oscillations. The ripple generation by inhibitory networks is studied in a greater detail in Malerba et al. (2016). Azizi et al. (2013) have explored the properties of a network that stores the topology of several environments and have shown that spike-frequency adaptation is an important mechanism for the movement of the activity bump within and between environments. In another modeling study, Romani and Tsodyks (2015) proposed that short-term synaptic depression is a potential mechanism for explaining the hippocampal activity both during mobility (theta-driven activity) and during immobility (fast replays).

Another class of models that aims to explain the origin of SWR events relies on the electrical coupling between axons of pyramidal cells in the CA3/CA1 regions (Draguhn et al., 1998; Schmitz et al., 2001; Traub et al., 2012). In a numerical model, Vladimirov et al. (2013) showed that the axonal plexus could explain the occurrence of SWs, the fast ripple oscillation, and moreover, account for the forward and reverse replay of sequences. Nevertheless, anatomical data to show the existence of such connections is still scarce (Hamzei-Sichani et al., 2007).

#### 2.4.2 Relation between recurrent and feedforward connectivity

What is the most efficient set of connectivities in terms of numbers of synapses used? To create an assembly of  $M$  neurons and to connect it to another assembly of the same size, we need  $M^2(p_{rc} + p_{ff})$  excitatory-to-excitatory synapses. The constraint  $\kappa = 1$  (Equation 2.7) then leads to a minimum total number of synapses at  $p_{rc} = 0$ . This result is somewhat surprising because it suggests that our proposed recurrent amplification provides a disadvantage.

However, another constraint might be even more important: to imprint an association in one-shot learning, as for example required for episodic memories, it might be an advantage to change as few synapses as possible so that one can retrieve the memory later via a replay. Therefore,  $p_{ff}$  should be low, in particular lower than the recurrent connectivity that is bound by the morphological connectivity that includes also weak or silent synapses. Minimizing  $p_{ff}$  under the constraint  $\kappa = 1$  implies, however, maximizing  $p_{rc}$ . Such large connectivities might require longer time to develop. A large  $p_{rc}$  is compatible with one-shot learning only if assemblies (that are defined by increased  $p_{rc}$  among a group of neurons) can be set up *prior* to the (feedforward) association of assemblies. Thus, episodic memories could benefit from strong preexisting assemblies. For setting up such assemblies, long time periods might be available to create new synapses and to morphologically grow synapses. Thus, we predict that for any episodic memory to be stored in one-shot learning in hippocampal networks such as CA3, a sufficiently strong representation of the events to be associated does exist *prior* to successful one-shot learning. In this case,  $p_{ff}$  (i.e., connectivity in addition to  $p_{rand}$ ) can be almost arbitrarily low. A natural lower limit is that the number of synapses per neuron  $Mp_{ff}$  is much larger than 1, say 10 as a rough estimate (in Figure 2.3 we have  $Mp_{ff} \sim 30$  for a rather low value of  $p_{rc} = p_{ff}$ , and 10 for  $p_{rc} = 0.30$ ; even 5 or more very strong synapses are sufficient in Figure 2.7). This can be interpreted in two ways: (1) Every neuron should activate several neurons in the subsequent assembly, and (2) every neuron in an assembly to be activated should receive several synapses from neurons in the previous assembly.

For example in the modeled network, for  $p_{ff} = 0.02$  and  $Mp_{ff} > 10$  we obtain  $M > 500$ , which is in agreement with an estimated optimal size of assemblies in the hippocampus (Leibold and Kempter, 2006). The total number of feedforward synapses required for imprinting an association is then  $M^2p_{ff} > 5,000$ , which is a relatively small number compared to the total number of background synapses  $(N^E)^2 p_{rand} = 4 \cdot 10^6$  for  $N^E = 20,000$  and  $p_{rand} = 0.01$ . Scaling up the network accordingly (see Section 2.5.8) to the size of a rodent CA3 network, i.e.,  $N^E = 240,000$  (a typical number for the rat hippocampus, e.g., West et al., 1991; Rapp and Gallagher, 1996), the number of new associative synapses is  $M^2p_{ff} > 17,000$ , while the total connections are more than  $0.5 \cdot 10^9$ .

To conclude, abundant recurrent connections within assemblies can decrease the feedforward connectivity required for a replay to almost arbitrary low values. Moreover, the ratio of memory synapses to background synapses decreases as the network is scaled to bigger size.

### 2.4.3 Mechanisms for assembly-sequence formation

For sequence replay, increasing the number of connections between groups has the same effect as scaling up the individual connection strengths. We conclude that structural and synaptic plasticity could play an equivalent role in the formation of assembly sequences. In the current study we have not considered plasticity mechanisms that could be mediating the formation of assembly sequences. Previous attempts of implementing a spike-timing-dependent plasticity (STDP) rule with an asymmetric temporal window (Bi and Poo, 1998; Gerstner et al., 1996; Kempter et al., 1999) in recurrent networks led to structural instabilities (Levy and Ruppin, 2000; Morrison et al., 2007; Lazar et al., 2009). However, it has been shown that under certain conditions the asymmetric STDP rule could encode sequences of connections (Jahnke et al., 2015), and moreover, maintain strong bidirectional synapses (Bush et al., 2010). More sophisticated learning rules better matched the experimentally observed plasticity protocols (Pfister and Gerstner, 2006; Clopath et al., 2010; Graupner and Brunel, 2012), and these rules combined with various homeostatic mechanisms could form Hebbian assemblies that remained stable over long time periods (Litwin-Kumar and Doiron, 2014; Sadeh et al., 2015; Zenke et al., 2015). Moreover, it has been shown that the triplet-based STDP rules (Pfister and Gerstner, 2006; Clopath et al., 2010) lead to strong bidirectional connections (Litwin-Kumar and Doiron, 2014; Sadeh et al., 2015), a network motif that has been reported in multiple brain regions (Song et al., 2005; Ko et al., 2011; Sadovsky and MacLean, 2013; Cossell et al., 2015; Guzman et al., 2016). Recent experimental work on the plasticity of the CA3-to-CA3 pyramidal cell synapses has revealed a symmetric STDP temporal curve (Mishra et al., 2016). Such a plasticity rule can be responsible for the encoding of stable assembly representations in the hippocampus.

Several plasticity rules have been successfully applied in learning sequences (Bush et al., 2010; Waddington et al., 2012; Brea et al., 2013; Kruskal et al., 2013; Jimenez Rezende and Gerstner, 2014; Scarpetta and de Candia, 2014; Jahnke et al., 2015). However, these studies focused purely on sequence replay and did not take into account its interaction with a balanced, asynchronous irregular background state.

### 2.4.4 Relations to hippocampal replay of behavioral sequences

The present model may explain the fast replay of sequences associated with the sharp-wave ripple (SWR) events, which originate in the CA3 region of the hippocampus predominantly during rest and sleep (Buzsáki, 1989). SWRs are characterized by a massive neuronal depolarization reflected in the local field potential (Csicsvari et al., 2000). Moreover, during SWRs, pyramidal cells in the CA areas fire in sequences that reflect their firing during prior awake experience (Lee and Wilson, 2002). Cells can fire in the same or in the reverse sequential order, which we refer to as forward and reverse replay, respectively (Foster and Wilson, 2006; Diba and Buzsáki, 2007). Our model, however, can not account for the slower replays that occur at near behaviour time scales during REM sleep (Louie and Wilson, 2001).

According to the two-stage model of memory trace formation (Buzsáki, 1989), the hippocampus is encoding new episodic memories during active wakefulness (stage one). Later, these memories are gradually consolidated into neocortex through SWR-associated replays (stage two). It has been proposed that acetylcholine (ACh) modulates the flow of information between the hippocampus and the neocortex and thereby mediates switches between these memory-formation stages (Hasselmo, 1999). During active wakefulness, the concentration of ACh in hippocampus is high, leading to partial suppression of excitatory glutamatergic

## 2.5 Materials and Methods

transmission (Hasselmo et al., 1995) and promoting synaptic plasticity (Halff et al., 2014). In this state, a single experience seems to be sufficient to encode representations of the immediate future in an environment (Feng et al., 2015). On the other hand, the level of ACh decreases significantly during slow-wave sleep (Marroso et al., 1995), releasing the synaptic suppression and resulting in strong excitatory feedback synapses, which suggests that this boost of recurrent and feedback connections leads to the occurrence of SWRs. In line with this hypothesis, the present model shows that increasing the synaptic strengths shifts the assembly-sequence dynamics from a no-replay regime to a spontaneous-replay regime. Also, we demonstrated that this regime supports both forward and reverse replay if assemblies are projecting symmetrically to each other and if recurrent connectivity exceeds severalfold the feedforward coupling.

Dragoi and Tonegawa (2011, 2013) showed that sequences can be replayed during SWRs also prior to the first exposure of the environment in which these sequences are represented. This finding challenges the standard framework according to which sequences are imprinted during exploration of the environment, i.e., the two-stage memory model (Buzsáki, 1989). An alternative model by Cheng (2013) proposes that the recurrent CA3 synaptic weights are relatively constant during learning, and no plasticity in CA3 is required during the formation of new memories. According to the CRISP model (Cheng, 2013), the storage of sequences is an intrinsic property of the CA3 network, and these sequences are formed offline prior to utilization due to the maturation of newly generated granule cells in the dentate gyrus. The model presented in this chapter concerns the storage of sequences in a recurrent network and is not in contradiction with the idea of preexisting sequences.

Our model deploys a single uniform inhibitory population which is, likely, an oversimplification of cortical and subcortical networks that are rich in expressing various interneuron types (Klausberger and Somogyi, 2008; Kullmann, 2011). However, the roles of the different inhibitory neurons during various brain states, and in particular, during SWRs are not well known. Strong candidates for interneurons that might be balancing the run-away excitation during SWR replay are the basket cells due to their fast dynamics and strong synapses. Moreover, they are one of the most active inhibitory neurons during SWRs. OLM cells with their slower input on the distal dendrites are good candidates for priming which assemblies/sequence might be replayed prior to the event.

In summary, a prediction of our assembly-sequence model is that prior to being able to store and recall a memory trace that connects events, strong enough representations of events in recurrently connected assemblies are necessary because recalling a minute memory trace requires amplification within assemblies. Another prediction of this model is based on the fact that the network is in an asynchronous-irregular state during the time intervals between replays. Hence, by increasing the activity of the excitatory neurons or by disinhibiting the network, e.g., by decreasing the activity of the interneuron population specialized in keeping the balance, one could increase the rate of spontaneous replays. Such disinhibition might explain the counter-intuitive observation that SWRs can be evoked by the activation of interneurons (Ellender et al., 2010; Schlingloff et al., 2014). Our model thus links a diverse set of experimental results on the cellular, behavioral, and systems level of neuroscience on memory retrieval and consolidation (Diekemann and Born, 2010).

## 2.5 Materials and Methods

The network simulations as well as the data analyses were performed in Python ([www.python.org](http://www.python.org)). The neural network was implemented in Brian (Goodman and Brette, 2009). For managing

## 2 Memory replay in balanced recurrent networks

the simulation environment and data processing, we used standard Python libraries such as NumPy, SciPy, Matplotlib, and SymPy.

### 2.5.1 Neuron model

Neurons are described by a conductance-based leaky integrate-and-fire model, where the subthreshold membrane potential  $V_i(t)$  of cell  $i$  obeys

$$C \frac{dV_i}{dt} = G^{\text{leak}}(V^{\text{rest}} - V_i) + G_i^E(V^E - V_i) + G_i^I(V^I - V_i) + I^{\text{ext}}. \quad (2.2)$$

The cells' resting potential is  $V^{\text{rest}} = -60$  mV, its capacitance is  $C = 200$  pF, and the leak conductance is  $G^{\text{leak}} = 10$  nS, resulting in a membrane time constant of 20 ms in the absence of synaptic stimulation. The variables  $G_i^E$  and  $G_i^I$  are the total synaptic conductances describing the time-dependent synaptic inputs to neuron  $i$ . The excitatory and inhibitory reversal potentials are  $V^E = 0$  mV and  $V^I = -80$  mV, respectively.  $I^{\text{ext}} = I^{\text{const}} + I^x$  is an externally applied current. To evoke activity in the network, a constant external current  $I^{\text{const}} = 200$  pA is injected into each neuron, which evokes a regular, intrinsically oscillating activity in the neuron, if considered in isolation. However, embedding such neurons in random recurrent networks can lead to irregular activity, as outlined below in the following two subsections. Only if explicitly stated (e.g., Figures 2.5 and 2.8), small additional current inputs  $I^x$  are applied to excitatory or inhibitory neurons, which we denote as  $I^e$  and  $I^i$ , respectively. As the membrane potential  $V_i$  reaches the threshold  $V^{\text{th}} = -50$  mV, neuron  $i$  emits an action potential, and the membrane potential  $V_i$  is reset to the resting potential  $V^{\text{rest}}$  for a refractory period  $\tau_{\text{rp}} = 2$  ms.

The dynamics of the conductances  $G_i^E$  and  $G_i^I$  of a postsynaptic cell  $i$  are determined by the spiking of the excitatory and inhibitory presynaptic neurons. Each time a presynaptic cell  $j$  fires, the synaptic input conductance of the postsynaptic cell  $i$  is increased by  $g_{ij}^E$  for excitatory synapses and by  $g_{ij}^I$  for inhibitory synapses. The input conductances decay exponentially with time constants  $\tau^E = 5$  ms and  $\tau^I = 10$  ms. The dynamics of the total excitatory conductance is described by

$$\frac{dG_i^E(t)}{dt} = \frac{-G_i^E(t)}{\tau^E} + \sum_{j,f} g_{ij}^E \delta(t - t_j^{(f)}). \quad (2.3)$$

Here the sum runs over the presynaptic projections  $j$  and over the sequence of spikes  $f$  from each projection. The time of the  $f^{\text{th}}$  spike from neuron  $j$  is denoted by  $t_j^{(f)}$ , and  $\delta$  is the Dirac delta function. The inhibitory conductance  $G_i^I$  is described analogously.

Amplitudes of recurrent excitatory conductances and excitatory conductances on inhibitory neurons are denoted with  $g_{ij}^E$  and  $g_{ij}^{IE}$ , respectively. If not stated otherwise, all excitatory conductance amplitudes are fixed and equal ( $g_{ij}^E = g_{ij}^{IE} = g^E = 0.1$  nS), which results in EPSPs with an amplitude of  $\approx 0.1$  mV at resting potential. The recurrent inhibitory synapses are also constant ( $g_{ij}^I = 0.4$  nS) while the inhibitory-to-excitatory conductances  $g_{ij}^{EI}$  are variable (see below). Irrespectively of the synaptic type, the delay between a presynaptic spike and a postsynaptic response onset is always 2 ms.

### 2.5.2 Network model

The modeled network consists of  $N^E = 20,000$  excitatory and  $N^I = 5,000$  inhibitory neurons. Our results do not critically depend on the network size (see Section “Scaling the network size” below). Initially, all neurons are randomly connected with a sparse probability  $p_{\text{rand}} = 0.01$ .

A cell assembly is defined as a group of recurrently connected excitatory and inhibitory neurons (Figure 2.1A). The assembly is formed by picking  $M$  excitatory and  $M/4$  inhibitory neurons from the network; every pair of pre- and post-synaptic neurons within the assembly is randomly connected with probability  $p_{\text{rc}}$ . The new connections are created independently and in addition to the already existing ones. Thus, if by chance two neurons have a connection due to the background connectivity and are connected due to the participation in an assembly, then the synaptic weight between them is simply doubled. Unless stated otherwise, assemblies are hence formed by additional connections rather than stronger synapses.

In the random network, we embed 10 non-overlapping assemblies with size  $M = 500$  if not stated otherwise. The groups of excitatory neurons are connected in a feedforward fashion, and a neuron from one group projects to a neuron of the subsequent group with probability  $p_{\text{ff}}$  (Figure 2.1B). Such a feedforward connectivity is reminiscent of a synfire chain. However, classical synfire chains do not have recurrent connections ( $p_{\text{rc}} = 0, p_{\text{ff}} > 0$ ), while here, neurons within a group are recurrently connected even beyond the random background connectivity ( $p_{\text{rc}} > 0, p_{\text{ff}} > 0$ ). We will refer to such a sequence as an “assembly sequence”. By varying the connectivity parameters  $p_{\text{rc}}$  and  $p_{\text{ff}}$ , the network structure can be manipulated to obtain different network types (Figure 2.1C). In the limiting case where feedforward connections are absent ( $p_{\text{rc}} > 0, p_{\text{ff}} = 0$ ) the network contains only largely disconnected Hebbian assemblies. In contrast, in the absence of recurrent connections ( $p_{\text{rc}} = 0, p_{\text{ff}} > 0$ ), the model is reduced to a synfire chain embedded in a recurrent network. Structures with both recurrent and feedforward connections correspond to Hebbian assembly sequences.

To keep the network structure as simple as possible and to be able to focus on mechanisms underlying replay, we use non-overlapping assemblies and we do not embed more than 10 groups. Nevertheless, additional simulations with overlapping assemblies and longer sequences indicate that our approach is in line with previous results on memory capacity (Leibold and Kempter, 2006, 2008; Trengove et al., 2013). Advancing the theory of memory capacity is, however, beyond the scope of this chapter.

### 2.5.3 Balancing the network

A naive implementation of the heterogeneous network as described above leads, in general, to dynamics characterized by large population bursts of activity. To overcome this epileptiform activity and ensure that neurons fire asynchronously and irregularly (AI network state), the network should operate in a balanced regime. In the balanced state, large excitatory currents are compensated by large inhibitory currents, as shown *in vivo* (Okun and Lampl, 2008; Cafaro and Rieke, 2010) and *in vitro* (Xue et al., 2014). In this regime, fluctuations of the input lead to highly irregular firing (van Vreeswijk and Sompolinsky, 1996, 1998), a pattern observed in the cortex (Abeles, 1991; Softky and Koch, 1993) as well as in the hippocampus during non-REM sleep (Csicsvari et al., 1999; Poe et al., 2010).

Several mechanisms were proposed to balance numerically simulated neural networks. One method involves structurally modifying the network connectivity to ensure that neurons receive balanced excitatory and inhibitory inputs (Renart et al., 2007; Roudi and Latham,

## 2 Memory replay in balanced recurrent networks

2007). It was shown that a short-term plasticity rule (Tsodyks and Markram, 1997) in a fully connected network can also adjust the irregularity of neuronal firing (Barbieri and Brunel, 2008).

Here, we balance the network using the inhibitory-plasticity rule (Vogels et al., 2011). All inhibitory-to-excitatory synapses are subject to a spike-timing-dependent plasticity (STDP) rule where near-coincident pre- and postsynaptic firing potentiates the inhibitory synapse while presynaptic spikes alone cause depression. A similar STDP rule with a symmetric temporal window was recently reported in the layer 5 of the auditory cortex (D’Amour and Froemke, 2015).

To implement the plasticity rule in a synapse, we first assign a synaptic trace variable  $x_i$  to every neuron  $i$  such that  $x_i$  is incremented with each spike of the neuron and decays with a time constant  $\tau_{\text{STDP}} = 20 \text{ ms}$ :

$$x_i \rightarrow x_i + 1, \text{ if neuron } i \text{ fires,}$$

$$\tau_{\text{STDP}} \frac{dx_i}{dt} = -x_i, \text{ otherwise.}$$

The synaptic conductance  $g_{ij}^{EI}(t)$  from inhibitory neuron  $j$  to excitatory neuron  $i$  is initialized with value  $g_0^I = 0.4 \text{ nS}$  and is updated at the times of pre/post-synaptic events:

$$g_{ij}^{EI} = g_{ij}^{EI} + \eta(x_i - \alpha), \text{ for a presynaptic spike in neuron } j,$$

$$g_{ij}^{EI} = g_{ij}^{EI} + \eta x_j, \text{ for a postsynaptic spike in neuron } i$$

where  $0 < \eta \ll 1$  is the learning-rate parameter, and the bias  $\alpha = 2\rho_0\tau_{\text{STDP}}$  is determined by the desired firing rate  $\rho_0$  of the excitatory postsynaptic neurons. In all simulations,  $\rho_0$  has been set to 5 spikes/sec, which is at the upper bound of the wide range of rates that were reported in the literature: e.g., 1 – 3 spikes/sec in Csicsvari et al. (2000); 3 – 6 spikes/sec in Kowalski et al. (2015); 1 – 76 spikes/sec in Felsen et al. (2005); 0.43 – 3.60 spikes/sec in Cheng and Ji (2013); 1 – 11 spikes/sec in English et al. (2014).

Existence of background connections and an implementation of the described inhibitory STDP rule drives typically the network into a balanced AI state. The excitatory and the inhibitory input currents balance each other and keep the membrane potential just below threshold while random fluctuations drive the firing (Figure 2.2A, B). The specific conditions to be met for a successful balance are discussed in the Results section. Similar effects could be achieved also in the absence of random background connections when input with appropriate noise fluctuations is applied to the neurons. We find this scenario, however, less realistic as neurons would be largely disconnected.

In the AI network regime, any perturbation to the input of an assembly will lead to a transient perturbation in the firing rate of the neurons within it. In the case of strong recurrent connections within the assembly, a small excitatory perturbation will lead to a stronger firing of both the excitatory as well as the inhibitory neurons. This amplification of input fluctuations into larger activity fluctuations is, unlike the Hebbian amplification, fast and does not show slowing of the activation dynamics for large connectivities. This phenomenon of transient pattern completion is known as balanced amplification (Murphy and Miller, 2009), where it is essential that each assembly has excitatory and inhibitory neurons and strong recurrent connectivity. Another advantage of the inhibitory subpopulations is the rapid negative feedback that can lead to enhanced memory capacity of the network

(Kammerer et al., 2013).

#### 2.5.4 Simulations and data analysis

Each network simulation consists of 3 main phases:

**1. Balancing the network.** Initially, the population activity is characterized by massive population bursts with varying sizes (avalanches). During a first phase, the network (random network with embedded phase sequence) is balanced for 50 seconds with decreasing learning rate ( $0.005 \geq \eta \geq 0.00001$ ) for the plasticity on the inhibitory-to-excitatory synapses. During this learning, the inhibitory plasticity shapes the activity, finally leading to AI firing of the excitatory population. Individual excitatory neurons then fire roughly with the target firing rate of 5 spikes/sec, while inhibitory neurons have higher firing rates of around 20 spikes/sec, which is close to rates reported in the hippocampus (Csicsvari et al., 2000; Cheng and Ji, 2013). After 50 seconds simulation time, the network is typically balanced.

**2. Reliability and quality of replay.** In a second phase, the plasticity is switched off to be able to probe an unchanging network with external cue stimulations. All neurons from the first group/assembly are simultaneously stimulated by an external input so that all neurons fire once. The stimulation is mimicked by adding an excitatory conductance in Equation 2.3 ( $g_{max} = 3 \text{ nS}$ ) that is sufficient to evoke a spike in each neuron. For large enough connectivities ( $p_{rc}$  and  $p_{ff}$ ), the generated pulse packet of activity propagates through the sequence of assemblies, resulting in a replay. For too small connectivities, the activity does not propagate. For excessively high connectivities, the transient response of one group results in a burst in the next group and even larger responses in the subsequent groups, finally leading to epileptiform population bursts of activity (Figure 2.3).

To quantify the propagation from group to group and to account for abnormal activity, we introduce a quality measure of replay. The activity of a group is measured by calculating the population firing rate of the underlying neurons smoothed with a Gaussian window of 2 ms width. We extract peaks of the smoothed firing rate that exceed a threshold of 30 spikes/sec. A group is considered to be activated at the time at which its population firing rate hits its maximum and is above the threshold rate. Activity propagation from one group to the next is considered to be successful if one group activates the next one within a delay between 2 and 20 ms. A typical delay is about 5 ms, but in the case of extremely small  $p_{ff}$  and large  $p_{rc}$  the time of propagation can take  $\sim 15$  ms. Additional rules are imposed to account for exceeding activity and punish replays that lead to run-away firing. First, if the activity of an assembly exceeds a threshold of 180 spikes/sec (value is chosen manually for best discrimination), the group is considered as bursting, and thus, the replay is considered as failed. Second, if the assembly activity displays 2 super-threshold peaks that succeed each other within 30 ms, the replay is unsuccessful. Third, a “dummy group” (of size  $M$ ) from the background neurons is used as a proxy for detecting activations of the whole network. In case that the dummy group is activated during an otherwise successful replay, the replay is failed. Thus, for each stimulation the “quality of replay” has a value of 1 for successful and a value of 0 for unsuccessful replays. The quality of replay for each set of parameters (Figure 2.3) is an average from multiple ( $\gtrsim 5$ ) stimulations of 5 different realizations of each network.

Additionally, we test the ability of the assembly sequence to complete a pattern by stimulating only a fraction of the neurons in the first group (Figure 2.4). Analogously to the full stimulation, the quality of replay is measured.

**3. Spontaneous activity.** In the last phase of the simulations, no specific input is

## 2 Memory replay in balanced recurrent networks

applied to the assemblies. As during the first phase of the simulation, the network is driven solely by the constant-current input  $I^{\text{const}} = 200 \text{ pA}$  applied to each neuron, and plasticity is switched off.

During this state, we quantify spontaneous replay (Figure 2.5). Whenever the last assembly is activated and if this activation has propagated through at least three previous assemblies, we consider this event as a spontaneous replay. Here, we apply the quality measure of replay, where bursty replays are disregarded. Additionally, we quantify the dynamic state of the network by the firing rate, the irregularity of firing, and the synchrony of a few selected groups from the sequence. The irregularity is measured as the average coefficient of variation of inter-spike intervals of the neurons within a group. As a measure of synchrony between 2 neurons, we use the cross-correlation coefficient of their spike trains binned in 5-ms windows. The group synchrony is the average synchrony between all pairs of neurons in a group.

### 2.5.5 Estimating response times of neurons and the network

How quickly do the neurons that receive a synchronous pulse packet react during a replay? Following the arguments of Diesmann et al. (1999), the response time is not determined by the membrane time constant of the neuron, but rather by the time it takes the neurons to reach threshold in response to the pulse packet. An analytical calculation can hence be obtained by considering the membrane potential dynamics in Equation 2.2. Let us assume that a neuron is at some initial voltage  $V_0$ . How fast does the neuron reach the threshold voltage when an external excitatory conductance  $G^{\text{inj}}$  is applied to the membrane? We can express the membrane potential  $V(t)$  explicitly:

$$V = (V_0 - V^*) \exp^{-\frac{t}{\tau^*}} + V^*$$

where the “driving” voltage is

$$V^* = \frac{G^{\text{leak}}V^{\text{rest}} + G^E V^E + G^I V^I + I^{\text{ext}} + G^{\text{inj}} V^E}{G^{\text{leak}} + G^E + G^I + G^{\text{inj}}}$$

and the time constant is

$$\tau^* = \frac{G^{\text{leak}}}{G^{\text{leak}} + G^E + G^I + G^{\text{inj}}} \tau_m .$$

Here,  $\tau_m = C/G^{\text{leak}} = 20 \text{ ms}$  is the leak time constant from Equation 2.2. The time that is needed for a neuron with initial membrane potential  $V_0$  to reach the voltage threshold  $V^{\text{th}}$  is:

$$t^{\text{AP}} = \tau^* \log \left( \frac{V_0 - V^*}{V^{\text{th}} - V^*} \right) .$$

Substituting with parameter values corresponding to the simulations ( $G^E = 0.6 \text{ nS}$ ,  $G^I = 5 \text{ nS}$ ,  $G^{\text{leak}} = 10 \text{ nS}$ ,  $G^{\text{inj}} = 3 \text{ nS}$ ,  $V_0 = -51 \text{ mV}$ ), we obtain  $t^{\text{AP}} = 1.4 \text{ ms}$ . Here, for  $G^{\text{inj}}$  we use a typical value of the peak excitatory conductance during a replay.

We also measured the activation time of the assemblies during pulse propagation in the simulated balanced network. A stimulation with step conductance  $G^{\text{inj}}$  applied to a group of random neurons leads to a fast increase in firing rates (20%-to-80% rise time is 1 ms).

In summary, in agreement with the literature (Gerstner, 1995; van Vreeswijk and Sompolinsky, 1996, 1998), the response time of the modeled network is indeed fast, i.e., faster

## 2.5 Materials and Methods

than the membrane time constant  $\tau_m = 20$  ms and the inter-spike interval (ISI  $\sim 12$  ms when  $G^{\text{inj}}$  is injected).

### 2.5.6 Estimating conditions for successful replay

An analytical description of conditions for successful replay is not easy to obtain. The most appropriate ansatz would be a generalization of the pulse-packet description of Goedeke and Diesmann (2008), which is unfortunately not trivial and beyond the scope of this paper. Instead, we choose a phenomenological approach and portray the network dynamics during replay by a linear dynamical system, which could be thought of as a linearization of a more accurate model. This ansatz allows to estimate a lower bound for the connectivities required for a successful replay.

The dynamics of an assembly  $i$  (Figure 2.1A, B) in the AI state is approximated by two differential equations:

$$\begin{aligned} \tau \frac{dr_i^E}{dt} &= -r_i^E + w_{\text{rc}} r_i^E - k w_{\text{rc}} r_i^I + \xi_i^E(t) \\ \tau \frac{dr_i^I}{dt} &= -r_i^I + w_{\text{rc}} r_i^E - k w_{\text{rc}} r_i^I \end{aligned} \quad (2.4)$$

where  $r_i^E$  and  $r_i^I$  are the deviations of the population firing rates of the excitatory (E) and inhibitory (I) populations from the spontaneous firing rates  $r_0^E$  and  $r_0^I$ , respectively. The parameter  $w_{\text{rc}}$  and the term  $-k w_{\text{rc}}$  represent the respective strengths of the excitatory and the inhibitory recurrent projections. The constant  $k$  describes the relative strength of the recurrent inhibition vs. excitation; for a balanced network, we assume that inhibition balances or dominates excitation, e.g.,  $k \geq 1$ . The weight  $w_{\text{rc}}$  is proportional to the average number  $M p_{\text{rc}}$  of recurrent synapses a neuron receives, and proportional to the synaptic strength  $g^E$ . The function  $\xi_i^E$  describes the external input to the assembly from the rest of the network. In this mean-field analysis, we neglect the influence of the noise on the network dynamics. Activities  $r_i^E$  and  $r_i^I$  are assumed to approach the steady state 0 with a time constant  $\tau$ . Based on the discussion in the previous subsection, we assume this time constant to be much faster than the membrane time constant.

The excitatory assemblies are sequentially connected, and we denote the strength of the feedforward projections as  $w_{\text{ff}}$ . The feedforward drive can be represented as an external input to an assembly:

$$\xi_i^E = w_{\text{ff}} r_{i-1}^E, \text{ for } i > 1.$$

Taking into account the feedforward input to population  $i$  from the preceding excitatory population  $i - 1$ , Equation 2.4 can be rewritten as

$$\tau \frac{d\mathbf{r}_i}{dt} = \begin{pmatrix} -1 + w_{\text{rc}} & -k w_{\text{rc}} \\ w_{\text{rc}} & -1 - k w_{\text{rc}} \end{pmatrix} \mathbf{r}_i + \begin{pmatrix} w_{\text{ff}} r_{i-1}^E \\ 0 \end{pmatrix}, \text{ for } i > 1 \quad (2.5)$$

where  $\mathbf{r}_i = \begin{pmatrix} r_i^E \\ r_i^I \end{pmatrix}$  is the 2-dimensional vector of firing rates in group  $i$ .

Assuming that the time duration of a pulse packet in group  $i - 1$  is much longer than the population time constant  $\tau$  in group  $i$ , we consider the solution of the stationary state ( $\tau \frac{d\mathbf{r}_i}{dt} = 0$ ) as an adequate approximation. By setting the left-hand side of Equation 2.5 to

## 2 Memory replay in balanced recurrent networks

zero, we can express the firing rate  $r_i^E$  as a function of  $r_{i-1}^E$ :

$$r_i^E = \left[ \frac{1 + kw_{rc}}{1 + (k - 1)w_{rc}} \right] w_{ff} r_{i-1}^E = \kappa r_{i-1}^E, \quad (2.6)$$

where  $\kappa$  is the “effective feedforward connectivity”.

Interestingly, the recurrent connections effectively scale up the efficiency of the feedforward connections and facilitate the propagation of activity. Assuming that  $(k - 1)w_{rc} \ll 1$ , that is, either small recurrent connectivity  $w_{rc}$  or an approximately balanced state  $k \approx 1$ , we can linearize in  $w_{rc}$ :

$$\kappa \approx w_{ff}(1 + w_{rc}). \quad (2.7)$$

For small  $\kappa$ , i.e.  $\kappa \ll 1$ , even large changes of the firing rate in group  $i - 1$  do not alter the rate in group  $i$ . For  $\kappa < 1$ , the pulse packet will steadily decrease while propagating from one group to another as  $r_i^E < r_{i-1}^E$ . On the other hand, if  $\kappa = 1$ , the propagation of a pulse packet is expected to be marginally stable. In the case of  $\kappa > 1$ , any fluctuation of firing rate in one assembly will lead to a larger fluctuation in the following assembly.

To connect the analytical calculations to the numerical simulations, we again note that a total connection strength is proportional to the number of inputs a neuron is receiving (e.g., the product of group size  $M$  and connection probability) and proportional to the synaptic strength:

$$w_{rc} = c M p_{rc} g^E \text{ and } w_{ff} = c M p_{ff} g_{ff}^E, \quad (2.8)$$

where  $M$  is the group size, and  $p_{rc}$  and  $p_{ff}$  are the recurrent and feedforward connectivities, respectively.  $g^E$  is the conductance of an excitatory recurrent synapse within a group, and  $g_{ff}^E$  is the conductance of feedforward synapses between groups. Unless stated otherwise, we assume  $g_{ff}^E = g^E$ . The parameter  $c$  is related to the slope of the neurons’ input-output transfer function, but given the phenomenological nature of the theoretical treatment, an accurate *ab initio* calculation of  $c$  is non-trivial. Instead, we use it as a fitting parameter. Using the critical value  $\kappa(p_{rc} = 0.08, p_{ff} = 0.04) = 1$  extracted from the simulation results (Figure 2.3), we find  $c = 0.25 \text{ nS}^{-1}$ . This value of  $c$  is used in all further analytical estimations for the effective connectivity  $\kappa$ .

In summary, the lower bound for the connectivities for a successful replay can be described as

$$p_{rc} = \frac{1}{cMg^E} \left( \frac{1}{cMp_{ff}g_{ff}^E} - 1 \right),$$

which is represented as a black line in Figures 2.3 and 2.5. For Figures 2.6 and 2.7, the black line is calculated analogously using the same constant  $c = 0.25 \text{ nS}^{-1}$ .

### 2.5.7 Calculating the slope $c$

In the previous section, the constant  $c$  was manually fitted to a value of  $0.25 \text{ nS}^{-1}$  to match analytical and numerical results. Here we express  $c$  analytically by utilizing a non-linear neuronal model and by using the parameter values from the simulations.

The resting firing rate  $\rho$  of a neuronal population that is in an asynchronous irregular (AI) regime can be expressed as a function of the mean  $\mu$  and the standard deviation  $\sigma$  of the membrane potential distribution (Ricciardi, 1977; Amit and Brunel, 1997; Brunel, 2000; Gerstner and Kistler, 2002):

$$\mu = \sum_k J_k \rho_k$$

## 2.5 Materials and Methods

$$\sigma = \sqrt{\sum_k J_k^2 \rho_k} , \quad (2.9)$$

where the sums over  $k$  run over the different synaptic contributions,  $\rho_k$  is the corresponding presynaptic firing rate, and  $J_k$  and  $J_k^2$  are the integrals over time of the PSP and the square of the PSP from input  $k$ , respectively. Here PSPs are estimated for the conductance-based integrate-and-fire neuron from Equation 2.2 for voltage values near the firing threshold  $V^{\text{th}}$ ,

$$J_k = \int_t \text{PSP}(t) dt = \tau^{\text{syn}}(V^{\text{syn}} - V^{\text{th}}) \frac{g_k^{\text{syn}}}{G^{\text{leak}}}$$

$$J_k^2 = \int_t \text{PSP}^2(t) dt = \frac{(\tau^{\text{syn}} g_k^{\text{syn}} (V^{\text{syn}} - V^{\text{th}}))^2}{2(\tau + \tau^{\text{syn}}) (G^{\text{leak}})^2},$$

where  $\tau$  is the membrane time constant,  $\tau^{\text{syn}}$  is the synaptic time constant,  $V^{\text{syn}}$  is the synaptic reversal potential, and  $g_k^{\text{syn}}$  is the synaptic conductance of connection  $k$ . Connections can be either excitatory or inhibitory.

Here we consider a network with random connections only, and look at a subpopulation of size  $M$ , where  $M \ll N^E$ . For a more convenient analytical treatment, the recurrent connections within the group are neglected. This assumption does not affect the estimation of the transfer function slope, as  $c$  is independent on the type of inputs. The firing rate-fluctuations of the neuronal group are calculated as in Equation 2.6:

$$r = c M g^E r_{\text{ext}}. \quad (2.10)$$

The membrane potential of an excitatory neuron from this subpopulation has several contributions:  $N^E p_{\text{rand}}$  excitatory inputs with firing rate  $\rho_0$  and efficacy  $J^E$ ; inhibitory inputs due to the background connectivity:  $N^I p_{\text{rand}} J^{EI} \rho_0^I$ ; injected constant current:  $I^{\text{ext}}/G^{\text{leak}}$ ; and input from an external group:  $M_{\text{ext}} J_{\text{ext}}^E \rho_{\text{ext}}$ . In summary, we find:

$$\mu = N^E p_{\text{rand}} J^E \rho_0 + N^I p_{\text{rand}} J^{EI} \rho_0^I + M_{\text{ext}} J_{\text{ext}}^E \rho_{\text{ext}} + \frac{I^{\text{ext}}}{G^{\text{leak}}}.$$

The standard deviation of the membrane potential is then, accordingly:

$$\sigma^2 = N^E p_{\text{rand}} J^{E^2} \rho_0 + N^I p_{\text{rand}} J^{EI^2} \rho_0^I + M_{\text{ext}} J_{\text{ext}}^{E^2} \rho_{\text{ext}}.$$

In the case of uncorrelated inputs, the following approximation can be used for the firing rate estimation (Ricciardi, 1977; Amit and Brunel, 1997; Brunel, 2000; Gerstner and Kistler, 2002):

$$\rho = \left( \tau_{\text{rp}} + \tau \sqrt{\pi} \int_{\frac{V^{\text{rest}} - \mu}{\sigma}}^{\frac{V^{\text{th}} - \mu}{\sigma}} e^{u^2} (1 + \text{erf}(u)) du \right)^{-1}, \quad (2.11)$$

where  $\tau_{\text{rp}}$  is the refractory period, and  $V^{\text{th}}$  and  $V^{\text{rest}}$  are membrane threshold and reset potential, respectively (see also section “Neural Model”).

To find the constant  $c$  used in the linear model, we estimate the firing rate  $\rho$  from Equation 2.11 and substitute in Equation 2.10, assuming a linear relation between firing-

## 2 Memory replay in balanced recurrent networks

rate fluctuations:

$$\rho(\rho_{\text{ext}}) - \rho_0 = cM_{\text{ext}}g^E(\rho_{\text{ext}} - 0), \quad (2.12)$$

and find:

$$c = \frac{\rho(\rho_{\text{ext}}) - \rho_0}{cM_{\text{ext}}g^E\rho_{\text{ext}}}. \quad (2.13)$$

Before calculating the constant  $c$  according to the method presented above, a preliminary step needs to be taken. As we set the firing rate of the excitatory population in the network to a fixed value  $\rho_0 = 5$  spikes/sec, there are two variables remaining unknown: the firing rate of the inhibitory population  $\rho_0^I$  and the inhibitory-to-excitatory synaptic conductance  $g_{\text{rand}}^{EI}$  that changes due to synaptic plasticity. Therefore, we first solve a system of 2 equations for the firing rates of the excitatory and the inhibitory populations expressed as in Equation 2.11. Once the unknowns  $\rho_0^I$  and  $g_{\text{rand}}^{EI}$  are calculated, we can estimate  $\rho(\rho_{\text{ext}})$  and  $c$  according to the method presented above. We note that the analytically calculated values of  $g_{\text{rand}}^{EI}$  and  $\rho_0^I$  match the measured values in the simulations.

The value we get after applying the above mentioned method for estimation of  $c$  is  $0.13 \text{ nS}^{-1}$ . The fit corresponding to the estimate of  $c$  is shown in Figure 2.3 with a white dashed line. It is worth noting that a slightly more involved calculation relying on the estimate  $c = \frac{1}{Mg} \frac{\partial r}{\partial r_{\text{ext}}}$  gives a similar result, concretely  $c = 0.11 \text{ nS}^{-1}$ .

Although the analytically calculated value  $c$  is a factor of 2 smaller than the manual fit  $c = 0.25 \text{ nS}^{-1}$ , it is in the same order of magnitude and not too far from describing the results for critical connectivity from the simulations.

The method applied above finds the slope of the transfer function for stationary firing rates. However, the spiking network replay is a fast and brief event, where a transient input in one assembly evokes a transient change in the output firing rate. The value discrepancy suggests that the transfer function of transients is even steeper than at the resting AI state.

### 2.5.8 Scaling the network size

So far we have been dealing with networks of fixed size  $N^E = 20,000$  neurons. How does the network size affect the embedding of assembly sequences? Is it possible to change the network size but keep the assembly size fixed?

Scaling the network size while keeping the connectivity  $p_{\text{rand}}$  constant leads to a change in the number of inputs that a neuron receives, and therefore, affects the membrane potential distributions. To compare replays in networks with different sizes  $N^E$  but identical  $M$ , we need to assure that the signal-to-noise ratio is kept constant, and the easiest way is to keep both the signal and the noise constant, which requires to change connectivities  $p_{\text{rc}}$  and  $p_{\text{ff}}$  and conductances.

While scaling the network from the default network size  $N^E = 20,000$  to a size  $\tilde{N}^E = \gamma N^E$ , we see that the noise  $\sigma$  scales as  $\sim g\sqrt{\gamma N^E}$  (Equation 2.9). To keep the input current fluctuations constant as we change  $\tilde{N}^E$ , all synaptic conductances are rescaled with a factor of  $1/\sqrt{\gamma}$ :  $\tilde{g} = g/\sqrt{\gamma}$  (van Vreeswijk and Sompolinsky, 1996). However, such a synaptic scaling leads to a change in the coupling between assemblies of fixed size  $M$ , which is proportional to the conductance. Therefore, the connectivities  $p_{\text{rc}}$  and  $p_{\text{ff}}$  are scaled with  $\sqrt{\gamma}$  to compensate the conductance decrease, leading to a constant coupling ( $cM\tilde{p}_{\text{rc}}\tilde{g}^E = cMp_{\text{rc}}g^E$  and  $cM\tilde{p}_{\text{ff}}\tilde{g}^E = cMp_{\text{ff}}g^E$ ), and hence, a constant signal-to-noise ratio.

What is the impact of such a scaling on the network capacity to store sequences? The number of connections needed to store a sequence is changed by a factor  $\sqrt{\gamma}$  as we change

## 2.5 Materials and Methods

$p_{rc}$  and  $p_{ff}$ . However, the number of background connections to each neuron is scaled with  $\gamma$ , resulting in sparser memory representations in larger networks. More precisely, for a neuron participating in the sequence, the ratio of excitatory memory connections to the total number of excitatory connections is

$$u = \frac{(p_{rc} + p_{ff})\sqrt{\gamma}M}{(p_{rc} + p_{ff})\sqrt{\gamma}M + p_{rand}\gamma N^E}.$$

Therefore, the proportion of connections needed for an association is scaled as  $1/\sqrt{\gamma}$  for  $\tilde{N}^E \gg M$ . To give a few numbers,  $u$  is equal to 0.23 for  $\tilde{N}^E = 20,000$ , and  $u = 0.09$  for  $\tilde{N}^E = 180,000$ . Other parameter values are:  $M = 500$ ,  $p_{rc} = p_{ff} = 0.06$ ,  $p_{rand} = 0.01$ .

The chosen scaling rule is applicable for networks of simpler units such as binary neurons or current-based integrate-and-fire neurons (Amit and Brunel, 1997; van Vreeswijk and Sompolinsky, 1998). This scaling is not valid in a strict mathematical framework for very large networks ( $\tilde{N}^E \rightarrow \infty$ ) consisting of conductance-based integrate-and-fire neurons (see Renart et al. (2007) for a detailed discussion). Simulations results, however, reveal that replays are possible in network sizes up to  $2 \cdot 10^5$  neurons.



# 3 Modulation of sharp-wave incidence

## 3.1 Summary

Recent *in vitro* studies have demonstrated that sharp-wave ripple events can be evoked after optogenetic stimulation of a parvalbumin-positive interneuron subpopulation (Schlingloff et al., 2014; Kohus et al., 2016). The 2-population model described in the previous chapter cannot explain this phenomenon. In this chapter, a 3-population model is discussed in detail as a hypothetical disinhibitory circuit that can generate the population bursts in the CA areas of the hippocampus. The main theme addressed here is how the GABAergic transmission modulates the incidence of sharp-wave ripple events. In particular, it is unknown how gabazine, a GABA<sub>A</sub> receptor antagonist, suppresses the generation of sharp-wave ripples. Analyzing data from *in-vitro* recordings and dissecting the 2-population model *in silico* and analytically gives a few possible explanation of the gabazine effect. The results are interpreted in the light of the proposed circuit. Another question explored here is whether the slow dynamics of GABA<sub>B</sub> receptors is modulating the long time scale of the inter-event intervals, that is in the order of hundreds of milliseconds to tens of seconds.

## 3.2 Introduction

Sharp-wave ripples (SWRs) are network events in the hippocampus that involve large numbers of cells that fire in synchrony within a time window of  $\sim 20 - 100$  ms (Buzsáki, 2015). During SWRs *in vivo*, principal neurons can fire in a temporal order that reflects the behaviour sequences from previous (Lee and Wilson, 2002) or future episodes (Dragoi and Tonegawa, 2011). Such replays are important for the consolidation of newly formed memories (Girardeau et al., 2009). Despite the concentrated effort and the progress in studying SWRs, some basic understanding of the emergence and the development of these events is still lacking. Therefore, *in-vitro* models have been developed to facilitate the study of this peculiar phenomenon (Maier et al., 2003). In particular, *in-vitro* preparations provide a better experimental control over the hippocampal circuit generating SWRs, e.g., facilitation of recording and imaging, isolation of specific microcircuits, pharmacological manipulation of substances, etc.

In this introduction, I review some general facts from the literature concerning the generation of SWRs. Because of the importance of inhibition (e.g., Maier et al., 2003; Schlingloff et al., 2014), I start with a brief overview of the main characteristics of the GABAergic neurons and the types of synapses they form in the hippocampus. In the following I will provide a brief discussion on some pharmacological substances that modulate the incidence of spontaneous SWRs *in vitro*. The last section of this introduction is dedicated to a hypothetical 3-population network model that can explain some of the more counterintuitive findings reported in the literature.

### 3 Modulation of sharp-wave incidence

#### 3.2.1 Inhibitory transmission in the hippocampus

$\gamma$ -Aminobutyric acid (GABA) is the main inhibitory neurotransmitter in the central neural system (Sivilotti and Nistri, 1991). GABA is produced by inhibitory neurons (INs) and stored in vesicles at the presynaptic terminals. GABA is released spontaneously or after a presynaptic neuronal action potential (AP). The action of GABA at the synapses is terminated by uptake mechanisms from the presynaptic side or from the surrounding glial cells. There are two major classes of receptors that are sensitive to the released GABA: GABA<sub>A</sub> and GABA<sub>B</sub> receptors.

##### GABA<sub>A</sub> receptors

The GABA<sub>A</sub> receptor (GABA<sub>AR</sub>) is a ligand-gated channel that selectively conducts chloride ions ( $\text{Cl}^-$ ) upon activation by agonists such as GABA. Typically, this results in an inhibitory postsynaptic potential (IPSP) and the hyperpolarization of the cell membrane. The reversal potential of the mediated IPSP is determined by the ratio of intracellular and extracellular chloride concentration and is typically  $\sim -70\text{ mV}$ . Inhibitory interneurons target with every compartment of the hippocampal principal cells (PCs), and GABA<sub>ARs</sub> can be found everywhere along the axo-dendritic axis of both PCs and INs (Kullmann et al., 2005).

Structurally, GABA<sub>ARs</sub> are protein complexes that consist of 5 subunits arranged in a ring. The subunits form a central pore through which chloride ions can flow (Figure 3.1). Multiple possible combinations of subunits (an incomplete list is shown in the chart in Figure 3.1) can form a receptor. The set of subunit determines basic kinetic properties such as activation and deactivation time constants (Benkowitz et al., 2004; Boileau et al., 2005), and also the affinity to GABA, benzodiazepines, steroids, barbiturates, ethanol, etc. The most abundant subunit combination is  $\alpha_1\beta_2\gamma_2$  (shown in Figure 3.1C). For example in the hippocampal CA3 area, 90% of the perisomatic synapses on PCs are immunopositive for the  $\alpha_1$  subunit (Kerti-Szigeti and Nusser, 2016). However, not all inhibitory synapses found by immunolabeling are active. Some inhibitory synapses might remain silent due to the lack of presynaptic GABA (Bekkers, 2005). Much like their excitatory cousins, the strength of inhibitory synapses is subjected to plasticity by various spike-timing-dependent-plasticity (STDP) rules (as reviewed by Vogels et al., 2013).

Not all GABA<sub>ARs</sub> are located at the synapses. A major subclass of GABA<sub>ARs</sub> containing the  $\delta$  subunit are located extrasynaptically on the membrane of cell bodies or dendrites. These receptors are especially sensitive to the ambient GABA that is released from presynaptic terminals and diffused from the synaptic cleft into the extracellular space (Semyanov et al., 2004; Farrant and Nusser, 2005). Their activation leads to a “tonic” hyperpolarization of the cell membrane, which contrasts the rapid dynamics of phasic IPSPs. Tonic GABA<sub>ARs</sub> express a wide range of modulations. Their activity depends on the amount of GABA released from the nearby located synapses, and by the changes in GABA uptake (Farrant and Nusser, 2005).

##### GABA<sub>B</sub> receptors

GABA<sub>B</sub> receptors (GABA<sub>BRs</sub>) are another major class of inhibitory GABAergic receptors that are expressed in most neurons of the central nervous system (Gassmann and Bettler, 2012). They are metabotropic receptors, that is, acting through G proteins. A functional

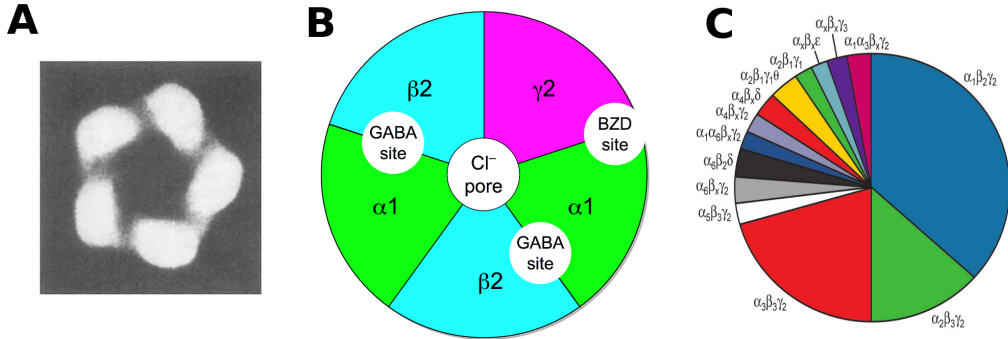


Figure 3.1: The GABA<sub>A</sub> receptor complex. **A**, Rotationally averaged representation of electron microscope image reveals a fivefold symmetry of the GABA<sub>A</sub>R (Nayeem et al., 1994; adapted with permission). The receptor diameter is  $\sim 10$  nM. **B**, Sketch of the most typical GABA<sub>A</sub>R  $\alpha_1\beta_2\gamma_2$  with the location of the GABA and benzodiazepines (BZD) binding sites (adapted from Wikipedia Commons). **C**, Chart showing the approximate distribution of GABA<sub>A</sub>R according to the subunits expression from a rat brain (Whiting, 2003; adapted with permission).

GABA<sub>B</sub>R consists of two subunits: GABA<sub>B1a</sub> or GABA<sub>B1a</sub>, and GABA<sub>B2</sub>. The GABA<sub>B</sub>Rs can be located at the post- or presynaptic side of the terminals. Postsynaptic GABA<sub>B</sub>Rs are located near the glutamatergic synapses but not at the inhibitory ones. There, they activate the G-protein-activated inwardly rectifying potassium channels (GIRKs) that inhibit the neuronal activity by generating a slow IPSP ( $\sim 500$  ms) with a low reversal potential of  $\sim -100$  mV (Booker et al., 2013). The postsynaptic receptor activation is considered important in the modulation of the long-term synaptic plasticity by controlling the back-propagation of APs (Leung and Peloquin, 2006). Presynaptic GABA<sub>B</sub>Rs can be located at excitatory or inhibitory terminals, acting as hetero- or autoreceptors, respectively. Activation of the presynaptic GABA<sub>B</sub>Rs reduces the permeability of the voltage-gated Ca<sup>2+</sup> channels (VGCCs) resulting in inhibition of Ca<sup>2+</sup> influx at the terminal, and thus, in reduction of the evoked and spontaneous neurotransmitter release (Gekel and Neher, 2008). Autoreceptors can be activated by a single AP of the cell they are located on (Kobayashi et al., 2012), while postsynaptic activation requires repetitive GABAergic firing (Scanziani, 2000).

In the hippocampus, the GABA<sub>B</sub>Rs are differentially expressed across the hippocampal layers and across neural populations. Postsynaptic, GIRK-coupled receptors are expressed over the whole somato-dendritic axis of the hippocampal principal cells, with the highest densities in the radiatum and in the distal dendrites in stratum lacunosum-moleculare in the CA regions (Degro et al., 2015). Compared to CA1 and dentate gyrus, pyramidal cells in area CA3 exhibit substantially stronger IPSPs induced by the GABA<sub>B</sub>R agonist baclofen (Degro et al., 2015). Interneurons show population-specific expression of postsynaptic GABA<sub>B</sub>Rs. For example, immunolabeling reveals high GABA<sub>B1</sub> subunit density at the extrasynaptic membrane of PVBC. In response to an extracellular stimulation in CA1, parvalbumin positive (PV<sup>+</sup>) basket cells have larger GABA<sub>B</sub>-mediated IPSCs compared to the ones evoked in the dendritic-targeting PV<sup>+</sup> interneurons (Lei and McBain, 2003). Synaptic transmission from both glutamatergic and GABAergic synapses on interneurons in the stratum radiatum is inhibited by GABA<sub>B</sub>R activation. Moreover, GABA<sub>B</sub>R activation reduces the frequency-dependent and short-term depression of inhibitory transmission and normalizes the IPSPs

### 3 Modulation of sharp-wave incidence

on principal cells. PV<sup>+</sup> dendritic-targeting interneurons show higher densities of GABA<sub>B</sub>Rs in the axons compared to PV<sup>+</sup> basket cells (Booker et al., 2013).

#### 3.2.2 GABAergic modulation of sharp-wave ripple incidence *in vitro*

*In-vitro* slice preparations are ideally suited to study the local hippocampal circuitry. Under certain experimental conditions, slices can express spontaneous events that resemble the SWRs observed *in vivo* (Hajos et al., 2009; Maier et al., 2009). These results suggest that a fraction of the hippocampal circuitry is sufficient for the generation of SWRs. *In-vitro* preparations have a slice thickness typically  $\sim 500\text{ }\mu\text{m}$ , containing  $\sim 20,000\text{--}40,000$  neurons in the CA areas (an estimate based on the numbers of neurons in the rat hippocampus and slice thickness; Boss et al., 1985; West et al., 1991; Bezaire and Soltesz, 2013). Moreover, mini-slice experiments show that isolated CA3 and CA1 areas can also generate SWRs in the absence of connections to neighboring regions (Maier et al., 2003). Despite the relatively small network size, the dynamics of the hippocampal circuit is not well understood, and a complete model of the SWR generation mechanism is still missing.

Because of the larger neuronal excitability of the ventral parts of the hippocampi (Dougherty et al., 2012), SWRs *in-vitro* models usually rely on ventral slices (e.g., Maier et al., 2003; Nimmrich et al., 2005). SWRs normally originate spontaneously in the CA3 region with a stereotypical waveform shape consisting of the sharp wave and the ripple oscillation in the field potential (Csicsvari et al., 1999). The activity then propagates to the CA1 area via the Schaffer collateral pathway. The ripples are, however, incoherent in both regions, suggesting an independent origin of the fast oscillation (Csicsvari et al., 2000; Both et al., 2008). The *in-vitro* model provides the opportunity of experimental control, and thus, to disentangle the contribution of various factors such as the contribution of different neuronal populations, neurotransmitter signalling, etc.

Inhibitory transmission plays a central role in the generation of SWRs (Maier et al., 2003; Schlingloff et al., 2014). Drugs altering the properties of inhibitory transmission can shed light on the different signaling paths involved the generation of SWRs. For example, SR-95531 (gabazine) is a widely used GABA<sub>A</sub> antagonist that has high affinity to the GABA binding site of phasic receptors (Ueno et al., 1997; Bai et al., 2001; Yeung et al., 2003). Low doses of gabazine *in vitro* decrease the incidence of SWRs, while larger doses block the events (Maier et al., 2003; Nimmrich et al., 2005; Ellender et al., 2010). Currently, it is unclear through what mechanisms gabazine affects the SWR incidence. On the other hand, thiopental is a barbiturate that increases the IPSP decay time constant, and thus, increases the total charge at the postsynaptic side (Dickinson et al., 2002). Low doses of thiopental decrease SWR incidence, while prolonging the duration and the peak of the spontaneous events, and interestingly, reduce the number of ripples per event (Papatheodoropoulos et al., 2007). Moreover, how can two drugs (i.e., gabazine and thiopental) that have opposite effects on the GABA synapses affect SWRs in a similar manner, i.e., decreasing the incidence of spontaneous SWRs?

Other major drugs affecting GABA<sub>A</sub>Rs such as diazepam and phenobarbital have non-linear effects on SWR incidence: for low doses the occurrence is increased, and for higher concentrations the incidence goes down (Papatheodoropoulos et al., 2007; Koniaris et al., 2011). These effects are not well understood.

The role in the modulation of SWRs of the other major inhibitory receptor, the GABA<sub>B</sub>R is unclear. Some studies have reported that blocking GABA<sub>B</sub>Rs in slices doesn't alter the SWR properties, such as incidence, amplitude, duration (Hollnagel et al., 2014; Hofer et al.,

2015). However, later in this chapter I will show that in the *in-vitro* model analysed here, the GABA<sub>B</sub>Rs antagonist SCH50,911 increases the incidence of SWRs. Blocking the GIRK channels with SCH23,390 also results in an increase of SWR incidence (Maier et al., 2012; personal communication with Nikolaus Maier). On the other hand, the application of GABA<sub>B</sub>R agonists decreases the incidence of SWR events (Maier et al., 2012; Hollnagel et al., 2014).

### 3.2.3 Sharp-wave events driven by inhibition

A counterintuitive experimental finding is the fact that SWRs can be evoked by driving inhibitory neurons to fire (Ellender et al., 2010; Schlingloff et al., 2014; Kohus et al., 2016). In particular, Schlingloff et al. (2014) have demonstrated that SWRs can be elicited by a transient optogenetic drive of a subpopulation of parvalbumin-positive (PV<sup>+</sup>) interneurons (Figure 3.2). The authors show that SWRs are evoked a few milliseconds after the onset of the light stimulation, and that the number of ripples is stable irrespective of the length of the impulse (Figure 3.2E). Spontaneous SWRs do not occur when ionotropic excitatory transmission is blocked, but nevertheless, events can be evoked by optogenetic stimulation of a PV<sup>+</sup> subpopulation. This finding suggests that inhibitory activity is sufficient for the generation of SWRs in the pyramidal layer, given that there is appropriate drive for the circuit, e.g., optical stimulation with duration of  $\sim 20\text{ ms}$ . In the control condition, when no synapses are blocked, the PV<sup>+</sup> stimulation recruits excitation. During the evoked SWRs, whole-cell voltage-clamp recordings from PV<sup>+</sup> interneurons reveal phasic excitatory postsynaptic potentials (Figure 3.3), meaning that the inhibitory stimulation leads to the release of excitation.

How does the PV<sup>+</sup> interneurons population lead to the excitatory drive observed in the *in-vitro* model? A simple two-population model consisting of single excitatory and inhibitory populations cannot explain the above-mentioned phenomenon. To better understand the mechanisms behind SWR generation one needs to look beyond the 2-population model (as presented in Chapter 2) and consider additional mechanisms. A few explanation have been proposed in the literature:

1. **Depolarizing effects of GABA<sub>A</sub>Rs.** It has been shown that during the early phases of development and during certain conditions of *in-vitro* preparations GABA<sub>A</sub>Rs can have depolarizing effects on the postsynaptic membrane potentials of pyramidal cells (Cohen et al., 2002; Gullidge and Stuart, 2003; Banke and McBain, 2006). In particular, Szabadics et al. (2006) demonstrated how activation of a single axo-axonic cell can trigger a depolarizing GABAergic postsynaptic potential or a postsynaptic action potential in pyramidal cell in cortical slices from rats and humans. In such a scenario, driving the PV<sup>+</sup> interneuron population (that includes the axo-axonic cells) would have an excitatory effect on the network activity.
2. **Inhibition leads to rebound excitation.** Cobb et al. (1995) have shown that inhibitory inputs to depolarized pyramidal neurons can lead to a brief depolarization (rebound) following the initial hyperpolarization. During the rebound depolarization cells can fire action potentials. Such effects taking place simultaneously in multiple neurons would effectively lead to their transient synchronization, and thus, to a possible population burst.
3. **Inhibition de-inactivates voltage-gated ion channels.** This idea is in line with Platkiewicz and Brette (2011) who have shown that the inactivation of Na<sup>+</sup> chan-

### 3 Modulation of sharp-wave incidence

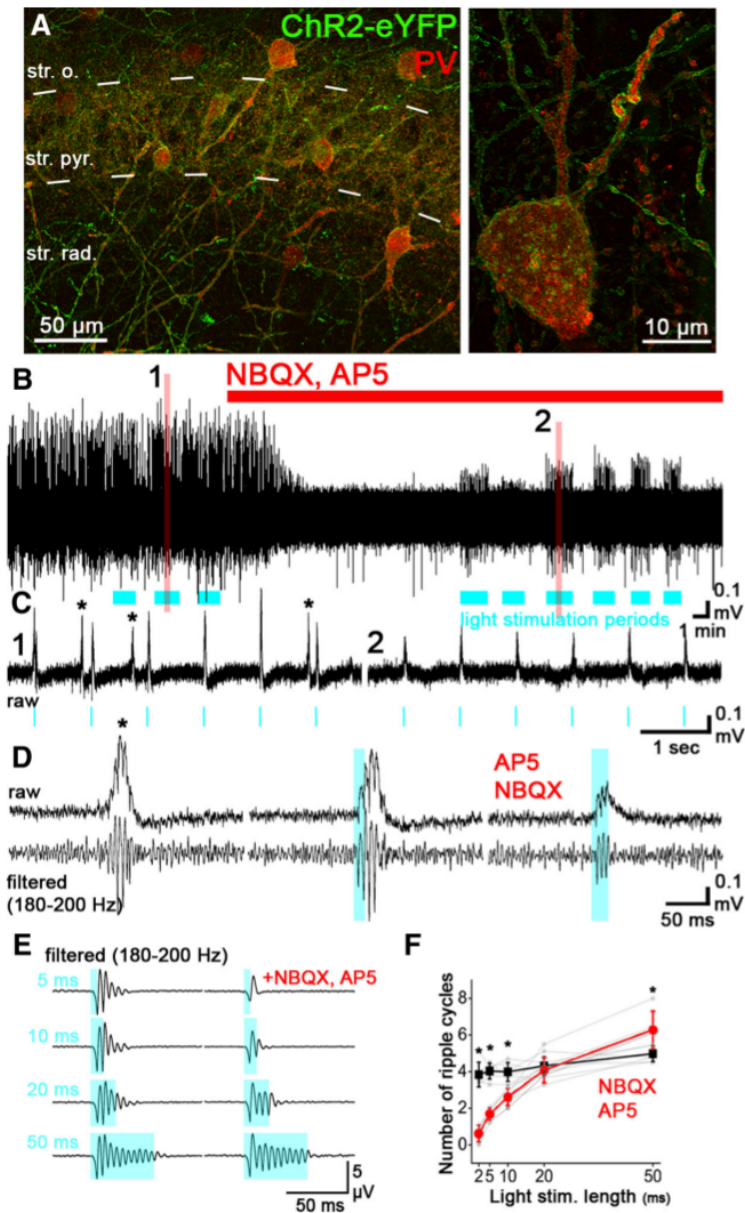


Figure 3.2: Sharp-wave ripples can be evoked by optogenetic drive to PV<sup>+</sup> interneurons (Schlingloff et al., 2014; adapted with permission). **A**, Fluorescent staining against parvalbumin (red) and ChR2 (green) shows that ChR2 is expressed exclusively in PV<sup>+</sup> interneurons. str. o., stratum oriens; str. rad., stratum radiatum; str. pyr., stratum pyramidale. **B**, Spontaneous and light-evoked (blue bars) SWRs recorded from a slice in control conditions. Spontaneous events disappear after a blockage of excitatory ionotropic transmission (red bar). **C**, A zoom in the local field potential from the periods denoted with 1 and 2 in **B**. Spontaneous events are denoted with stars, evoked events are denoted with a blue bar indicating the timing of the light pulse. During the excitatory blockage no spontaneous SWRs occur, but only evoked (right panel). **D**, Examples of a spontaneous SWR (left), an evoked SWR (right), and an evoked SWRs with excitation blocked. **E**, **F**, Light pulses with different durations evoke SWRs. In control condition, the length of the SWR event is relatively independent on the light duration, which is not the case when excitation is blocked.

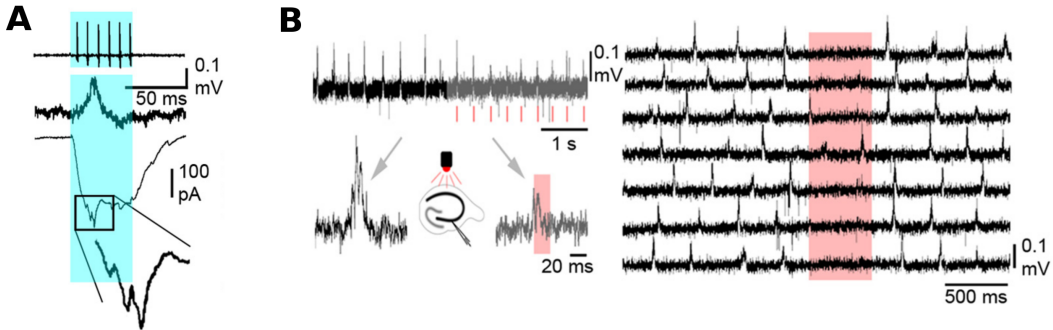


Figure 3.3: Optogenetic control of PV<sup>+</sup> interneurons modulates SWRs (Schlingloff et al., 2014; adapted with permission). **A**, Optogenetic drive of PV<sup>+</sup> interneurons evoked repetitive action potentials in PV<sup>+</sup> cells (loose-patch recording in top trace) as well as a SWR in the LFP (second trace). A whole-cell, voltage-clamp recording from a PV<sup>+</sup> interneuron shows phasic EPSC < 10 ms after the onset of the impulse (two bottom traces). **B**, Optogenetic silencing of PV<sup>+</sup> cells interrupts (left panel) and blocks the generation of spontaneous SWRs (right panel).

nels impacts the neuron's firing threshold. A brief inhibitory/hyperpolarizing input might be sufficient to de-inactivate channels that have been inactivated due to continuous depolarization. This mechanism can be extended also to other voltage-gated ion channels.

4. **Disinhibition.** A possible disinhibitory loop includes basket cells, which are shown to project to dendritic-targeting interneurons (DTIs) (Cobb et al., 1997; Kohus et al., 2016). According to this hypothesis activation of BC leads to strong inhibition of the DTI that actively suppress PC from firing between the events. This inhibition of inhibition would be the direct cause of the following SWR.

The above-mentioned mechanisms are not mutually exclusive as possible causes for the inhibitory-driven evoked events. However, some of these explanations seem more plausible than others. For example, currently there is no evidence that GABA<sub>A</sub>R has depolarizing effects in the *in-vitro* SWR models. Experimental support for membrane potential rebounds after inhibitory inputs from PVBCs is also scarce. This hypothesis comes with clear predictions that can be tested experimentally *in-vitro*: i) a patch-clamped recordings from PC should show a rebound spike after driving one or more PV<sup>+</sup> interneurons; and ii), blocking de-inactivation of the voltage-gated ion channels should prevent the inhibitory-driven SWRs.

### 3.2.4 Hypothesis on the CA3 circuitry giving rise to sharp-wave ripples

The fact that silencing a PV<sup>+</sup> subpopulation can interrupt an ongoing SWR event and significantly reduce the incidence of spontaneously occurring events (Schlingloff et al., 2014) supports the last hypothetical mechanisms, the disinhibitory circuit (Figure 3.4). The hypothesis presented below aims to explain some paradoxical results reported in the literature. The proposed model relies on a number of assumptions that are to be tested in experiments. Moreover, it comes with some predictions that can validate or invalidate the proposed model.

A minimal disinhibitory model consists of 3 populations: pyramidal cells (PC), parvalbumin-positive basket cells (PVBC), and another class of interneurons, which I will refer to as mysterious interneurons (mINs). The circuit can operate in two regimes: a balanced state with

### 3 Modulation of sharp-wave incidence

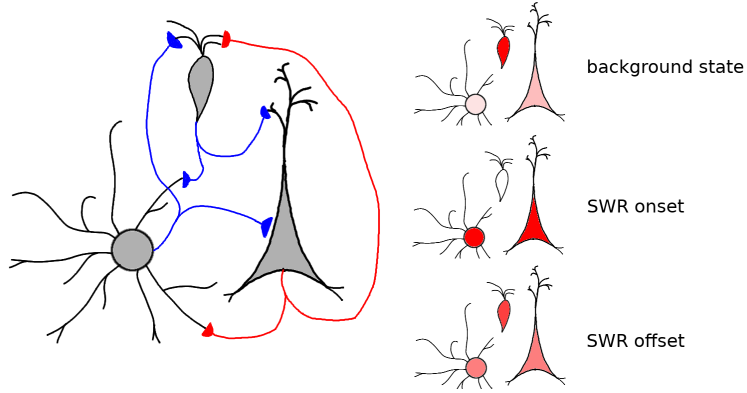


Figure 3.4: A sketch of a minimal model consisting of 3 neuronal populations. **left:** The network consists of 3 populations: PC (right), PVBC (left), and mIN (top). Populations are all-to-all connected, including recurrent connections (not shown). Axons and synapses are color-coded with red for excitation and blue for inhibition. **right:** Population activity before and during a SWR represented in three snapshots. The degree of population activation is color-coded where higher saturation of the red color denotes higher activity. In the background state, PCs and PVBCs have low firing rates, while the mIN population has its highest activity. At the onset of events, PCs and PVBCs are active, while mINs are silent because of the fast inhibition from PVBC. Towards the end of the event, mINs get activated by the excitatory neurons, and thus, start suppressing the SWR event.

low firing rates that describes the CA3 network dynamics between events, and a high-firing state corresponding to a SWR event (Figure 3.4). In the background state the PCs are in a low-firing (Csicsvari et al., 1999) balanced state and are heavily inhibited by the active mINs. The PVBCs are virtually silent in the background state (Klausberger et al., 2003; Varga et al., 2012). Spontaneous SWRs occur when, due to a build-up of activity, pyramidal neurons excite the PVBCs, and then PVBCs inhibit the mIN population, effectively disinhibiting the pyramidal population. Thus, during a SWR event, the network activity turns around, the PC and PVBC populations are firing with high rates (Klausberger et al., 2003; Varga et al., 2012), while the mINs are silent. The conditions in which this disinhibitory circuit operates are explored in detail in a separate project by Roberta Evangelista. Preliminary results predict a strong PC-PVBC-mIN connection pathway in comparison to PC-mIN connections, as well as stronger connections on the PVBC-mIN-PC pathway in comparison to PVBC-PC connections.

According to the model, activation of the PC or PVBC population would activate the disinhibitory pathway, leading to a SWR. The model is in line with the reports that find a gradual build-up of PC activity tens of milliseconds prior to spontaneous SWR events (Ellender et al., 2010; Schlingloff et al., 2014; Hulse et al., 2016). Moreover, depolarization of a small group (few tens up to hundred) of neighboring pyramidal neurons could evoke a SWR *in vivo* (Stark et al., 2014). And Bazelet et al. (2016) showed that driving a single pyramidal cell to firing (200 pA, for 200 ms) can prime the occurrence of SWRs *in vitro*. Interestingly, the PC stimulation leads to the recruitment of perisomatic-targeting inhibitory interneurons reflected in the field IPSP at the initial phase of the evoked SWs. According to the proposed hypothesis, the stimulated PCs (Stark et al., 2014; Bazelet et al., 2016) drive a subpopulation of PVBCs that consequently disinhibit the local circuit. Also in line with the disinhibitory model is the fact that silencing PV<sup>+</sup> cells stops an ongoing SWR and leads

to suppression of spontaneous SWs (Schlingloff et al., 2014).

The 3-population model is not fully in line with who Ellender et al. (2010) have shown that during a continuous (500 ms) drive of a single perisomatic-targeting interneuron, the incidence of SWR occurrence decreases, and after termination of the stimulation, the SWR incidence increases with a significant peak of occurrence 1 to 2 seconds after the stimulation offset. It is worth noting that these results hold only for a fraction of the stimulated cells (6/24). Perisomatic-targeting interneurons are a family of different classes of interneurons that include cholecystokinin-positive basket cells, parvalbumin-positive basket cells, and axo-axonic cells (Freund and Buzsáki, 1996). It is not known which, if any particular, class of these interneurons is involved in this temporal suppression of SWRs. It is still an open question why stimulating a single perisomatic-targeting neuron can suppress SWRs and can release SWRs immediately after the stimulation (Ellender et al., 2010), while optical stimulation of small populations gives rise to SWRs just  $\sim 1$  ms after the onset of the stimulation (Schlingloff et al., 2014). However, exciting a small subpopulation of PV<sup>+</sup> interneurons (<5 cells) does not evoke any SWR events, and even suppresses ongoing events *in vivo* (Stark et al., 2014). This might be explained by the fact that while Schlingloff et al. (2014) illuminate the whole slice, and thus activate most of the PV<sup>+</sup> interneurons, Ellender et al. (2010) and Stark et al. (2014) activate one or a very few neurons which is not sufficient for disinhibition, and thus, to initiate an event. Another interesting disagreement of results is that Ellender et al. (2010) did not observe a rise of the SWR incidence after driving single pyramidal neurons in contrast to the report from Bazelet et al. (2016).

To make a more complete model of the SWR generation, one should also consider mechanisms that control the duration of a SWR and the time interval between events. One requires processes on a relevant time scale on the order of hundreds of milliseconds to seconds. An important component of such mechanisms could be the short-term plasticity of inhibitory transmission. It has been shown that basket cells exhibit short-term depression (STD) of synaptic transmission both on pyramidal cells and on other interneurons as well (Kraushaar and Jonas, 2000; Kohus et al., 2016). During a SWR event, PVBCs fire multiple times with a high frequency, and therefore, the efficacies of their synapses decrease significantly towards the end of an event. Considering such depression on the PVBC-mIN synapses would lead to a weaker inhibition on the mINs in the advanced phase of the sharp wave, resulting in mINs recruitment. Once active again, mINs inhibit the PC population, leading to the termination of the SWR. The recovery of the PVBCs synapses is a relatively slow process on the order of hundreds of milliseconds (Kohus et al., 2016). Once the synapses recover from depression, the PVBC population is able to disinhibit the CA3 circuit again and lead to the next event. In line with the STD hypothesis, a prolonged optogenetic drive (400 ms) to the PC population leads to ripple oscillations that decrease in amplitude and frequency after 50 ms (Stark et al., 2014). The decrease in frequency is likely due to the depression of the PVBC-PVBC synapses that are crucial for the ripple oscillation generation (Donoso et al., 2017), while the amplitude decrease is due to the depression of PVBC-PC synapses that are the main contributor to the ripple LFP in the pyramidal cell layer.

To summarize, here I propose a phenomenological three-population model as a minimal circuit that can give rise to the SWR events observed *in vitro* and *in vivo* (see Figure 3.4). In the background state, in the intervals between events, the pyramidal cell (PC) and the PV<sup>+</sup> basket cell (PVBC) population exhibit low firing rates, while being inhibited by another (not identified yet) inhibitory population (mINs). Before the onset of an event, there is a build-up of excitatory activity recruiting PVBCs which inhibit the mIN population, and

### 3 Modulation of sharp-wave incidence

thus, the disinhibited circuit enters a high firing-rate regime, where the balance of activity is maintained by the pyramidal cells and the PVBCs. The high firing rates of PVBCs during the event leads to short-term depression of their efferent synapses. In particular, as the PVBC-mIN pathway is depressed, the mINs are recruited back into the network, and thus, terminate the event by inhibiting the excitatory PC population.

Such a model circuit comes with a number of assumptions/predictions that can be tested experimentally. A basic model requirement is the third population of unidentified interneurons, the mINs. To help narrow down the search for this population, there are a few features that should be exhibited according to the model:

- mINs are active in the low-firing background state, are silent in the initial stage of the SWR events, and are active again at the advanced phase of the SWRs. Possible candidates are ivy cells (Hájos et al., 2013), axo-axonic cells (Viney et al., 2013), enkephalin-expressing interneurons (Fuentealba et al., 2008b), or neurogliaform cells (Karayannis et al., 2010). However, neurogliaform cells and ivy cells have bigger time constants (Fuentealba et al., 2008a; Karayannis et al., 2010), and their slow IPSPs are unlikely to modulate the network activity on a millisecond time scale upon PV<sup>+</sup> interneuron stimulation.
- a transient inhibition applied to the mIN population should trigger a SWR event.
- a constant drive applied to the mINs should suppress the generation of SWRs.
- the mINs are parvalbumin negative (PV<sup>-</sup>) interneurons.
- the mINs are heavily suppressed by a PV<sup>+</sup> subpopulation during SWR events.
- due to the lack of observed IPSPs in patch-clamped pyramidal cell recordings, it's likely that mINs target the distal dendrites of PCs.
- a current-source density (CSD) analysis from multi-electrode recordings might show the location the current source evoked by mINs in the background state.

However, the proposed disinhibitory hypothesis has to deal with a few weaknesses at its incarnation. The following issues need to be addressed properly by experiments or extension of the model:

- A light stimulation to the PV<sup>+</sup> neurons recruits the excitatory population shortly ( $\sim 10$  ms) after the onset of the light impulse (see Figure 3.3). This result suggests that the membranes of pyramidal cells are in a tight balance of excitatory and inhibitory inputs, and the suppression of mINs leads to a rapid increase of firing. An interesting question is: Where does the excitatory drive originate? In what conditions is the low firing rate of the *in-vitro* circuit sufficiently high to drive the population bursts upon disinhibition?
- As mentioned above, patch-clamp recordings from pyramidal cells rarely show signatures of IPSPs (from the data provided by Nikolaus Maier, and also in Maier et al. (2011); Schlingloff et al. (2014)). Assuming that the lack of IPSPs is due to a filtering of the dendritic tree, in which conditions can this filtering happen?

- Given the aforementioned points, it is possible that other mechanisms can take the role of the mINs? For example, an alternative, or complementary, mechanism to the disinhibition circuit could manifest itself through inhibition that would de-inactivate voltage-gated  $\text{Na}^+$  channels.

In the following Results section, I discuss the findings from *in-vitro* data in the light of the phenomenological model presented here.

### 3.3 Results

In this section I analyse *in-vitro* recordings provided by Nikolaus Maier. All recordings are performed in CA3 stratum pyramidale of hippocampal slices that exhibit spontaneous SWRs. The results are interpreted in the light of the hypothetical 3-population circuit. Additionally, for explaining the experimental findings of gabazine effects in the SWR incidence, I used numerical and analytical methods applied to the 2-population network presented in Chapter 2.

#### 3.3.1 Serial correlations between peak amplitudes of SWRs and intervals between them

The time intervals between consecutive SWR events *in vitro* vary from tens of milliseconds to tens of seconds depending on the experimental setup and the slice preparation. Currently, we do not know the underlying biological processes that control the dynamics on time scales much larger than tens of milliseconds. However, a natural assumption is that there is some kind of slow recovery of the system after each SWR event, which might have been caused by e.g., depletion of synaptic and neuronal resources (Cohen and Fields, 2004; Jones et al., 2007), receptor saturation (Trussell et al., 1993), or short-term depression (Romani and Tsodyks, 2015; Kohus et al., 2016). Moreover, slow dynamics can arise from a slower inhibition evoked by ambient GABA on the extrasynaptic  $\text{GABA}_\text{A}$ Rs (Brown et al., 1978; Ben-Ari et al., 1994) or an activation of synaptic/extrasynaptic  $\text{GABA}_\text{B}$ Rs (Scanziani, 2000; Hollnagel et al., 2014; Lang et al., 2014).

The type of data that is analysed here (extracellular recording at a single location) does not allow to discriminate between the mechanisms listed above as they all predict serial correlations between SWR events. For example, if some of the mechanisms is involved indeed, then after a longer interval since the last event, the circuit will be more recovered, and the following SWR event is expected to be larger in amplitude (see sketch in Figure 3.5, top panel). Moreover, if the SWR peak amplitude reflects the degree to which the (local) circuit is involved into the population burst, then events with larger amplitudes will cause stronger activation of these mechanisms, and thus, a longer interval until the following event is expected. To test whether any of the arguments above hold, this section examines the serial correlations between inter-SWR-interval and the amplitude peak of the following SWR (interval-peak), and also the serial correlations between SWR amplitudes peaks and the following time interval (peak-interval).

Does the recovery time affects the size of the following events? To test this, I calculated the serial correlation between the inter-event time intervals and the peak amplitude of the following SWR (typical example recording shown in Figure 3.5, middle-left panel). Most slices show significant and positive correlations ( $p < 10^{-3}$ ; 18 out of 20 recordings; Figure 3.5, bottom-left panel). This means that after a long interval the amplitude peak of the following

### 3 Modulation of sharp-wave incidence

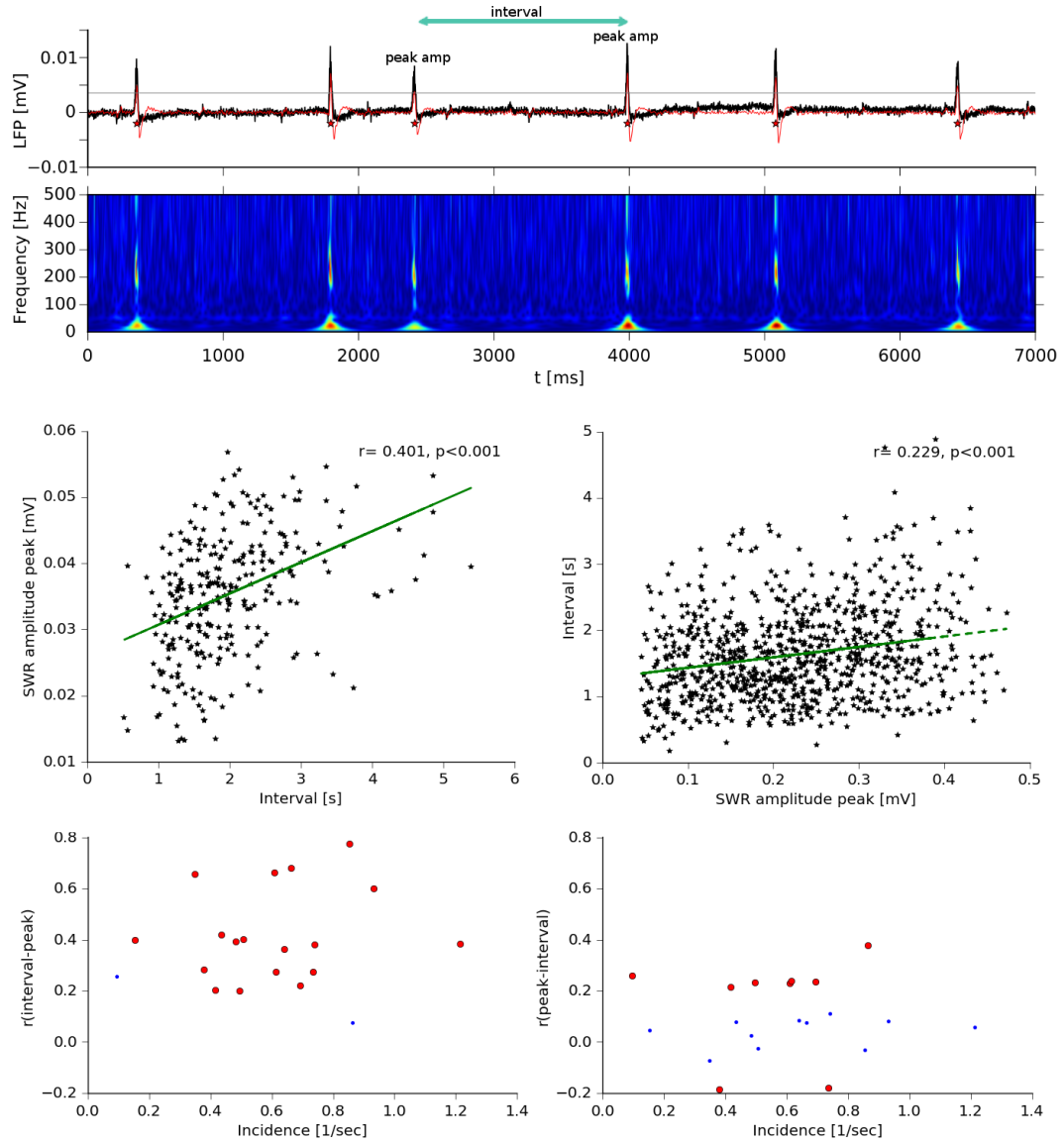


Figure 3.5: Serial correlations of sharp-wave ripples. **top:** An example of extracellular recording. Black and red lines are the raw and the band-pass filtered (3–50 Hz) LFP signal, respectively. The colored panel below shows the respective spectrogram. **middle:** Typical examples of interval-peak (left panel,  $n = 294$ ) and peak-interval (right panel,  $n = 1118$ ) relations from two different recordings show positive correlations. Note the order of magnitude difference in the SWR peak amplitude in both examples. **bottom:** Distribution of interval-peak (right panel) and peak-interval (left panel) correlations in respect to the SWR incidence; the red circles denote significant ( $p < 10^{-3}$ ) correlations, blue dots denote insignificant correlations.

### 3.3 Results

SWR is big, and after a brief interval, the following SWR has a smaller peak amplitude. After dividing the recordings into 5-minute time windows, each slice shows at least once positive and significant serial correlation (interval-peak) during the course of the recording. Negative correlations are not present. The interval-peak correlations found in the data have been recently confirmed by Kohus et al. (2016).

In the analysed data, the incidence of spontaneous SWs ranges from 0.1 to  $\sim 1.2$  event/sec across slices. The degree of recovery might be pronounced better for shorter intervals and less pronounced after longer intervals. Therefore, a natural question is whether the incidence influences the interval-peak correlation. Statistical tests on the aggregated data (Figure 3.5, bottom-left panel) show that this dependence is, however, statistically insignificant ( $r=0.2$ ,  $p=0.4$ ). Moreover, dividing each recording into 5-minute time windows, and testing the serial correlation of events within that window in respect to the incidence also does not show a strong relation (18 out of 20 recordings show insignificant ( $p > 10^{-3}$ ), 1/20 positive ( $r = 0.77$ ,  $p < 10^{-6}$ ), and 1/20 negative ( $r = 0.93$ ,  $p < 10^{-6}$ ) correlation between incidence and interval-peak correlations). Therefore, the conclusion is that the interval-peak serial correlation does not depend on the incidence of SWR events.

Does the SWR peak amplitude influence the time interval until the following events? To test that, the peak-interval serial correlation are calculated. From 20 slices, only 9 show correlations that are significant ( $p < 10^{-3}$ ) with a median correlation coefficient of around 0.2 (Figure 3.5, bottom-right panel).

The majority of recordings shows a missing peak-interval correlation (11/20). Even though recovery might control inter-SWR intervals, a low peak-interval correlation cannot rule out this mechanism. A possible explanation for this observation is that the SWR peaks are a local phenomenon, and while being large at the recording location, SWs peaks can be smaller at other locations of the slice. The next event is then triggered in a site where the peak has been rather low and the local resources are less depleted. Therefore, we can not predict the time of the next event based on the measured amplitude at a particular site because SWs can originate elsewhere in the slice. In such cases, the local depletion recovery does not play a role in controlling the timing of next events. Following this line of reasoning gives us a hypothetical explanation about the surprisingly low correlations between peaks and intervals.

To test the hypothesis relying on the locality of SWR peak amplitudes stated above, I analyse data from multi-electrode array (MEA) recordings. The dataset is provided by Roberta Evangelista, where multiple sites in the CA3 area of hippocampal slices are measured simultaneously. In single recordings, the peak amplitudes of SWR events measured at different locations show very high co-variability (an example is shown Figure 3.6). Moreover, the aggregated data from 20 different slices show that every pair of locations in a CA3 slice has a positive and significant ( $p < 10^{-3}$ , 2116 total pairs) correlations between the measured SWR peaks (Figure 3.7). The high correlations between different sites rule out the hypothesis that the amplitude of SWRs is a local phenomenon in slices.

In summary, the majority of slices (18/20) show positive and significant ( $p < 10^{-3}$ ) correlations between the time interval since the last event and the peak amplitude of the following SWR. On the other hand, smaller correlation between SWR peak amplitude and the interval until the following event are found in 9/20 slices. This weak peak-interval serial correlation can not be explained by some locality of the events as SWR peaks are a non-local phenomenon, and a large SWR measured at one location is likely to be large in the whole CA3 region.

### 3 Modulation of sharp-wave incidence

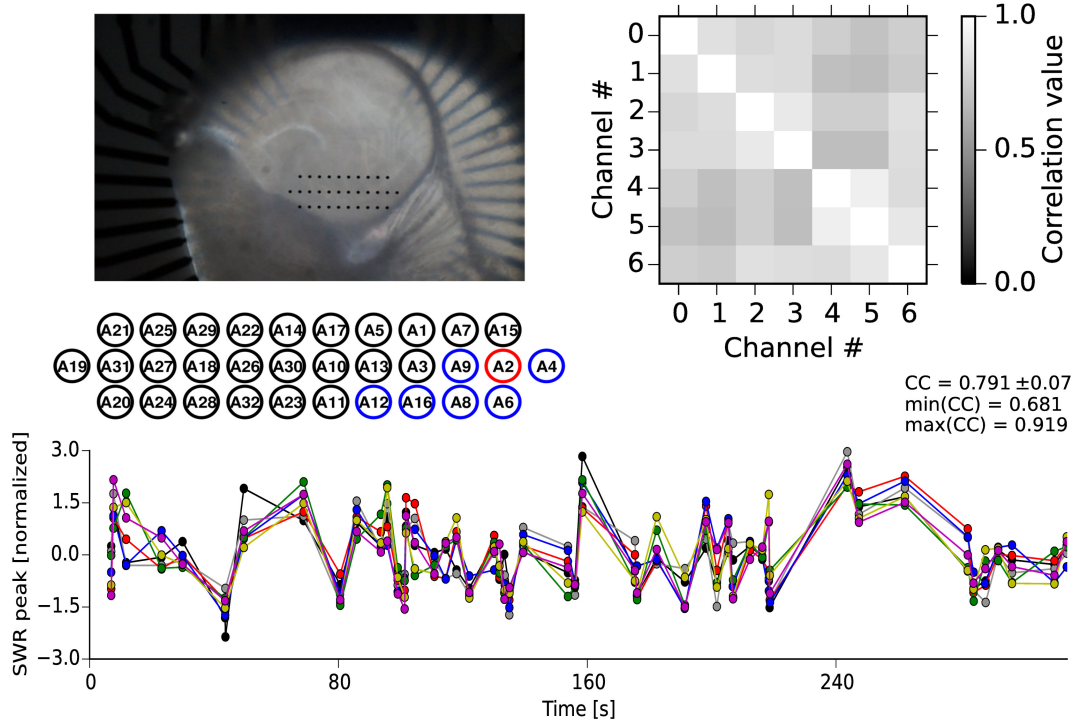


Figure 3.6: An example multi-electrode array recording *in vitro*. **top-left:** A hippocampal slice with recording sites in black. The colored circles (red and blue) denote recording channels that are considered to be in the stratum pyramidale and have a reliable signal of the SWR events. **bottom:** Example of a recording sweep, where SWR peak amplitudes measured at 7 recording electrodes are plotted in time. For better comparison, peaks are normalized by subtracting the mean and dividing by the standard deviation of peaks of peak amplitudes for each recording site. **top-right:** A matrix of the pair-wise correlation coefficients (CC) between SWR peak amplitudes measured at the different electrodes.

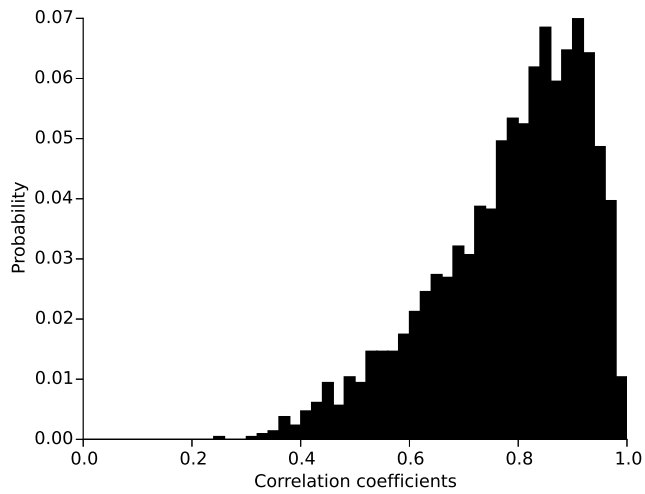


Figure 3.7: Distribution of correlation coefficients between pairs of SWR peak amplitudes measured at different locations in CA3; aggregated data from 20 hippocampal slices.

The high interval-peak correlations found in the data have been recently confirmed by Kohus et al. (2016). The authors propose that a recovery from short-term depression (STD) on the inhibitory synapses affects the amplitudes of SWR peaks observed in the local field potential, and moreover, suggest that STD is a possible mechanism controlling the SWR incidence. The field potential in stratum pyramidale is dominated by the inhibitory synaptic activity (Schönberger et al., 2014). Therefore, the amplitude of SWR peaks in the stratum pyramidale are modulated by the local inhibitory synaptic currents. A recovery from STD of the PVBC-PC synapses (and possibly PVBC-PVBC) is a strong candidate for the modulation of SWR peak amplitudes. Thus, the high amplitudes of SWRs observed after longer time intervals since last event are caused by recovered inhibitory synapses in the pyramidal layer. However, the positive peak-interval correlation observed in some slices (7/20) suggests that the SWR amplitude might also reflect the PVBC firing rate to a smaller degree. In the light of the 3-population hypothesis stated in Section 3.2.4, the incidence of SWRs is controlled by the STD recovery time constant on the inhibitory PVBC-mINs synapses, and higher firing PVBC firing would lead to a larger depression, and thus, to a longer interval until the next event.

### 3.3.2 Gabazine effects on sharp-wave ripples *in vitro*

Hippocampal slices exhibit network dynamics shaped by excitatory and inhibitory activities that balance each other (Csicsvari et al., 1999; Maier et al., 2011; English et al., 2014; Hulse et al., 2016). It is intuitively expected that by decreasing the total inhibitory coupling (connections from inhibitory to all the other neurons are weakened) the network would get more excitable. However, from previous work (e.g., Nimmrich et al., 2005) it is known that application of low concentrations of gabazine (a GABA<sub>A</sub>R antagonist) decreases the rate of spontaneously occurring SWRs, while larger concentrations block SWRs (Maier et al., 2003; Ellender et al., 2010). It is not clear how the application of gabazine affects the network activity.

An underlying assumption in the presented analysis is that the decrease of SWR incidence is due to a decrease of the firing rate of the excitatory population outside of SWRs. But how does a decrease of inhibition lead to a more inhibited network? To tackle this paradox, in this section I analyse some data provided by Nikolaus Maier in which gabazine is applied to hippocampal slices.

Gabazine (SR-95531) is a GABA<sub>A</sub>R antagonist that binds to the GABA-binding site, effectively decreasing inhibitory conductance. Low drug concentrations block phasic but not tonic GABA<sub>A</sub>Rs (Bai et al., 2001; Yeung et al., 2003; Behrens et al., 2007). In the experiments analysed here, after a few minutes of stable baseline recording, low concentrations of gabazine (100 nM) were applied to the hippocampal slices. A typical example is shown in Figure 3.8 where gabazine was applied 27 minutes after the recording onset (application duration denoted with a horizontal red line). Shortly after the drug infusion, the incidence of spontaneous events goes down from 0.32 to 0.15 events/second (values are measured in 5-minute time windows from before and during drug application, independent two-sample t-test with p-value < 10<sup>-6</sup>). The averaged LFP waveforms associated with SWRs (arranged relative to the peak of the filtered signal) show a stereotypical SWR waveform before and during the drug application (Figure 3.8, bottom panels). There is also slight but significant increase of the SWR peak amplitudes and duration after the gabazine application ( $p < 10^{-3}$ ). After the washout (end of red bar, at 43 minutes) the incidence of SWs increases back to the values before the drug infusion.

### 3 Modulation of sharp-wave incidence

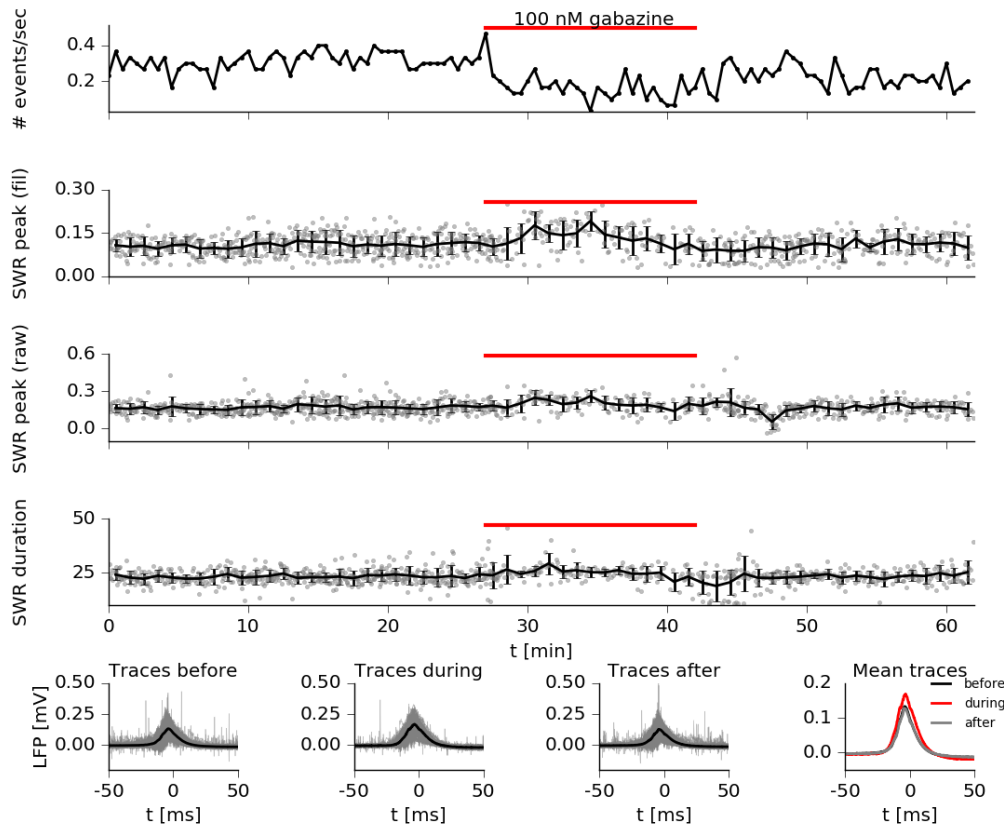


Figure 3.8: An extracellular recording from CA3 where gabazine concentration is applied to the hippocampal slice. Time of drug application is denoted with a horizontal red bar. The top panel shows the SWR incidence in time with a half-minute time resolution. The two panels below show the SWR amplitude peaks, where “fil” and “raw” denote band-passed filtered ( $\sim 5\text{--}50\text{ Hz}$ , for details see the Methods section) and raw voltage traces, respectively; units are in mV. The gray dots represent single events, and the black lines represent the mean, and errors bar the standard deviation of the amplitude peak in one-minute time windows. Analogously, the forth panel shows the SWR duration in milliseconds. The panels on the bottom row show all events before, during, and after drug application (panels from left to right) overlaid in gray, and the mean wave-forms are in black. The right-most panel shows a comparison between the mean events from before during, and after gabazine application.

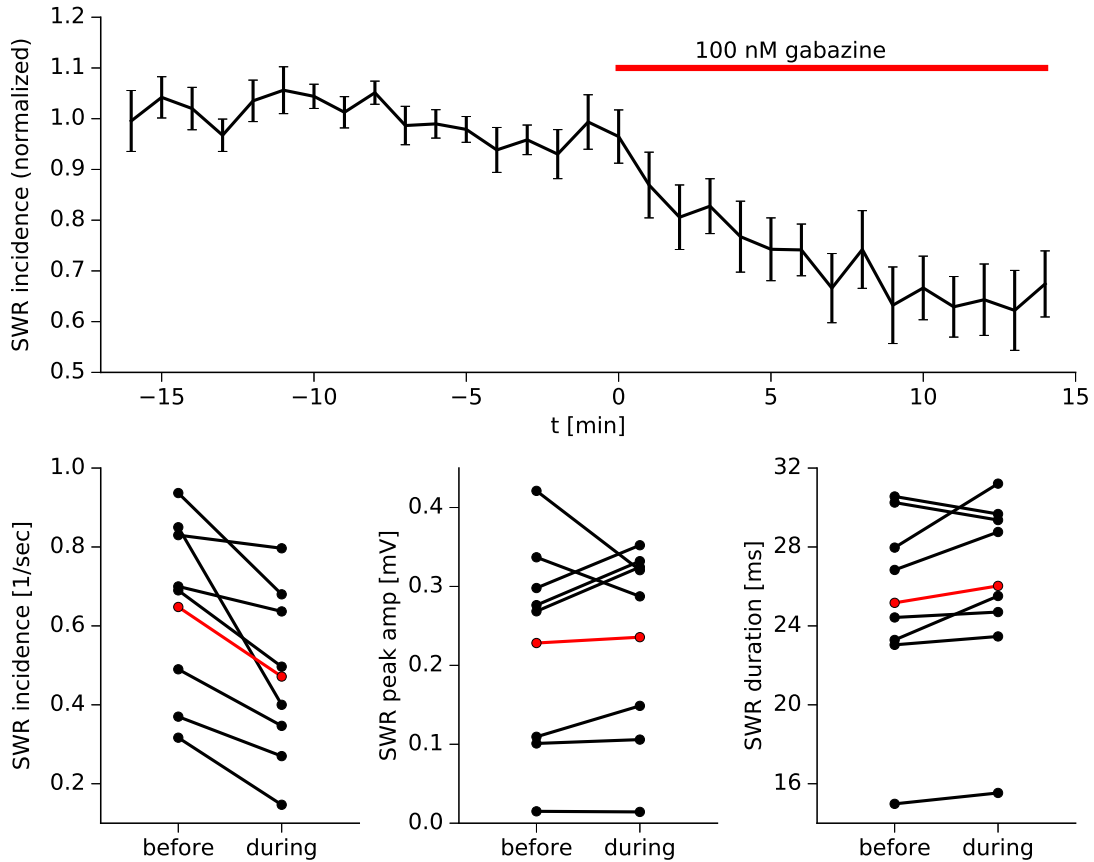


Figure 3.9: The GABA<sub>A</sub>R antagonist gabazine affects SWRs. **top:** SWR incidence in time aggregated from all recordings ( $n = 8$ ), where the incidence is normalized to 1 by dividing by the mean incidence from before the drug application. The red bar shows the time of drug application. **bottom:** The average SWR incidence, peak, and duration measured in 5-minute time windows before ( $[-7, -2]$  minutes) and during ( $[6, 11]$  minutes) gabazine application. Each slice is denoted with two black dots that are connected by a line. The red dots are the averages from all slices.

Gabazine decreased the incidence in all 8 slice recordings. In 6 slices the decrease was significant ( $p < 10^{-3}$ ). The average effect is shown in Figure 3.9, where the incidence is normalized (to value of 1 for the incidence 5 minutes prior to drug application). Gabazine starts affecting the incidence already 1 minute after application and takes around 5 minutes to take a full effect.

To better characterize how the drug affects the network dynamics, the further analysis focuses on the events in constrained time windows. Events from the window  $[-7, -2]$  minutes (before drug application) and  $[6, 11]$  minutes (after drug application) were used to calculate properties of SWs (Figure 3.9 bottom row). As already mentioned, there is a significant effect on the incidence (around 37% decrease on average). However, somewhat weaker effects are observed on the SWR peak amplitude and duration. On average, events tend to be larger after gabazine application, where 4 out of 8 recordings show significant ( $p < 0.002$ ) increase in SWR amplitude peak after the drug application, and 2/8 show a decrease in amplitudes. It is not known whether this increase in amplitudes is due to direct effects of gabazine or

### 3 Modulation of sharp-wave incidence

because of the decreased incidence, and thus, the longer recovery time.

The found effect of gabazine on the SWR amplitude is at odds with the finding of Schlingloff et al. (2014) who showed that a local puff of gabazine *in vitro* dramatically decreases the SWR amplitude around the application site. A possible explanation is that due to the large concentration of gabazine in the local application ( $10\text{ }\mu\text{M}$ ), the local inhibitory currents, which modulate the field potential in the stratum pyramidale (Schönberger et al., 2014), are totally suppressed, and thus the local amplitude is small.

Does gabazine have an effect on the serial correlation between consecutive SWR events? To answer this question, the serial correlations (peak-interval and interval-peak) were measured before and after drug application in 5-minute time windows as described above (Figure 3.10). While the peak-interval correlation remains low and does not change after the gabazine application, there is a trend of increase in the interval-peak correlation. Showing the relation between incidence and interval-peak correlation for individual recording (Figure 3.10, bottom panel) reveals the tendency of decreasing incidence and increased interval-peak correlations (6 out of 8 recordings).

In summary, gabazine has the counterintuitive effect of decreasing the incidence of SWRs. Moreover, gabazine application slightly increases the SWR amplitude and the serial correlation between inter-sharp-wave interval and the peak of the following SWR. Due to the small dataset (8 recordings), I can not present a conclusive evidence of the drug effects. However, it is interesting that decreasing the inhibitory synaptic transmission increases the peak of SWs in the pyramidal layer (6/8 slices, 4 of which significant). Ideas on how gabazine affects the generation of SWRs in the 3-population model are discussed in a greater detail in the Discussion (Section 3.4.1). In the following section, using numerical and analytical modelling, I study the effects of gabazine in a simpler 2-population model.

#### 3.3.3 Gabazine effects on sharp-wave incidence *in silico*

To better understand how gabazine affects the incidence of SWRs *in silico*, I deploy the assembly-sequence concept (described in Chapter 2) as a model for the spontaneously occurring SWs. Here, numerical simulations of balanced networks with embedded assembly sequences and a linear firing-rate model are used as tools to describe the network dynamics under the influence of gabazine.

In the numerical simulations, sequences of neural assemblies consisting of both excitatory and inhibitory neurons are embedded into a randomly connected network. Recurrent connectivity ( $p_{rc} = 0.08$ ) describes the connection probability within an assembly while a feedforward connectivity ( $p_{ff} = 0.06$ ) is the connectivity between the excitatory neurons of subsequent assemblies in the sequence (sketch of network connectivity is shown in Figure 2.1). With these parameters values, noise fluctuations in the firing rates get amplified by the feedforward structure resulting in spontaneous replays (Figure 2.4). For a more detailed description of the numerical model and the parameter values, please refer to Chapter 2.

The effects of gabazine are modeled by decreasing the conductances of the targeted inhibitory synapses by a fixed fraction. The network dynamics is stable when the conductances are decreased up to  $\sim 10\%$  from their original value, while a larger decrease leads to an epileptiform activity. In Figure 3.11, “*in-silico* gabazine” decreases the conductance of inhibitory synapses by 5%, a value which is likely to be smaller than the effect of  $100\text{ nM}$  in the experiments (Nimmrich et al., 2005).

Not surprisingly, *in-silico* gabazine drastically increased the rate of spontaneous replays of assembly sequences in the modelled network. This is illustrated in Figure 3.11, where

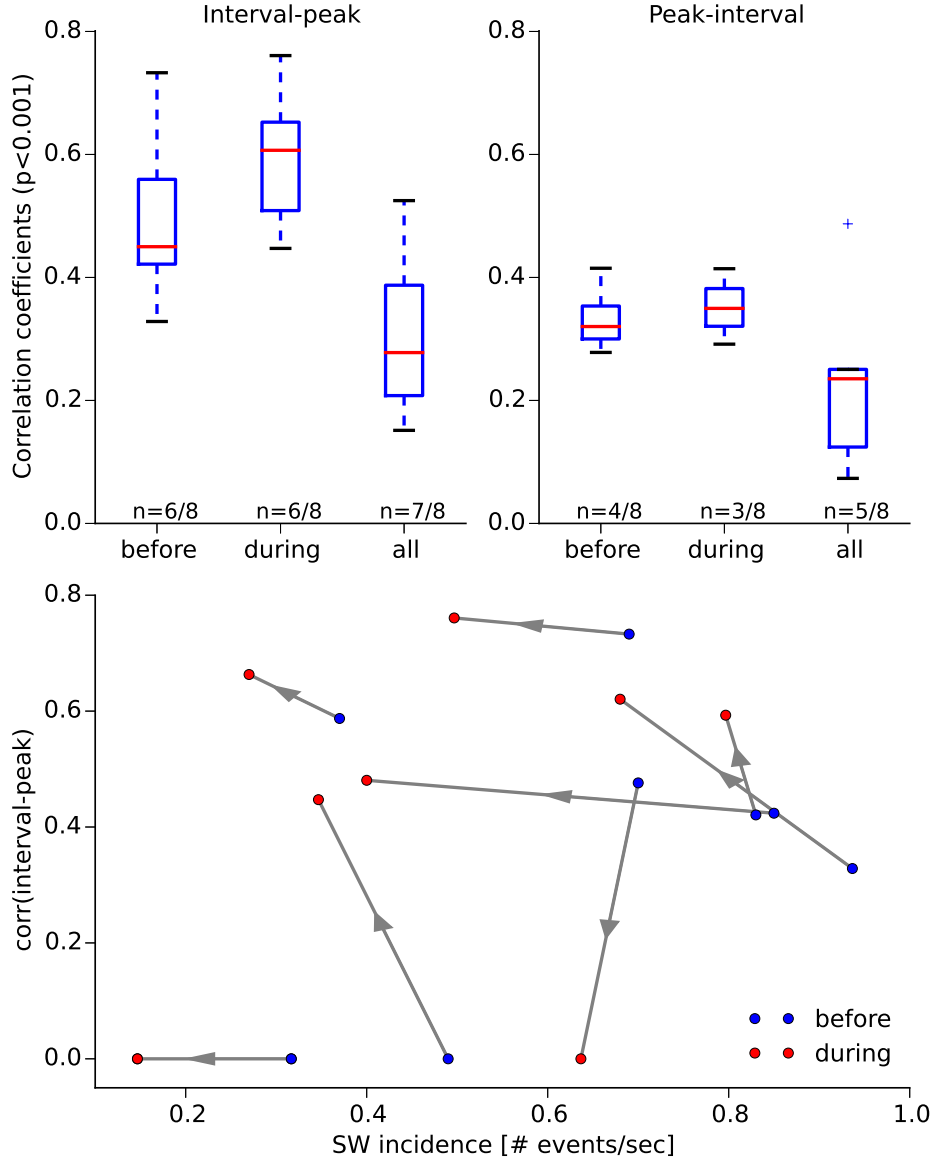


Figure 3.10: Gabazine effect on the serial correlations. **top:** Serial correlation before and during gabazine are calculated in 5-minute long time windows, where  $n$  shows the number of recordings with significant correlations ( $p < 0.001$ ) before gabazine application (before), during application (during), and aggregated data from a whole recording (all). **bottom:** Serial correlations coefficients between time interval since last event and the following SWR peak (interval-peak) are plotted against recorded incidence; arrows show the change after gabazine application. Insignificant correlations are considered to be 0.

### 3 Modulation of sharp-wave incidence

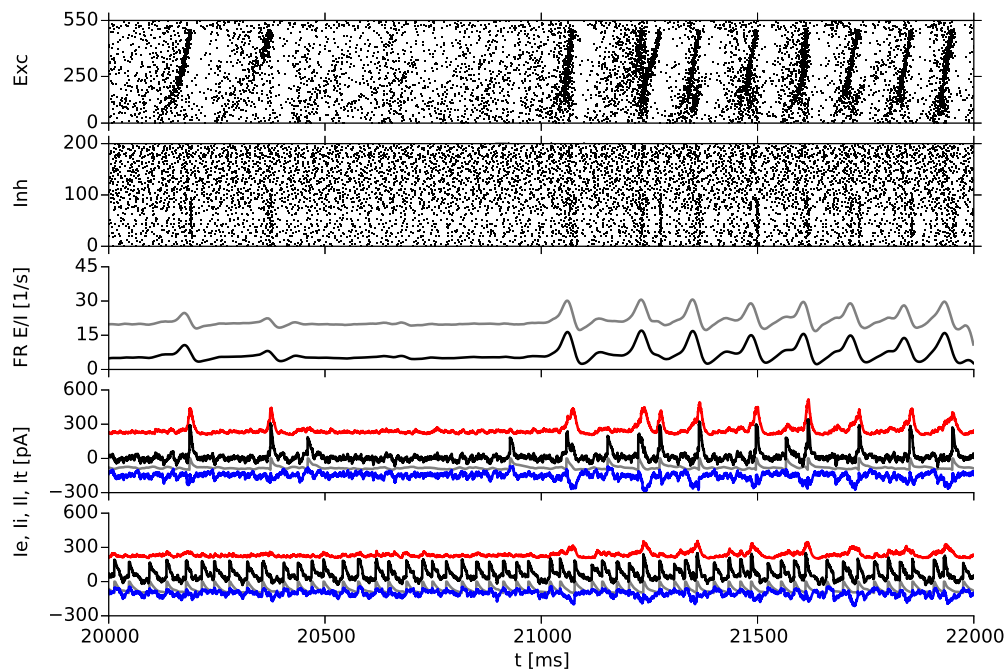


Figure 3.11: Gabazine *in silico* increases the rate of spontaneous replays. Decreasing all inhibitory conductances (at 21<sup>st</sup> second by 5%) leads to an increase in the incidence of spontaneous replays in balanced-network simulations. The two upper panels show raster plots of subpopulations of excitatory (Exc) and inhibitory (Inh) neurons, where each black dot denotes a spike. The middle plot shows the firing rate (FR) of the excitatory and inhibitory populations. The last two panels show the currents experienced by one excitatory and one inhibitory neuron. Red, blue, gray, and black colors denote excitatory ( $I_e$ ), inhibitory ( $I_i$ ), leak ( $I_{II}$ ), and total ( $I_t$ ) currents.

### 3.3 Results

gabazine is applied to all inhibitory synapses after the 21<sup>st</sup> second of the simulation. The top two panels show raster plots of example excitatory and inhibitory neurons; black dots show individual spikes, and black stripes are bursts of synchronous activity during which many neurons fire in close temporal proximity. The replays during these activity bursts are used as a model of the SWR events. The frequency of these population events is increased immediately after the simulated gabazine infusion, as seen in the number of replays (the top panel), and in the firing rates (third panel). This result is in direct opposition with the gabazine effects that are reported *in vitro* (Section 3.3.2).

Can a relatively simple two-populations balanced network explain the gabazine-associated decrease of SWR incidence reported in experiments? GABA<sub>A</sub>Rs are known to be complex channels with five subunits that can come in various combinations (for the curious readers, see Section 3.2.1). The expressed subunits largely determine the receptor properties, i.e., time constants, affinity to GABA and other neurotransmitters. For example tonic GABA<sub>A</sub>R are insensitive for gabazine (Bai et al., 2001; Yeung et al., 2003; Behrens et al., 2007) at low concentrations while phasic GABA<sub>A</sub>Rs show various affinities depending on the subunit expression. The subunit expression is largely determined by the type of the postsynaptic neuron and by the location of the channels on the morphological tree (Sieghart and Sperk, 2002). One hypothesis to explain the gabazine-associated decrease of SWR events relies on the assumption that gabazine has differential effects on the different GABA<sub>A</sub> synapses. And more specifically, if inhibitory-to-inhibitory synapses are affected to a larger degree than the inhibitory-to-excitatory synapses, one would expect a network that is less disinhibited, and thus, the excitatory population receives more inhibition resulting in smaller firing rates. In what follows, I test whether such assumptions would really decrease the incidence of modeled events.

As a toy example in numerical simulation, I consider the extreme case where gabazine affects the inhibitory-to-inhibitory synapses only. *In-silico* gabazine indeed decreases the firing rate of the excitatory neurons (Figure 3.12, top panel). However, the network shows also a decrease in the firing rate of the inhibitory population as well. How is it possible that excitatory neurons receiving weaker inhibition (smaller input from inhibitory population), fire less? To better understand the effects of gabazine, further, I present an analytical approach.

To capture the dynamics of the simulated network, I apply a linear model to a two-population balanced network and analyse how the firing rates depend on gabazine. The network dynamics is described by a system of differential equations:

$$\begin{aligned}\tau \frac{dr^E}{dt} &= -r^E + w_{ee} r^E - w_{ei} r^I + I_0 \\ \tau \frac{dr^I}{dt} &= -r^I + w_{ie} r^E - w_{ii} r^I + I_0\end{aligned}\tag{3.1}$$

where the notation is as in Chapter 2.  $r^E$  and  $r^I$  are excitatory and the inhibitory firing rates, respectively. The connection from populations  $x$  to  $y$  is described by a dimensionless connection weight variable  $w_{yx}$  ( $x, y = e, i$ ). The population time constant is  $\tau$ , and the external input to the populations is denoted with  $I_0$ .

Assuming that the network is in a steady state, then the rates are constant, i.e.,  $\frac{dr^E}{dt} = 0$

### 3 Modulation of sharp-wave incidence

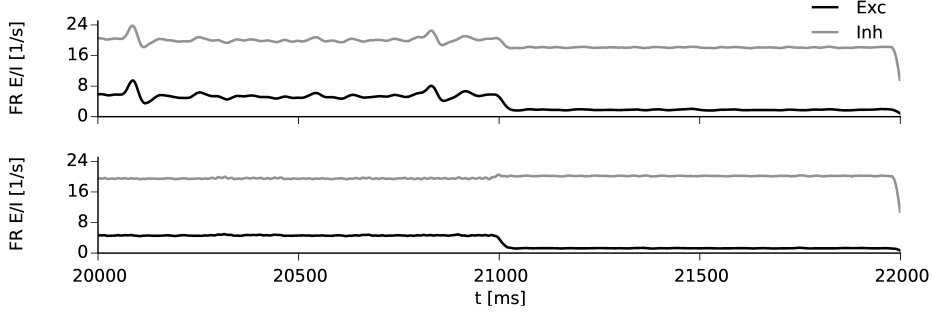


Figure 3.12: Gabazine *in silico* applied only to inhibitory-to-inhibitory synapses decreases the rate of spontaneous replays. **top:** Spontaneous replays occur during the peaks of the excitatory and inhibitory firing rates. Decreasing the inhibitory-to-inhibitory conductances (at 21<sup>st</sup> second by 5%) decreases the firing rates and abolishes the spontaneous replays in balanced-network simulations. **bottom:** Gabazine applied only on inhibitory-to-inhibitory synapses can result in decrease of excitatory and increase of inhibitory firing rates, when excitatory-to-excitatory synapses are very weak in comparison to all other synapses. Here  $g^{EE} = 0$ .

and  $\frac{dr^I}{dt} = 0$ . In this condition, one can express the stationary solution:

$$\begin{aligned} r^E &= \frac{(1 + w_{ii} - w_{ei})}{w_{ie}w_{ei} - (1 + w_{ii})(-1 + w_{ee})} I_0 \\ r^I &= \frac{(1 + w_{ie} - w_{ee})}{w_{ie}w_{ei} - (1 + w_{ii})(-1 + w_{ee})} I_0 \end{aligned} \quad (3.2)$$

To estimate how the gabazine-induced decrease of inhibitory connections affects the firing rates, we can look at the derivatives of the steady-state rates in respect to the gabazine concentration  $c_{gbz}$ :

$$\frac{\partial r^E}{\partial c_{gbz}} = \frac{\partial r^E}{\partial w_{ei}} \cdot \frac{\partial w_{ei}}{\partial c_{gbz}} + \frac{\partial r^E}{\partial w_{ii}} \cdot \frac{\partial w_{ii}}{\partial c_{gbz}} \quad (3.3)$$

and

$$\frac{\partial r^I}{\partial c_{gbz}} = \frac{\partial r^I}{\partial w_{ei}} \cdot \frac{\partial w_{ei}}{\partial c_{gbz}} + \frac{\partial r^I}{\partial w_{ii}} \cdot \frac{\partial w_{ii}}{\partial c_{gbz}}. \quad (3.4)$$

The partial derivatives of inhibitory weights ( $w_{ei}$  and  $w_{ii}$ ) in respect to the drug concentration  $c_{gbz}$  is negative due to the antagonist effects of gabazine. The partial derivatives of the rates in respect to the inhibitory weights can easily be estimated from Equation 3.2:

$$\begin{aligned} \frac{\partial r^E}{\partial w_{ii}} &= I_0 \frac{w_{ei}(1 + w_{ie} - w_{ee})}{D^2} \\ \frac{\partial r^I}{\partial w_{ii}} &= I_0 \frac{(-1 + w_{ee})(1 + w_{ie} - w_{ee})}{D^2} \end{aligned} \quad (3.5)$$

$$\begin{aligned} \frac{\partial r^E}{\partial w_{ei}} &= I_0 \frac{-(1 + w_{ii})(1 + w_{ie} - w_{ee})}{D^2} \\ \frac{\partial r^I}{\partial w_{ei}} &= I_0 \frac{-w_{ie}(1 + w_{ie} - w_{ee})}{D^2} \end{aligned} \quad (3.6)$$

### 3.3 Results

where  $D = w_{ie}w_{ei} - (1 + w_{ii})(-1 + w_{ee})$ .

If we now assume that gabazine has the same effect on all inhibitory synapses, i.e.,  $\frac{\partial w_{ei}}{\partial c_{gbz}} = \frac{\partial w_{ii}}{\partial c_{gbz}}$ , and substitute Equations 3.5 and 3.6 in 3.3 and 3.4, the change of firing rate due to gabazine is:

$$\begin{aligned}\frac{\partial r^E}{\partial c_{gbz}} &= \frac{\partial w_{ii}}{\partial c_{gbz}} \cdot I_0 \frac{-(1 + w_{ii} - w_{ei})(1 + w_{ie} - w_{ee})}{D^2} = -\frac{\partial w_{ii}}{\partial c_{gbz}} \cdot \frac{r^E r^I}{I_0} > 0 \\ \frac{\partial r^I}{\partial c_{gbz}} &= \frac{\partial w_{ii}}{\partial c_{gbz}} \cdot I_0 \frac{-(1 + w_{ie} - w_{ee})^2}{D^2} = -\frac{\partial w_{ii}}{\partial c_{gbz}} \cdot \frac{r^I r^I}{I_0} > 0.\end{aligned}\quad (3.7)$$

In line with the simulations, the derivatives above are always positive (if  $\frac{\partial w_{ii}}{\partial c_{gbz}} < 0$ ), i.e., gabazine always increases the rate of both excitatory and inhibitory populations.

Can this simple linear model capture the simulation results in which gabazine affects only inhibitory-to-inhibitory synapses? There we saw a decrease not only in the excitatory but also in the inhibitory firing rates (Figure 3.11, bottom panel). Taking the rate derivatives with respect to  $w_{ii}$  only (in Equations 3.3 and 3.4, we assume that  $\frac{\partial w_{ei}}{\partial c_{gbz}} = 0$ ), we obtain:

$$\begin{aligned}\frac{\partial r^E}{\partial c_{gbz}} &= \frac{\partial w_{ii}}{\partial c_{gbz}} \cdot I_0 \frac{w_{ei}(1 + w_{ie} - w_{ee})}{D^2} \\ \frac{\partial r^I}{\partial c_{gbz}} &= \frac{\partial w_{ii}}{\partial c_{gbz}} \cdot I_0 \frac{(-1 + w_{ee})(1 + w_{ie} - w_{ee})}{D^2}.\end{aligned}\quad (3.8)$$

Here, the term  $1 + w_{ie} - w_{ee}$  determines the change of excitatory firing rate. As the connection weights are proportional to the conductances (e.g.,  $w_{ee} \propto g_{ee}$ , see Chapter 2 for details), and the excitatory conductances used in the simulations are all equal  $g_{ee} = g_{ie}$ , one can see that  $1 + w_{ie} - w_{ee} > 0$ . In that case, it is easy to see that  $\frac{\partial r^E}{\partial c_{gbz}} < 0$ , meaning that excitatory rate decreases when  $w_{ii}$  is depressed. This line of arguments is supported by the simulations, where gabazine applied only to the inhibitory-to-inhibitory connections decreases the excitatory firing rate (Figure 3.12). On the other hand,  $r^I$  shows more interesting behaviour that depends on the excitatory weights. For intermediate values  $w_{ee} \in (1, 1+w_{ie})$ , the inhibitory rate decreases during gabazine application as well (as seen in Figure 3.12, top panel). For values of  $w_{ee}$  outside of this interval, one would expect increase of inhibitory firing after the drug infusion. As a proof of concept, networks with  $g_{ee} = 0$  nS show that the inhibitory firing rate goes up after the simulated drug application (Figure 3.12, bottom panel).

To summarize the results from this section, by using numerical simulations and a linear analytical description, I showed that in a balanced network a gabazine application is increasing the firing rates of both inhibitory and excitatory populations if all inhibitory synapses are similarly affected by the drug. This increase of firing leads to a higher incidence of spontaneous replays, which is in odds with the decrease of SWR incidence observed *in vitro*. Therefore, I tested whether a differential effect of gabazine on different synapses can explain the experimental results. I considered the extreme case when gabazine affects only inhibitory-to-inhibitory synapses and showed that in this case the firing rate of the excitatory population can decrease. This result suggests that a stronger effect of gabazine on the inhibitory-to-inhibitory synapses can explain the decreased SWR incidence after gabazine application *in vitro*.

Here I examine a minimal model consisting of only two populations, which can neverthe-

### 3 Modulation of sharp-wave incidence

less provide some means for studying *in-vitro* models. A similar approach can also be applied to the more accurate 3-population nonlinear model currently developed by Roberta Evangelista, and utilized to examine in what conditions gabazine decreases the network excitability. Is it possible that in the 3-population model, a gabazine application to all inhibitory synapses can decrease the rate of spontaneous events? Or would it be required that the disinhibitory synapses (from PVBC to the mysterious inhibitory neurons) are affected to a larger degree?

A strong assumption in the foundation of the current framework is that the decrease of SWR incidence is due to a decrease of firing of the excitatory population. Whether this is indeed the case can be tested in *in-vitro* experiments. It is also not known how gabazine affects the firing of the inhibitory populations. Numerical and analytical results show that gabazine applied only on the inhibitory-to-inhibitory connections can decrease not only the excitatory but also the inhibitory firing rates. This result is interesting by its own as it demonstrates that intuitive interpretations of a relatively simple model can be misleading and should be used with caution.

#### 3.3.4 Involvement of GABA<sub>B</sub> receptors in sharp-wave ripples

SWRs are huge population events where the vast majority of interneurons are firing with increased rates, and single interneurons often fire multiple times during the event (Klausberger, 2009; Hájos et al., 2013). It has been shown that the repetitive firing of interneurons can activate extrasynaptic GABA<sub>B</sub>Rs, possibly through increased concentrations of ambient GABA in the extracellular space (Scanziani, 2000; Wang et al., 2010). The inhibition from GABA<sub>B</sub>Rs is relatively slow, lasting several hundreds of milliseconds, which is close to the time scale of the typical inter-SWR intervals. Here, I study the possibility that the relatively long time intervals between SWR events are determined by GABA<sub>B</sub>Rs.

First, to investigate whether GABA<sub>B</sub>Rs are involved in the SWR incidence in the *in-vitro* model, I analysed extracellular recordings where the GABA<sub>B</sub>R antagonist SCH50,911 (further referred as SCH) was applied in slices. The number of analysed slices is 12 (see the Methods section). An example of the SCH effects in a slice is shown in Figure 3.13. The drug affects the network dynamics already during the first minute of application by increasing the incidence of spontaneous SWRs (Figure 3.13, top panel). An independent two-sample t-test of the incidence (measured as number of events per sweep in confined 5-minute time intervals) shows a significant increase of incidence ( $p$ -value  $< 10^{-7}$ ). Other main properties, such as peak amplitude and duration are decreased after SCH application ( $p$ -values  $< 10^{-10}$ , and  $< 10^{-3}$ , respectively).

Blocking the GABA<sub>B</sub>Rs resulted in increase of the average incidence of spontaneous SWRs from all slices ( $\sim 50\%$  on average). The drug effects are visible already in the first minute after the application and saturate around 2-3 minutes later (Figure 3.14, top panel). To better assess the effects of SCH, further, the analysis focuses on the events in 5-minute long time windows, i.e., in the intervals  $[-5, 0]$  minutes, that is before and  $[2, 7]$  minutes, that is during drug application. Comparing the data from these two intervals shows that SCH increases the incidence in every recording (10/12 show a significant increase; independent 2-sample t-test,  $p < 2 \cdot 10^{-3}$ ). On average, SCH resulted in a decrease of SWR peak amplitudes (Figure 3.14, bottom middle panel), where 6/12 slices show a significant decrease ( $p < 10^{-3}$ ), and in 2/12 slices the amplitudes were increased ( $p < 10^{-3}$ ). The SWR duration also decreased on average, but this change is not significant ( $p > 0.01$  in 11/12 slices). While the result for every recording varies depending on the exact 5-minute time windows that are used for the analysis, the summary results do not change qualitatively.

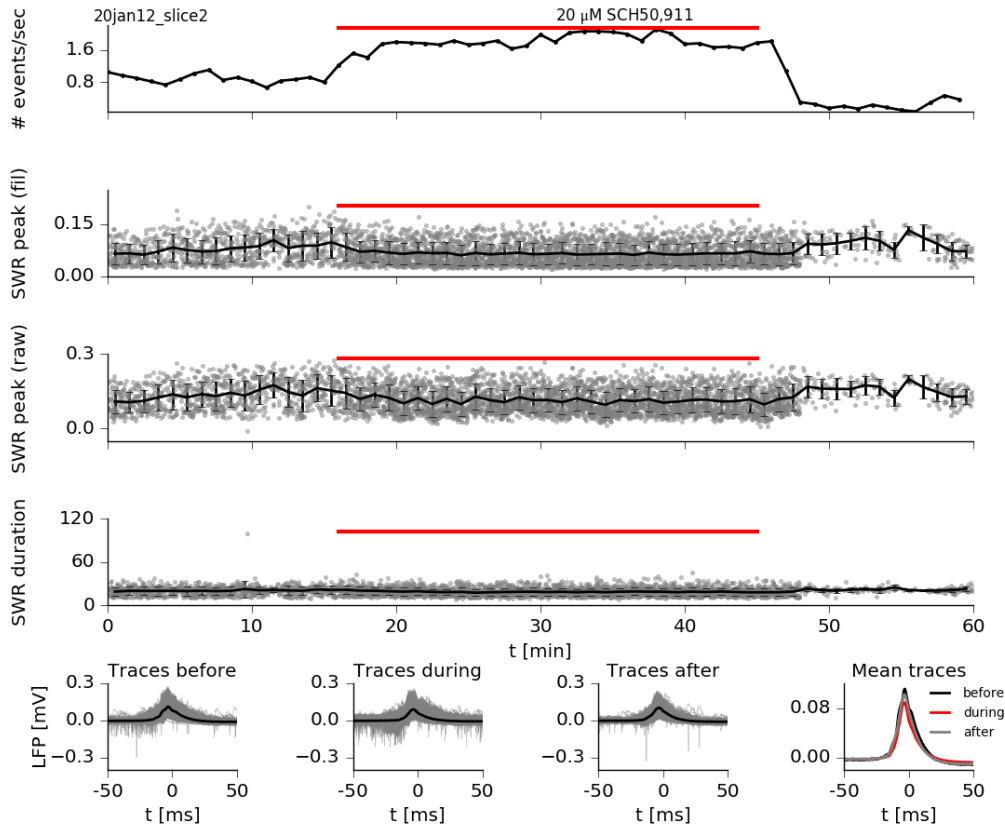


Figure 3.13: Extracellular recording from the pyramidal layer of CA3 area where the GABA<sub>B</sub>R antagonist SCH50,911 is applied to a hippocampal slice. The time of drug application is denoted with a horizontal red bar. The top panel shows the SWR incidence in time with a minute time resolution. The two panels below show the SWR peaks amplitude, where “fil” and “raw” stand for band-passed filtered ( $\sim 5 - 50$  Hz, for details see the Methods section) and raw voltage traces, respectively; units are in mV. The gray dots represent single events, and the black lines represent the mean and the standard deviation of the amplitude peak in a minute time window. Analogously, the forth panel shows the SWR duration in milliseconds. The panels on the bottom row show all events before, during, and after drug application overlaid in gray, and the mean wave-forms are in black. The right-most panel shows a comparison between the mean events from before and during SCH application.

### 3 Modulation of sharp-wave incidence

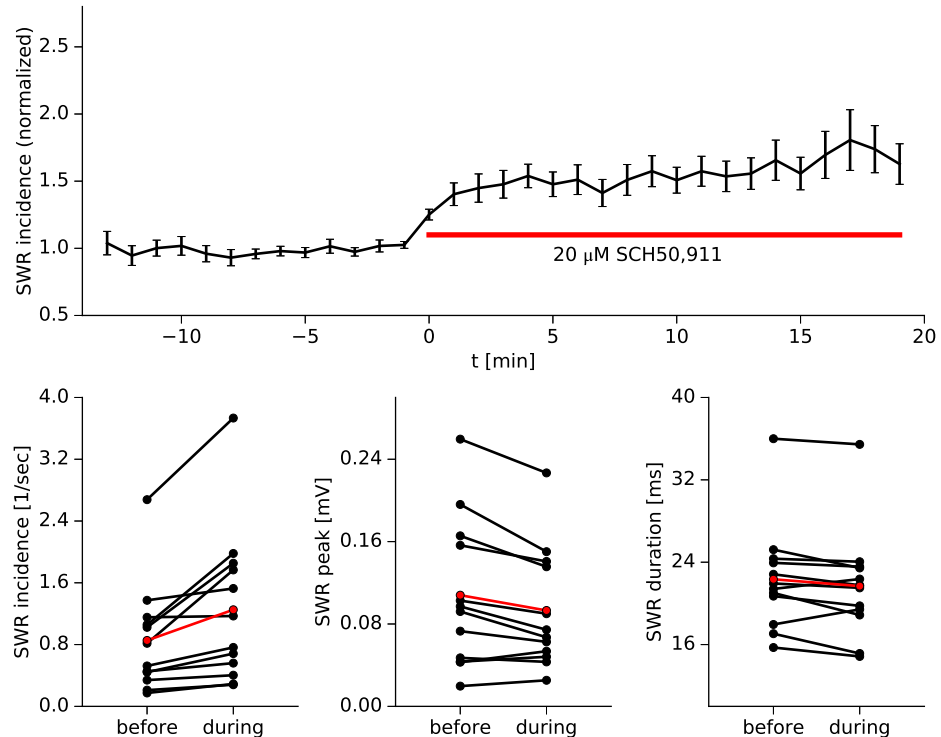


Figure 3.14: The GABA<sub>B</sub>R antagonist SCH50,911 affects SWRs. **top:** SWR incidence in time aggregated from all recordings ( $n = 12$ ), where the incidence is normalized to 1 by dividing by the mean incidence before the drug application. The red bar shows the time of drug application. **bottom:** The average SWR incidence, peak and duration measured in 5-minute time windows before ( $[-5, 0]$  minutes) and during ( $[2, 7]$  minutes) SCH application for each slice are denoted with black dots. The red dots are the averages from all slices.

### 3.3 Results

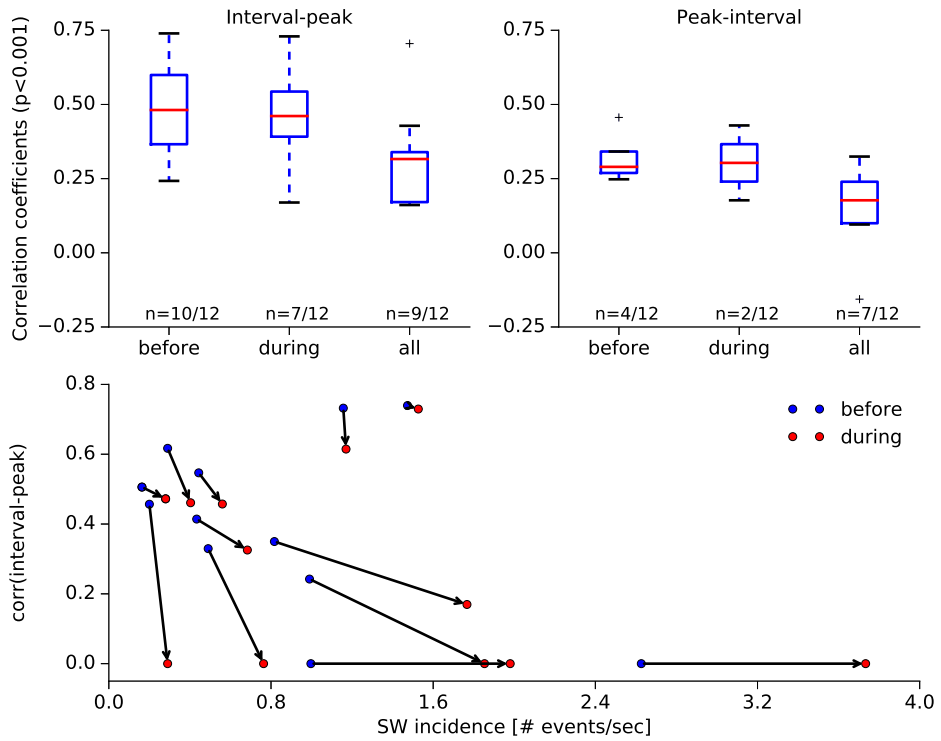


Figure 3.15: GABA<sub>B</sub>R antagonist SCH50,911 effect on the serial correlations. **top:** Serial correlation before and during SCH are calculated in 5-minute long time windows, where  $n$  shows the number of recordings with significant correlations ( $p < 0.001$ ) before SCH application (before), during application (during), and aggregated data from the whole recording (all). **bottom:** Serial correlations coefficients between time interval since last event and the following SWR peak are plotted against recorded incidence; arrows show the change after SCH application.

Next, I inquire whether blocking GABA<sub>B</sub>Rs affects also the serial (interval-peak) correlation between events. At first glance the pooled data does not reveal any change in the correlations, as the correlation distributions from before and during SCH application (Figure 3.15, top panels) are statistically similar. However, looking at the effects in the individual recordings (Figure 3.15, bottom panel) one can see that there is a decrease of serial correlation after drug application in 10 out of 12 slices (the 2 remaining recordings show no significant correlations).

To summarize the findings above, GABA<sub>B</sub>Rs are taking part in the SWR modulation. In contrast to previous reports (i.e., Hollnagel et al., 2014; Hofer et al., 2015), the analysed data shows that GABA<sub>B</sub>R antagonist (SCH50,911) increases the incidence of spontaneous SWR events. However, due to the small increase in incidence ( $\sim 50\%$ ), the GABA<sub>B</sub>R is not the only factor controlling the time between events as hypothesized initially. This result suggests that there are other mechanisms different than GABA<sub>B</sub> that act on slow time scales and are involved in controlling the incidence. Moreover, application of the GABA<sub>B</sub>Rs antagonist results in a decrease of the SWR peak amplitudes and in a decrease in the serial correlations between interval and peaks. To investigate how do GABA<sub>B</sub>Rs influence the SWR incidence, it is worth having a closer look at the possible involvement of the different GABA<sub>B</sub>Rs.

### 3 Modulation of sharp-wave incidence

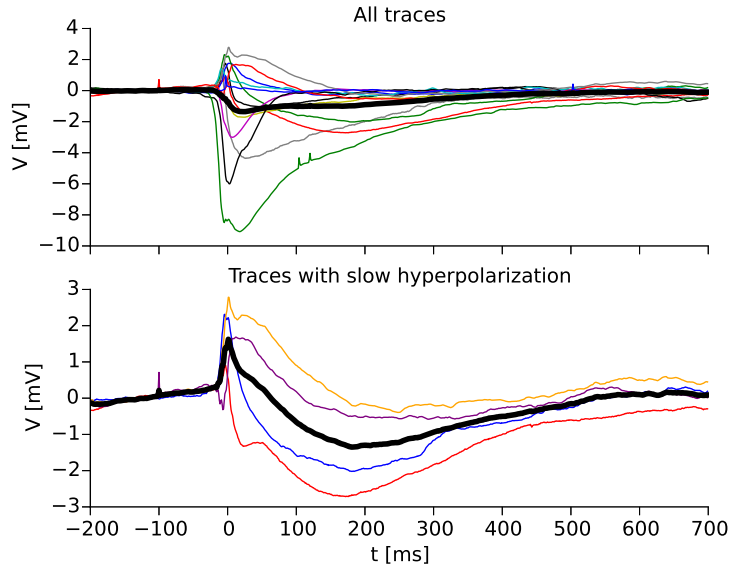


Figure 3.16: Patch-clamp recordings from pyramidal cells during SWRs. **top:** Mean voltage traces associated to SWRs from each slice are color coded; the thick black line is the mean of the means. **bottom:** Mean voltage traces of cells that show slow, possibly GABA<sub>B</sub>R-mediated hyperpolarization (4/13 cells). Membrane potentials are normalized by subtracting the mean depolarization in a 200-millisecond interval preceding the event.

#### 3.3.5 Role of postsynaptic GABA<sub>B</sub> receptors

It is been shown that a repetitive firing of certain interneurons can evoke slow and strong inhibition due to activation of postsynaptic or extrasynaptic GABA<sub>B</sub>Rs on pyramids (Scanziani, 2000; Gassmann and Bettler, 2012). As SWRs are population events that recruit many neurons, and especially the perisomatic targeting interneurons (Klausberger, 2009; Hájos et al., 2013), it is likely that ambient GABA in this region is increased (Hollnagel et al., 2014; Lang et al., 2014). Next, I ask whether GABA<sub>B</sub>Rs located postsynaptically on pyramidal cells are indeed activated after SWs, and whether they play any role in the modulation of SWs. To test this hypothesis, here I analyse data from simultaneous (paired) extracellular and intracellular recordings (kindly sponsored by Nikolaus Maier) performed in the stratum pyramidale of the hippocampal CA3 area and a pyramidal cell in the CA3, respectively. By averaging the intracellular traces across events, we can see that pyramidal cells exhibit a rich membrane potential dynamics during SWR events, with various combination of depolarization and hyperpolarization (Figure 3.16, top panel). A slow, possibly GABA<sub>B</sub>R-mediated hyperpolarization is present in a few recordings, but is not visible in the average trace from all cells (Figure 3.16, top panel, thick black line). In the recordings that show a slow hyperpolarization (4 out of 13 cells, Figure 3.16, bottom panel) the trough in the membrane potential is around 200 ms after the population event and lasts for about 500 ms. Interestingly, one recording reveals well-pronounced slow as well as fast inhibition (red trace).

Is the slow hyperpolarization correlated in any way with the amplitude of the SWs? To test this, I separated the events in each recording in two groups: big and small events, i.e., the 30% largest SWR peaks and 30% smallest events, respectively. Plotting the mean intracellular trace during small and big events, shows that the SWs with larger amplitudes are associated with larger hyperpolarization (Figure 3.17, top panel). Interestingly, the mean

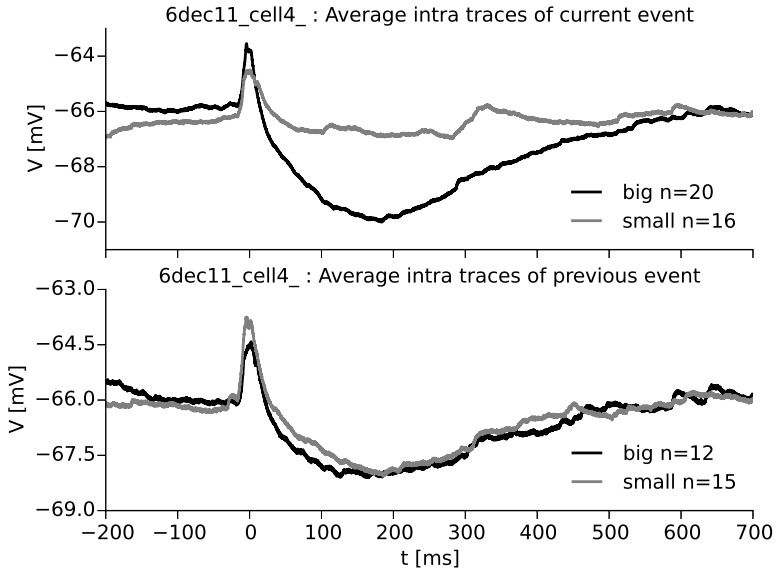


Figure 3.17: Sharp-waves ripples with larger peak amplitudes evoke stronger hyperpolarization. **top:** Big events (30 % of the largest SWR events) are associated with a well-pronounced slow hyperpolarization. Smaller events (30% of the smallest SWRs) did not evoke a GABA<sub>B</sub>-associated response. The difference of membrane potentials prior to events is a recording artifact (see the Methods section). **bottom:** There is no correlation between the depolarisation of a cell and the peak amplitude of the following SWR event.

traces before big and small events are virtually indistinguishable (Figure 3.17, bottom panel), suggesting that the amount of hyperpolarization does not determine the size of the following event. This result holds for all four recordings that exhibit slow inhibition in the membrane potential.

Moreover, the slow hyperpolarization does not affect the time interval until the following event (not shown here). There is a correlation between the inter-SWR interval and the amplitude of the following hyperpolarization, which is expected given the fact that longer intervals are followed by larger SWs, and thus, larger hyperpolarization.

The last recording data of intracellular and extracellular recordings reveals that slow, possibly GABA<sub>B</sub>-mediated hyperpolarization occurs in a fraction of the CA3 pyramidal neurons *in vitro*. The magnitude of the received inhibition is not correlated with the size or the time interval until the next event. Therefore, intracellular recordings suggest that the time interval between events is not controlled by the postsynaptic GABA<sub>B</sub>Rs on pyramids.

## 3.4 Discussion

In this chapter I analysed the serial correlations between sharp-wave ripple events measured in the stratum pyramidale of CA3 area in hippocampal slices. To briefly summarize, the results reveal a strong correlation between time interval since the last event and the peak amplitude of the following SWR (significant correlation in 18/20 slices, mean correlation  $\sim 0.4$ ). On the other hand, there is a lower serial correlation between the events size and the time interval (significant positive correlation in 7/20 slices, significant negative correlation in 2/20 slices, mean correlation  $\sim 0.2$ ) until the following event. There isn't a locality of the

### *3 Modulation of sharp-wave incidence*

SWR events because multi-electrode array recordings revealed that SWR peak amplitudes are a non-local phenomenon, and a large SWR measured at one location is likely to be large in the whole CA3 region.

Application of the GABA<sub>A</sub>R antagonist gabazine decreased the incidence of SWRs (in agreement with Nimmrich et al., 2005). Moreover, gabazine increased the size of SWR events measured in stratum pyramidale (significant change in 4/8 slices), and increased the interval-peak serial correlations.

In contrast to previous reports (i.e., Hollnagel et al., 2014; Hofer et al., 2015), here I showed that the GABA<sub>B</sub>R antagonist SCH50,911 increased the incidence of spontaneous SWR events (10/12 slices). On average, the SCH50,911 application resulted in a decrease of SWR amplitudes (significant decrease in 6/12; significant increase in 2/12 slices) and in a decreased interval-peak correlation. Moreover, intracellular recordings suggested that the time interval between events is not controlled by postsynaptic GABA<sub>B</sub>Rs on pyramids due to the absence of a correlation between the slow hyperpolarization and the inter-event interval.

The results above do not reveal the mechanisms controlling the generation of SWRs, but provide some insights about the possible circuitry, which are discussed in detail in what follows.

#### **3.4.1 Hypotheses on how gabazine affects sharp-wave ripples**

It has been shown that gabazine, which is a GABA<sub>A</sub>R antagonist, leads to a lower incidence of SWRs. Here, I give an interpretation of the counterintuitive result that a reduction of inhibition leads to a reduction of SWR incidence.

#### **Hypothesis on how gabazine affects sharp-wave amplitude**

An interesting observation is that the application of gabazine tends to increase the amplitudes of the field potential measured in stratum pyramidale during SWRs. Similarly, Steidl et al. (2006) reported increase of the stimulus-evoked field potential in the pyramidal layer after the application of 500 nM gabazine, while no significant changes were observed in other layers. The field potential in the pyramidal layer is dominated by inhibitory synaptic currents (Schönberger et al., 2014), most likely from the fast local perisomatic synapses (Ylinen et al., 1995). Therefore, I conclude that although gabazine decreases the unitary (i.e., single spike activated) postsynaptic currents, there is an increase in the firing rate of perisomatic-targeting interneurons, resulting in a net increase of inhibitory currents during a SWR. The exact identity of these neurons is to be found. Because the parvalbumin-positive basket cells (PVBCs) are among the most active interneurons during SWRs, and their projections to the pyramidal cells (PCs) are located in the pyramidal cell layer (where the recordings are performed), further, I assume that PVBC are among the cells with increased firing rate.

#### **Hypothesis on how gabazine affects sharp-wave incidence**

In the numerical simulations of the 2-population network model, the spontaneous replay of assembly sequences was used as a model for SWRs. As intuitively expected, decreasing all inhibitory conductances in the balanced network led to an increase of replay incidence. However, a differentiated role of gabazine on the inhibitory-to-excitatory (I-to-E) and I-to-I synapses in the simulations could replicate the original gabazine experiment. More specifically, if I-to-I synapses are affected to a larger degree than the I-to-E synapses, then

### 3.4 Discussion

the incidence of spontaneous bursts is decreased. Currently, it is not clear whether the same argument can be applied to the 3-population hypothesis (see Section 3.2.4). It may be possible that a “gabazine application” to all inhibitory synapses can decrease the rate of spontaneous events in the non-linear 3-population model. A detailed mathematical analysis, similar to the one presented in Section 3.3.3 could answer these questions.

The hypothesised increased firing of the perisomatic-targeting interneurons, as discussed above, can decrease the SWR incidence through two major pathways. First, repetitive firing of an interneuron can lead to excess of GABA at the synaptic cleft, leading to a diffusion into the extracellular space (Farrant and Nusser, 2005). The ambient GABA can then (i) activate the tonic GABA<sub>A</sub>Rs that are especially sensitive to GABA (Semyanov et al., 2004), or (ii) activate GABA<sub>B</sub>Rs at the pyramidal cell bodies (Scanziani, 2000). Both of these extrasynaptic receptor types are slow in comparison to phasic inhibition and can keep cells hyperpolarized for longer time intervals, which are in the order of the inter-event time intervals.

The two pathways can explain why gabazine and thiopental, which have opposite effects on the inhibitory transmission, result in a similar SWR modulation. Both drugs lead to diffusion of GABA to the extrasynaptic GABAergic receptors. For example, larger concentrations of gabazine (5 μM) applied to hippocampal slices lead to a persistent hyperpolarization of the pyramidal cells of ~ 9 mV below the membrane potential measured in control conditions (Behrens et al., 2007). It is not known whether this is the case with the lower gabazine concentrations in the SWR model analysed here, but this effect can be tested experimentally. Intracellular recordings can reveal whether small concentrations of gabazine (~ 100 nM) also lead to a persistent hyperpolarization. If this is the case, an additional local application of a tonic GABA<sub>A</sub>R antagonist (e.g., DPP-4-PIO; Boddu et al., 2014) or a GABA<sub>B</sub>R antagonist could reveal the identity of the involved extrasynaptic receptors. In a “reversal experiment”, if a GIRK-channel blocker applied after the gabazine reverses the SWR incidence to a control level, it would be a hint that gabazine modulates SWRs through activation of postsynaptic GABA<sub>B</sub>Rs. Or in an “occlusion experiment” for example, if gabazine does not affect the incidence in slices with already bocked tonic GABA<sub>A</sub>R, it would suggest that the tonic GABA<sub>A</sub>R are involved.

The other major mechanism explaining SWR incidence modulation is in line with the numerical and analytical analysis (see Section 3.3.3) of gabazine affecting the disinhibitory pathway to a larger degree compared to the inhibitory pathway on PCs. On the one hand, due to its antagonist properties, gabazine decreases the efficacies of the PVBC-mIN synapses. On the other hand, the increased spiking of PVBC during events would lead to a stronger short-term depression on the PVBC-mIN synapses compared to control conditions. Both mechanisms could contribute to the elevation of the mINs firing rate, and thus, to the increase of dendritic inhibition on pyramidal neurons after drug application. The plausibility of gabazine affecting the disinhibitory pathway can be tested experimentally, once the mIN population is identified.

#### Hypothesis on how gabazine affects the serial correlations

What is the mechanism of the observed gabazine-mediated increase of the interval-peak correlations in the majority of slices? This observation is puzzling: for a decreased incidence, one would expect decreased correlations because of the longer time for synaptic recovery from STD. However, the hypothesised higher firing rate of PVBCs (after gabazine) leads to a stronger synaptic depression, and thus, to a longer recovery time of the PVBC afferent

### 3 Modulation of sharp-wave incidence

synapses (PVBC-PC, particularly). This implies that in ‘control’ *in-vitro* experiments, the STD after SWR events is not saturated to its maximal value.

#### Other mechanisms

Up to this point, it has been considered that gabazine targets exclusively the GABA<sub>A</sub>Rs. However, it has been shown that gabazine (as well as bicuculline) blocks also the glycine receptors (Wang and Slaughter, 2005; Li and Slaughter, 2007). Glycine receptors are ionotropic inhibitory receptors that (upon activation) produce chloride flow into the cell membrane. They are present in the hippocampus in smaller quantities relative to other brain areas (van den Pol and Gorcs, 1988) and cluster around the inhibitory synapses on pyramidal cells and interneurons (Lévi et al., 2004). Whether the incidence of SWRs is influenced by gabazine blocking the glycine receptors can be tested in experiments. In particular, does the application of a glycine receptor antagonist occlude the effect of gabazine or bicuculline?

#### 3.4.2 Hypothesis on how GABA<sub>B</sub> receptors influence the sharp-wave incidence

Currently, it is not known through what mechanisms the GABA<sub>B</sub>Rs influence the SWR incidence. In contrast to previous reports (e.g., Hollnagel et al., 2014; Hofer et al., 2015), the slice recordings analysed here showed a significant increase of SWR incidence after application of the GABA<sub>B</sub>R antagonist SCH50,911. On the other hand, agonists of GABA<sub>B</sub>R led to a decrease of SWR incidence (Maier et al., 2012; Hollnagel et al., 2014). Five different GABA<sub>B</sub>R-mediated pathways can explain these results in the framework of the phenomenological 3-population model.

- **Postsynaptic GABA<sub>B</sub>Rs on PCs.** A possible location of GABA<sub>B</sub>R is on the postsynaptic sites on pyramidal cells. It is been shown that the activation of these receptors leads to slow IPSPs with high amplitudes in CA3 principal cells (Knowles et al., 1984). Such hyperpolarization would result in a lower spontaneous firing rate of the PC population, and thus, a lower incidence of SWs. There are experimental evidences that GABA<sub>B</sub>R are located along the whole somato-dendritic axis on the principal cells, with highest concentrations in the stratum radiatum and lacunosum moleculare layer (Degro et al., 2015). Moreover, GABA<sub>B1</sub> receptors cluster with GIRK channels at the dendritic spines of PCs mostly in the stratum oriens, stratum radiatum and lacunosum moleculare (Kulik et al., 2006). The activation of postsynaptic GABA<sub>B</sub>Rs requires a repetitive firing of one or more presynaptic interneurons (Scanziani, 2000).
- **Postsynaptic GABA<sub>B</sub>Rs on PVBCs.** Because of the hypothesised disinhibitory role of the PVBCs, postsynaptic GABA<sub>B</sub>Rs on the PVBCs would also suppress the initiation of SWs upon activation and facilitate SWR generation upon suppression. Immunolabeling shows that GABA<sub>B</sub>Rs are co-localised with GIRK channels predominantly at the dendrites and the soma of the PV<sup>+</sup> interneurons (Booker et al., 2013), and to a smaller degree on the axons. Moreover, slow GABA<sub>B</sub>-mediated IPSPs are present in the perisomatic-targeting, but not in the dendritic-targeting PV<sup>+</sup>INs (Booker et al., 2013).
- **GABA<sub>B</sub> heteroreceptors on PCs.** Activation of GABA<sub>B</sub>Rs at the presynaptic side of the recurrent excitatory synapses suppresses glutamate release, and thus, the

### 3.4 Discussion

network excitability. It has been shown that both GABA<sub>B1</sub> and GABA<sub>B2</sub> are expressed at the presynaptic terminals of CA3 recurrent synapses (López-Bendito et al., 2004), and that these receptors can modulate the AMPA receptors (Lei and McBain, 2003). Moreover, GIRK channels cluster with GABA<sub>B1</sub> at the excitatory axons (Kulik et al., 2006). However, the functionality of these receptors is not clear. For example, Lei and McBain (2003) have shown that the baclofen-mediated inhibition of EPSPs is larger compared to the inhibition of IPSPs, and that the GABA<sub>B</sub>R antagonist CGP55,845 enhanced the IPSPs but not the EPSPs.

- **GABA<sub>B</sub> heteroreceptors on PVBCs.** Activation of presynaptic GABA<sub>B</sub>Rs on the PC-PVBC connections would suppress the excitability of PVBCs, which would lead to a suppression of SWRs. It is been shown that presynaptic GABA<sub>B</sub>Rs on the glutamatergic synapses can inhibit the excitatory transmission on CA3 interneurons (Lei and McBain, 2003), but the identity of these interneurons is unknown.
- **GABA<sub>B</sub> autoreceptors on PVBC-mIN synapses.** Activation of GABA<sub>B</sub>Rs located presynaptically on the PVBC-mIN connections would decrease the inhibition on mINs, and thus, decrease the incidence of SWRs. Lei and McBain (2003) have shown that inhibitory transmission to hippocampal interneurons is modulated by presynaptic GABA<sub>B</sub>Rs. Particularly, Booker et al. (2013) showed that the output of perisomatic-targeting PV<sup>+</sup> interneurons is modulated by GABA<sub>B</sub>Rs.

There are anatomical evidences supporting each of the hypotheses described above. However, which, if any of these GABA<sub>B</sub>Rs are activated indeed during SWRs is unknown. Some experimental evidences from the literature point to a presynaptic modulation. For example, Hollnagel et al. (2014) suggest that the GABA<sub>B</sub>R agonist baclofen decreases SWR incidence due to presynaptic glutamatergic suppression. However, the used *in-vitro* model is different as SWs occur spontaneously just after a train of external stimulations, and GABA<sub>B</sub>R antagonist did not lead to an increase in the SWR incidence. A study by Maier et al. (2012) shows that adenosine (activates GIRK channels, and suppresses glutamate transmitter release) suppresses SWRs because of presynaptic modulation. Moreover, there is no evidence that the postsynaptic GABA<sub>B</sub>R-mediated hyperpolarization (on PCs) is associated with the interval until next spontaneous event in the intracellular recordings analysed here. However, data (from personal communication with Nikolaus Maier) points out that application of GIRK-channel blocker (SCH23,390) increases SWR incidence, and moreover, a later application of GABA<sub>B</sub>R antagonist does not suppress the SWR incidence. This result suggests that the postsynaptic GIRK-coupled GABA<sub>B</sub>R are involved in the modulation of SWs, but not the presynaptic ones. Moreover, the GABA<sub>B</sub>R antagonist CGP52432, that acts predominantly on the autoreceptors (Lanza et al., 1993), did not influence SWR incidence in the *in-vitro* model used by Hofer et al. (2015). Such result hints that the reported here increase of SWR incidence might be not due to presynaptic GABA<sub>B</sub>Rs on inhibitory synapses.

There are more possible location sites for the GABA<sub>B</sub>Rs that haven't been discussed here. Through the prism of the 3-population model, the sites not mentioned here (e.g., presynaptic GABA<sub>B</sub>Rs on the outgoing mIN synapses) would modulate SWR incidence in the opposite direction as observed experimentally. Only the five pathways described above would lead to the experimentally observed effects of GABA<sub>B</sub>R modulators. The question whether one or more of these mechanisms are deployed simultaneously is to be answered. Cocktails of drugs could help us to better disentangle the different mechanism of receptors

### 3 Modulation of sharp-wave incidence

modulation. For example, more experiments with a sequential application of GIRK-channel blocker and GABA<sub>B</sub>R antagonist could be performed, where first one of the drugs applied, and after a few tens of minutes the other. Another experiment to test the postsynaptic modulation is to apply a GABA<sub>B</sub>R agonist, which will decrease the incidence, and to apply a GIRK-channel blocker afterwards to check whether the incidence is normalized. If the experiments favor a presynaptic modulation, the differential distribution of GABA<sub>B</sub> subunits (i.e., GABA<sub>B(1a,2)</sub> and GABA<sub>B(1b,2)</sub>) on different neurons could help narrow down the list of suspected receptors. However, one should be careful with the interpretation of the results as the effects of GABA<sub>B</sub>R are nonlinear (Brenowitz et al., 1998). Upon activation, presynaptic (Schwenk et al., 2010), as well as postsynaptic (Wetherington and Lambert, 2002) GABA<sub>B</sub>R can get desensitized.

Another possible influence of the GABA<sub>B</sub>Rs is through the modulation of short-term inhibitory plasticity, which is hypothesised to control the SWR incidence and amplitude. Short-term depression (STD) is usually mediated presynaptically (Kraushaar and Jonas, 2000). Moreover, the STD of inhibitory neurons can be modulated by GABA<sub>B</sub>Rs (Lei and McBain, 2003). It would be interesting to find out whether STD of PVBCs is also modulated by the GABA<sub>B</sub>Rs.

In summary, activation or inactivation of GABA<sub>B</sub>Rs can facilitate or depress the spontaneous generation of SWRs, respectively. Here, I proposed a few possible pathways of modulation. However, unlike hypothesised initially at the beginning of this project, the GABA<sub>B</sub>R does not seem to be the crucial mechanism defining the relatively long time scale between events.

#### 3.4.3 Overview

After over two decades of research, the mechanisms of sharp-wave ripple generation are still under debate. While some of the early theories focused exclusively on the role of excitation (e.g., Draguhn et al., 1998 and Memmesheimer, 2010, but also Ylinen et al., 1995), a number of evidences from the last years point out the importance of inhibitory transmission not only for the ripple oscillation, but also for the generation of the whole population event (Maier et al., 2011; Schlingloff et al., 2014; Stark et al., 2014; Kohus et al., 2016). While the build-up of excitation is an important requirement for the generation of spontaneous events (de la Prida et al., 2006; Ellender et al., 2010; Schlingloff et al., 2014; Hulse et al., 2016), SWR-like events can also be evoked by a spontaneous experimentator (Maier et al., 2003; Nimmrich et al., 2005; Both et al., 2008; Kohus et al., 2016) even in the absence of excitatory transmission (Schlingloff et al., 2014).

A phenomenological 3-population model relying on disinhibition explains some intriguing results from the literature. In particular, the model relies on a network circuit that can switch between two states: one state is characterised by a low firing rate of principal neurons and an unknown interneuron population, and another (transient) state by high firing rates of the principal and parvalbumin-positive basket neurons. However, currently the model is too general to explain all experimental findings. A number of possible experiments have been proposed in the preceding sections that can help us refine the model, and possibly validate or invalidate it.

To find the missing link between the SWR events and the slow time scale of the inter-event interval, one possibility is to look beyond the neural circuit. The astrocyte network, in particular, operates on a slower time scale ( $\sim 500$  ms, Sasaki et al., 2014), and has been known to modulate neural activity through complex and not well-understood mechanisms.

For example, astrocytes control neural excitability through gliotransmitters (e.g., glutamate, Parpura et al., 1994; ATP, Newman, 2001; GABA, Liu et al., 2000) and through modulation of the extracellular concentration of  $K^+$  (Wang et al., 2012). The astrocyte network can propagate  $Ca^{2+}$  waves triggered by neurotransmitters such as glutamate (e.g., Cornell-Bell et al., 1990). Recently, Zhang et al. (2017) showed that acute induction of astrocyte  $Ca^{2+}$  influx led to a suppression of neural activity on one-second time scale in a drosophila model. It is unclear whether similar mechanism are active in the hippocampus. Currently, the connections between SWRs and astrocyte activity is largely unexplored. It would be interesting to see if the occurrence of SWRs is correlated with the calcium waves in the astrocyte network or in the astrocytic compartments (Oschmann et al., 2017), and if yes, through what mechanism they are coupled. In particular, it is feasible that *in-vitro* preparations that show clock-like rhythmicity of SWRs occurrence are controlled predominantly by the slow oscillations of the neural-astrocyte network activity. While in slices with irregular SWRs (as most of the data analysed here), the neural-astrocyte network might contribute to a smaller degree. SWRs could be triggered by neural firing rate fluctuations that activate the disinhibitory circuit on top of the slow recovery of excitability.

## 3.5 Methods

The results in this chapter are based on the analysis of data kindly provided by Nikolaus Maier from the lab of Dietmar Schmitz (Neuroscience Research Center at Charité, Berlin). Here, five datasets of *in-vitro* recordings are analysed, one of which was jointly recorded by Roberta Evangelista and Nikolaus Maier. All recordings were performed in the CA3 area of horizontal hippocampal slices. Here I give a brief summary about the data and provide some details on the techniques applied during the analysis.

### 3.5.1 Data and data analysis

The slice preparations were done after “standard” procedures (Maier et al., 2003, 2012) according to the guidelines of the local authorities (Berlin). The slices were obtained by cutting mice hippocampi through the horizontal plane. All analyzed extracellular recordings were done in the pyramidal cell layer (stratum pyramidale) of CA3.

Sharp waves (SWs) were detected as positive deflections in the band-pass filtered signal of extracellular electrode recordings. A typical frequency band used in the analysis was 2–60 Hz (Butterworth filter), but due to noise, some recordings were filtered in the band 5–60 Hz. The threshold for SWR detection was set manually for each slice after visual inspection of the data. In recordings that show small deviations of the signal, 2 standard deviations (SDs) above the mean were sufficient to capture all SWR events. For “noisy” recordings with substantial deviations in the recorded signal, the threshold could be up to 5 SDs. Only events of duration between 10 and 70 ms were considered as sharp-wave events. The amplitudes positive deflections of the filtered signal were used to quantify the SWR peaks in the Results (Section 3.3). The measure of inter-SWR intervals was based on the difference of peak times. The time interval between events from different sweeps were not considered in the analysis.

#### Dataset 1: hippocampal slices

The first dataset consists of extracellular recordings from 20 hippocampal slices. Recordings were performed in the years 2007–2014. The temporal sampling frequency was 5 or 10 kHz.

### *3 Modulation of sharp-wave incidence*

The recording durations were between 8 and 55 minutes.

#### **Dataset 2: multi-electrode arrays**

The second set of data was jointly collected by Roberta Evangelista and Nikolaus Maier as part of Roberta's Master thesis. Data were recorded on multi-electrode arrays (MEA) from 25 slices of 8 animals in 2014 and 2015. While each array consisted of 32 electrodes, only recordings from stratum pyramidale of CA3 were considered in this analysis, i.e., between 6 and 13 recording sites in different slices. Due to data preprocessing, the amplitudes of the raw field-potential traces (instead of the filtered) were considered for the calculation of the SWR peak amplitudes. Moreover, the SWR peak amplitudes values were normalized by subtracting the mean and dividing by the SD of SWR peaks at the particular recording site.

#### **Dataset 3: gabazine**

The effects of gabazine on the hippocampal circuit were experimentally investigated in eight slices by Nikolaus Maier in the years 2012–2014. Here, the extracellular field potentials in stratum pyramidale were measured in intact slices. A few tens of minutes (between 16 and 40 mins) after the recording onset, a low concentration (100 nM) of the GABA<sub>A</sub>R antagonist gabazine was applied with artificial cerebrospinal fluid (ACSF). In 2 of the slices, there was a washout of gabazine that reversed the effects on incidence and amplitudes of SWRs. Events from the window [-7, -2] minutes (before drug application) and [6, 11] minutes (after drug application) were used to compare the properties of SWs.

#### **Dataset 4: GABA<sub>B</sub>R blocker**

This dataset contains extracellular recordings from 13 hippocampal slices. Here, the extracellular field potential was measured for several minutes, after which 20 μM GABA<sub>B</sub>R of a antagonist (SCH50,911) was applied to the ACSF. In two of the recordings, SCH50,911 was washed out after ~ 20 minutes of application, and in one of the recording the wash-out normalized the SWR incidence to the levels prior to application; in the other recording, incidence increased even further. Events from the window [-5, 0] minutes (before drug application) and [2, 7] minutes (after drug application) were used to compare the properties of SWs. One recording was excluded as there were virtually no events prior to the drug application, and thus, the average results were heavily skewed.

#### **Dataset 5: intracellular recordings**

The last dataset consists of 13 recording pairs performed between 2008 and 2012. Two simultaneous recordings were performed in CA3 area, one extracellular and one intracellular recording from a patched pyramidal cell in a current clamp mode. The data consists of multiple sweeps of around 5–20 seconds. The length of each recording is rather short, ranging from 40 seconds up to 10 minutes, with sampling rates between 5 and 40 kHz. At the beginning of each sweep, a large negative current pulse was injected into the patched cells to determine potential changes in cell's input resistance resulting into a negative deflection (~ 10 mV) of the membrane potential. Therefore, events that occurred in the first 200 ms of the sweep were ignored. In a couple of recordings this hyperpolarization was still present in the membrane potential prior to SWs and reflected in the voltage trace differences in Figure 3.16 (top panel).

### 3.5.2 Simulations

The network simulations were based on the model presented in Chapter 2. Spontaneous replays of assembly sequences are used as a model for the SWR events (Section 3.3.3). The connectivity values were  $p_{rc} = 0.08$  and  $p_{ff} = 0.06$ . The remaining parameters were unchanged. The gabazine modulation was modelled by decreasing the values of inhibitory conductances  $g_{ii}$  and  $g_{ei}$  by 5%.



## 4 Outlook

The aim of this final chapter is to put into perspective the problems that have been analysed so far. In particular, what is the relevance of the assembly sequence in the framework of the disinhibitory 3-population model? Moreover, I openly discuss some ideas that have spontaneously occurred over the course of the last few years.

### 4.1 Bridging the assembly sequence model and the 3-population hypothesis

Neural assemblies connected in a feedforward manner can explain the replay of behaviour sequences observed in the hippocampus. The sequence replay can be evoked by an external input cue, or occur spontaneously. As described in Chapter 2, a spontaneous replay requires higher connectivities between assemblies than the evoked replay. Moreover, the spontaneous replay largely depends on the network excitability, and a small change of the net input can shift to or from spontaneous replay regime. For example, decreasing the total input to the network abolishes spontaneous events, while an increase of the input facilitates them. However, such circuitry relying on two populations (an excitatory and an inhibitory one) cannot account for the inhibitory-evoked SWRs observed *in vitro* (e.g., Schlingloff et al., 2014; Kohus et al., 2016). Therefore, in Chapter 3, I described a phenomenological model of a hippocampal network consisting of 3 populations (one excitatory and two inhibitory populations). The underlying idea is that the activation of one inhibitory population activates a disinhibitory circuit, leading to a population burst. An ultimate goal, that has not been achieved in this thesis, is to combine these two models (e.g., the assembly sequence and the 3-population model) into a single framework. Is the high-firing-rate regime during a population burst going to dramatically decrease the connectivities required for a replay?

A possible limitation of the presented assembly-sequence model is the fact that it relies on ‘rigid’ assemblies of neurons that are uniformly connected among themselves. Experimental data on the synaptic organisation in hippocampus, as well as in the cortex, show heavily skewed distributions of synaptic strength and connectivity (e.g., Takahashi et al., 2010; Buzsáki and Mizuseki, 2014; Cossell et al., 2015). Lognormal distributions of connectivities and synaptic weights between neurons would be a more plausible model for a cell assembly. Then, a few ‘central’ neurons will fire reliably during assembly activation, while the participation of the ‘periphery’ neurons will depend more on the strength and the type of input stimulation. To what degree such modification of the model will affect the results of sequence replay is not known.

### 4.2 Further implications of the disinhibitory circuit

The 3-population hypothesis is a plausible general mechanism for achieving multistability of local networks. Particularly, a disinhibitory pathway can lead to a rapid activation of the excitatory network upon command. Such a mechanism might underlie the gating of

## 4 Outlook

spontaneous activity not only in the hippocampus, but also in local cortical networks. Luczak et al. (2013) suggested that the sensory cortex is constantly processing the inputs in a background, low-firing rate regime, i.e., the ‘down state’. Upon a top-down request from higher-order areas, the sensory cortex switches to an ‘up state’, and thus, gates the sensory information upstream. Such up states might be achieved through a rapid disinhibition.

A line of research from Brecht lab points out to the plausibility of the disinhibitory hypothesis in cortical networks. Brecht et al. (2004) has shown that a repetitive stimulation of a single pyramidal neurons in the rat motor cortex can evoke whisker movement. The stimulation evoked a marked change of pattern activity reflected in the field potential and increased firing of the fast spiking, putative inhibitory interneurons (Houweling and Brecht, 2007; Doron et al., 2014). Moreover, stimulation of fast spiking, putative inhibitory interneurons in somatosensory cortex led to stronger effects detected in the animal’s behaviour compared to a stimulation of principal cells (Doron et al., 2014). The stimulations were typically followed by a ‘long-lasting’ inhibition of firing rates measured in the micro-circuit (Doron et al., 2014). Experiments targeting the disinhibitory neurons would address explicitly the question of disinhibition in cortical networks.

### 4.3 Why a hippocampal replay?

According to the standard 2-stage memory model, behaviour sequences are imprinted in the CA3 recurrent networks upon experience (Marr, 1971; Buzsáki, 1989). However, such view has been challenged in the last years as reports have shown that the hippocampal replay is not a simple function of experience (e.g., Gupta et al., 2010). Even more explicitly, Dragoi and Tonegawa (2011, 2013) showed that sequences are replayed in the hippocampus already prior to the first exposure of the environment which these sequences represent. What could be the role of the observed replays?

Dragoi suggested<sup>1</sup> that the role of CA3 is to create blank sequences that are mapped later to experience. Cheng (2013) proposed the CRISP model which goes along these lines. According to the model, CA3 sequences are formed offline prior to utilization due to the maturation of newly generated granule cells in the dentate gyrus. During the first exposure to the environment, granule cells that carry sparse information about the environment are instantly mapped to the CA3 sequences via the mossy fibers. While this is a plausible explanation of how the hippocampal input is mapped to the blank hippocampal sequences, it is not clear how the hippocampal output during a following offline replay is mapped back to the context it represents. Such mapping would require highly plastic synapses that are able to encode information in a single experience. Cheng (2013) hypothesises that the internal sequences are mapped back to the behavioural information via the feedforward synapses from CA1 to the deep EC layers. Such learning might be facilitated by the preplays that occur prior to experience. In this way, the internal CA3 sequences would not be purely blank, but are already integrated with activity patterns in the deep layers of the EC.

---

<sup>1</sup>The episodic event took place during a public talk at BCCN-Berlin in 2013.

# Bibliography

- Abeles, M. (1991). *Corticonics: Neural circuits of the cerebral cortex*. Cambridge University Press.
- Albert, C. Y. and Margoliash, D. (1996). Temporal hierarchical control of singing in birds. *Science*, 273(5283):1871.
- Almeida-Filho, D. G., Lopes-dos Santos, V., Vasconcelos, N. A., Miranda, J. G., Tort, A. B., and Ribeiro, S. (2014). An investigation of Hebbian phase sequences as assembly graphs. *Frontiers in Neural Circuits*, 8:34.
- Amit, D. J. and Brunel, N. (1997). Model of global spontaneous activity and local structured activity during delay periods in the cerebral cortex. *Cerebral Cortex*, 7(3):237–252.
- Andersen, P. (2007). *The hippocampus book*. Oxford University Press.
- Atwood, H. L. and Wojtowicz, J. M. (1999). Silent synapses in neural plasticity: current evidence. *Learning & Memory*, 6(6):542–571.
- Aviel, Y., Horn, D., and Abeles, M. (2004). Synfire waves in small balanced networks. *Neurocomputing*, 58:123–127.
- Aviel, Y., Mehring, C., Abeles, M., and Horn, D. (2003). On embedding synfire chains in a balanced network. *Neural Computation*, 15(6):1321–1340.
- Aviel, Y., Pavlov, E., Abeles, M., and Horn, D. (2002). Synfire chain in a balanced network. *Neurocomputing*, 44:285–292.
- Axmacher, N., Elger, C. E., and Fell, J. (2008). Ripples in the medial temporal lobe are relevant for human memory consolidation. *Brain*, 131(7):1806–1817.
- Azizi, A. H., Wiskott, L., and Cheng, S. (2013). A computational model for preplay in the hippocampus. *Frontiers in Computational Neuroscience*, 7:161.
- Bai, D., Zhu, G., Pennefather, P., Jackson, M. F., MacDonald, J. F., and Orser, B. A. (2001). Distinct functional and pharmacological properties of tonic and quantal inhibitory postsynaptic currents mediated by  $\gamma$ -aminobutyric acidA receptors in hippocampal neurons. *Molecular Pharmacology*, 59(4):814–824.
- Balaguer-Ballester, E., Lapish, C. C., Seamans, J. K., and Durstewitz, D. (2011). Attracting dynamics of frontal cortex ensembles during memory-guided decision-making. *PLoS Computational Biology*, 7(5):e1002057.
- Banke, T. G. and McBain, C. J. (2006). GABAergic input onto CA3 hippocampal interneurons remains shunting throughout development. *Journal of Neuroscience*, 26(45):11720–11725.

## Bibliography

- Barbieri, F. and Brunel, N. (2008). Can attractor network models account for the statistics of firing during persistent activity in prefrontal cortex? *Frontiers in Neuroscience*, 2:114–122.
- Bathellier, B., Ushakova, L., and Rumpel, S. (2012). Discrete neocortical dynamics predict behavioral categorization of sounds. *Neuron*, 76(2):435–449.
- Bazelot, M., Teleńczuk, M. T., and Miles, R. (2016). Single CA3 pyramidal cells trigger sharp waves *in vitro* by exciting interneurones. *Journal of Physiology*, 594(10):2565–2577.
- Behrens, C., Van Den Boom, L., and Heinemann, U. (2007). Effects of the GABA<sub>A</sub> receptor antagonists bicuculline and gabazine on stimulus-induced sharp wave-ripple complexes in adult rat hippocampus *in vitro*. *European Journal of Neuroscience*, 25(7):2170–2181.
- Behrens, C. J., van den Boom, L. P., de Hoz, L., Friedman, A., and Heinemann, U. (2005). Induction of sharp wave-ripple complexes *in vitro* and reorganization of hippocampal networks. *Nature Neuroscience*, 8(11):1560–1567.
- Bekkers, J. M. (2005). Presynaptically silent GABA synapses in hippocampus. *Journal of Neuroscience*, 25(16):4031–4039.
- Ben-Ari, Y., Tseeb, V., Ragozzino, D., Khazipov, R., and Gaiarsa, J. (1994).  $\gamma$ -Aminobutyric acid (GABA): a fast excitatory transmitter which may regulate the development of hippocampal neurones in early postnatal life. *Progress in Brain Research*, 102:261–273.
- Benkowitz, C., Banks, M. I., and Pearce, R. A. (2004). Influence of GABA<sub>A</sub> receptor  $\gamma_2$  splice variants on receptor kinetics and isoflurane modulation. *Journal of the American Society of Anesthesiologists*, 101(4):924–936.
- Berkes, P., Orbán, G., Lengyel, M., and Fiser, J. (2011). Spontaneous cortical activity reveals hallmarks of an optimal internal model of the environment. *Science*, 331(6013):83–87.
- Bezaire, M. J. and Soltesz, I. (2013). Quantitative assessment of CA1 local circuits: Knowledge base for interneuron-pyramidal cell connectivity. *Hippocampus*, 23(9):751–785.
- Bi, G.-q. and Poo, M.-m. (1998). Synaptic modifications in cultured hippocampal neurons: dependence on spike timing, synaptic strength, and postsynaptic cell type. *Journal of Neuroscience*, 18(24):10464–10472.
- Bischofberger, J., Engel, D., Frotscher, M., and Jonas, P. (2006). Timing and efficacy of transmitter release at mossy fiber synapses in the hippocampal network. *Pflügers Archiv*, 453(3):361–372.
- Bliss, T. V. and Lømo, T. (1973). Long-lasting potentiation of synaptic transmission in the dentate area of the anaesthetized rabbit following stimulation of the perforant path. *Journal of Physiology*, 232(2):331–356.
- Bloch, D. K. (2007). *Aristotle on memory and recollection*. Brill.
- Boddum, K., Frølund, B., and Kristiansen, U. (2014). The GABA<sub>A</sub> antagonist DPP-4-PIOL selectively antagonises tonic over phasic GABAergic currents in dentate gyrus granule cells. *Neurochemical Research*, 39(11):2078–2084.

## Bibliography

- Boileau, A. J., Pearce, R. A., and Czajkowski, C. (2005). Tandem subunits effectively constrain GABA<sub>A</sub> receptor stoichiometry and recapitulate receptor kinetics but are insensitive to GABA<sub>A</sub> receptor-associated protein. *Journal of Neuroscience*, 25(49):11219–11230.
- Booker, S. A., Gross, A., Althof, D., Shigemoto, R., Bettler, B., Frotscher, M., Hearing, M., Wickman, K., Watanabe, M., Kulik, Å., et al. (2013). Differential GABA<sub>B</sub>-receptor-mediated effects in perisomatic-and dendrite-targeting parvalbumin interneurons. *Journal of Neuroscience*, 33(18):7961–7974.
- Boss, B. D., Peterson, G. M., and Cowan, W. M. (1985). On the number of neurons in the dentate gyrus of the rat. *Brain Research*, 338(1):144–150.
- Boss, B. D., Turlejski, K., Stanfield, B. B., and Cowan, W. M. (1987). On the numbers of neurons on fields CA1 and CA3 of the hippocampus of Sprague-Dawley and Wistar rats. *Brain Research*, 406(1-2):280–287.
- Bostock, D. (1986). *Plato's Phaedo*. Oxford University Press.
- Both, M., Bähner, F., von Bohlen und Halbach, O., and Draguhn, A. (2008). Propagation of specific network patterns through the mouse hippocampus. *Hippocampus*, 18(9):899–908.
- Bragin, A., Jandó, G., Nádasdy, Z., Hetke, J., Wise, K., and Buzsáki, G. (1995). Gamma (40–100 Hz) oscillation in the hippocampus of the behaving rat. *Journal of Neuroscience*, 15(1):47–60.
- Brea, J., Senn, W., and Pfister, J.-P. (2013). Matching recall and storage in sequence learning with spiking neural networks. *Journal of Neuroscience*, 33(23):9565–9575.
- Brecht, M., Schneider, M., Sakmann, B., and Margrie, T. W. (2004). Whisker movements evoked by stimulation of single pyramidal cells in rat motor cortex. *Nature*, 427(6976):704–710.
- Brenowitz, S., David, J., and Trussell, L. (1998). Enhancement of synaptic efficacy by presynaptic GABA<sub>B</sub> receptors. *Neuron*, 20(1):135–141.
- Brown, D., Adams, P., Higgins, A., and Marsh, S. (1978). Distribution of GABA-receptors and GABA-carriers in the mammalian nervous system. *Journal de Physiologie*, 75(6):667–671.
- Brown, T. G. (1914). On the nature of the fundamental activity of the nervous centres; together with an analysis of the conditioning of rhythmic activity in progression, and a theory of the evolution of function in the nervous system. *Journal of Physiology*, 48(1):18–46.
- Brunel, N. (2000). Dynamics of sparsely connected networks of excitatory and inhibitory spiking neurons. *Journal of Computational Neuroscience*, 8(3):183–208.
- Brunel, N. and Wang, X.-J. (2003). What determines the frequency of fast network oscillations with irregular neural discharges? I. Synaptic dynamics and excitation-inhibition balance. *Journal of Neurophysiology*, 90(1):415–430.
- Buhl, D. and Buzsáki, G. (2005). Developmental emergence of hippocampal fast-field “ripple” oscillations in the behaving rat pups. *Neuroscience*, 134(4):1423–1430.

## Bibliography

- Bush, D., Philippides, A., Husbands, P., and O’Shea, M. (2010). Dual coding with STDP in a spiking recurrent neural network model of the hippocampus. *PLoS Computational Biology*, 6(7):e1000839.
- Buzsáki, G. (1989). Two-stage model of memory trace formation: a role for “noisy” brain states. *Neuroscience*, 31(3):551–570.
- Buzsáki, G. (2002). Theta oscillations in the hippocampus. *Neuron*, 33(3):325–340.
- Buzsáki, G. (2010). Neural syntax: cell assemblies, synapsembles, and readers. *Neuron*, 68(3):362–385.
- Buzsáki, G. (2015). Hippocampal sharp wave-ripple: A cognitive biomarker for episodic memory and planning. *Hippocampus*, 25(10):1073–1188.
- Buzsáki, G., Buhl, D., Harris, K., Csicsvari, J., Czeh, B., and Morozov, A. (2003). Hippocampal network patterns of activity in the mouse. *Neuroscience*, 116(1):201–211.
- Buzsáki, G., Lai-Wo, L. S., and Vanderwolf, C. H. (1983). Cellular bases of hippocampal EEG in the behaving rat. *Brain Research Reviews*, 6(2):139–171.
- Buzsáki, G. and Mizuseki, K. (2014). The log-dynamic brain: how skewed distributions affect network operations. *Nature Reviews Neuroscience*, 15(4):264–278.
- Buzsáki, G. and Wise, K. (1992). High-frequency network oscillation in the hippocampus. *Science*, 256(5059):1025.
- Cafaro, J. and Rieke, F. (2010). Noise correlations improve response fidelity and stimulus encoding. *Nature*, 468(7326):964–967.
- Câteau, H. and Fukai, T. (2001). Fokker–Planck approach to the pulse packet propagation in synfire chain. *Neural Networks*, 14(6):675–685.
- Cheng, J. and Ji, D. (2013). Rigid firing sequences undermine spatial memory codes in a neurodegenerative mouse model. *eLife*, 2:e00647.
- Cheng, S. (2013). The CRISP theory of hippocampal function in episodic memory. *Frontiers in Neural Circuits*, 7:88.
- Chenkov, N., Sprekeler, H., and Kempfer, R. (2017). Memory replay in balanced recurrent networks. *PLoS Computational Biology*, 13(1):e1005359.
- Cicero, M. T., Sutton, E. W., and Rackham, H. (1948 (55BC)). *De Oratore*. Harvard University Press.
- Clark, R. E. and Squire, L. R. (2013). Similarity in form and function of the hippocampus in rodents, monkeys, and humans. *Proceedings of the National Academy of Sciences*, 110(Supplement 2):10365–10370.
- Clopath, C., Büsing, L., Vasilaki, E., and Gerstner, W. (2010). Connectivity reflects coding: a model of voltage-based STDP with homeostasis. *Nature Neuroscience*, 13(3):344–352.

## Bibliography

- Cobb, S., Buhl, E., Halasy, K., Paulsen, O., and Somogyi, P. (1995). Synchronization of neuronal activity in hippocampus by individual GABAergic interneurons. *Nature*, 378(6552):75.
- Cobb, S., Halasy, K., Vida, I., Nyíri, G., Tamás, G., Buhl, E., and Somogyi, P. (1997). Synaptic effects of identified interneurons innervating both interneurons and pyramidal cells in the rat hippocampus. *Neuroscience*, 79(3):629–648.
- Cohen, I., Navarro, V., Clemenceau, S., Baulac, M., and Miles, R. (2002). On the origin of interictal activity in human temporal lobe epilepsy *in vitro*. *Science*, 298(5597):1418–1421.
- Cohen, J. E. and Fields, R. D. (2004). Extracellular calcium depletion in synaptic transmission. *The Neuroscientist*, 10(1):12–17.
- Colgin, L. L., Kubota, D., Brucher, F. A., Jia, Y., Branyan, E., Gall, C. M., and Lynch, G. (2004). Spontaneous waves in the dentate gyrus of slices from the ventral hippocampus. *Journal of Neurophysiology*, 92(6):3385–3398.
- Contreras, E. J. B., Schjetnan, A. G. P., Muhammad, A., Bartho, P., McNaughton, B. L., Kolb, B., Gruber, A. J., and Luczak, A. (2013). Formation and reverberation of sequential neural activity patterns evoked by sensory stimulation are enhanced during cortical desynchronization. *Neuron*, 79(3):555–566.
- Corkin, S. (1968). Acquisition of motor skill after bilateral medial temporal-lobe excision. *Neuropsychologia*, 6(3):255–265.
- Corkin, S. (2002). What's new with the amnesic patient HM? *Nature Reviews Neuroscience*, 3(2):153–160.
- Cornell-Bell, A. H., Finkbeiner, S. M., Cooper, M. S., and Smith, S. J. (1990). Glutamate induces calcium waves in cultured astrocytes: long-range glial signaling. *Science*, 247(4941):470.
- Cossart, R., Aronov, D., and Yuste, R. (2003). Attractor dynamics of network up states in the neocortex. *Nature*, 423(6937):283–288.
- Cossell, L., Iacaruso, M. F., Muir, D. R., Houlton, R., Sader, E. N., Ko, H., Hofer, S. B., and Mrsic-Flogel, T. D. (2015). Functional organization of excitatory synaptic strength in primary visual cortex. *Nature*, 518(7539):399–403.
- Cowansage, K. K., Shuman, T., Dillingham, B. C., Chang, A., Golshani, P., and Mayford, M. (2014). Direct reactivation of a coherent neocortical memory of context. *Neuron*, 84(2):432–441.
- Csicsvari, J., Hirase, H., Czurkó, A., Mamiya, A., and Buzsáki, G. (1999). Oscillatory coupling of hippocampal pyramidal cells and interneurons in the behaving rat. *Journal of Neuroscience*, 19(1):274–287.
- Csicsvari, J., Hirase, H., Mamiya, A., and Buzsáki, G. (2000). Ensemble patterns of hippocampal CA3–CA1 neurons during sharp wave–associated population events. *Neuron*, 28(2):585–594.

## Bibliography

- Dave, A. S. and Margoliash, D. (2000). Song replay during sleep and computational rules for sensorimotor vocal learning. *Science*, 290(5492):812–816.
- de la Prida, L. M., Huberfeld, G., Cohen, I., and Miles, R. (2006). Threshold behavior in the initiation of hippocampal population bursts. *Neuron*, 49(1):131–142.
- Debanne, D., Gähwiler, B. H., and Thompson, S. M. (1998). Long-term synaptic plasticity between pairs of individual CA3 pyramidal cells in rat hippocampal slice cultures. *Journal of Physiology*, 507(1):237–247.
- Degro, C. E., Kulik, A., Booker, S. A., and Vida, I. (2015). Compartmental distribution of GABA<sub>B</sub> receptor-mediated currents along the somatodendritic axis of hippocampal principal cells. *Frontiers in Synaptic Neuroscience*, 7:6.
- Diba, K. and Buzsáki, G. (2007). Forward and reverse hippocampal place-cell sequences during ripples. *Nature Neuroscience*, 10(10):1241–1242.
- Dickinson, R., de Sousa, S. L., Lieb, W. R., and Franks, N. P. (2002). Selective synaptic actions of thiopental and its enantiomers. *Journal of the American Society of Anesthesiologists*, 96(4):884–892.
- Diekelmann, S. and Born, J. (2010). The memory function of sleep. *Nature Reviews Neuroscience*, 11(2):114–126.
- Diesmann, M., Gewaltig, M.-O., and Aertsen, A. (1999). Stable propagation of synchronous spiking in cortical neural networks. *Nature*, 402(6761):529–533.
- Donoso, J., Maier, N., Schmitz, D., and Kempter, R. (2017). Ripple oscillations in hippocampal inhibitory networks. *Hippocampus (under review)*.
- Doron, G., von Heimendahl, M., Schlattmann, P., Houweling, A. R., and Brecht, M. (2014). Spiking irregularity and frequency modulate the behavioral report of single-neuron stimulation. *Neuron*, 81(3):653–663.
- Dougherty, K. A., Islam, T., and Johnston, D. (2012). Intrinsic excitability of CA1 pyramidal neurones from the rat dorsal and ventral hippocampus. *Journal of Physiology*, 590(22):5707–5722.
- Doupe, A. J., Solis, M. M., Kimpo, R., and BOETTIGER, C. A. (2004). Cellular, circuit, and synaptic mechanisms in song learning. *Annals of the New York Academy of Sciences*, 1016(1):495–523.
- Dragoi, G. and Buzsáki, G. (2006). Temporal encoding of place sequences by hippocampal cell assemblies. *Neuron*, 50(1):145–157.
- Dragoi, G. and Tonegawa, S. (2011). Preplay of future place cell sequences by hippocampal cellular assemblies. *Nature*, 469(7330):397–401.
- Dragoi, G. and Tonegawa, S. (2013). Distinct preplay of multiple novel spatial experiences in the rat. *Proceedings of the National Academy of Sciences*, 110(22):9100–9105.
- Draguhn, A., Traub, R., Schmitz, D., and Jefferys, J. (1998). Electrical coupling underlies high-frequency oscillations in the hippocampus *in vitro*. *Nature*, 394(6689):189–192.

## Bibliography

- D'amour, J. A. and Froemke, R. C. (2015). Inhibitory and excitatory spike-timing-dependent plasticity in the auditory cortex. *Neuron*, 86(2):514–528.
- Ekstrom, A. D., Kahana, M. J., Caplan, J. B., Fields, T. A., Isham, E. A., Newman, E. L., and Fried, I. (2003). Cellular networks underlying human spatial navigation. *Nature*, 425(6954):184–188.
- Ellender, T. J., Nissen, W., Colgin, L. L., Mann, E. O., and Paulsen, O. (2010). Priming of hippocampal population bursts by individual perisomatic-targeting interneurons. *Journal of Neuroscience*, 30(17):5979–5991.
- English, D. F., Peyrache, A., Stark, E., Roux, L., Vallentin, D., Long, M. A., and Buzsáki, G. (2014). Excitation and inhibition compete to control spiking during hippocampal ripples: intracellular study in behaving mice. *Journal of Neuroscience*, 34(49):16509–16517.
- Eschenko, O., Mölle, M., Born, J., and Sara, S. J. (2006). Elevated sleep spindle density after learning or after retrieval in rats. *Journal of Neuroscience*, 26(50):12914–12920.
- Eschenko, O., Ramadan, W., Mölle, M., Born, J., and Sara, S. J. (2008). Sustained increase in hippocampal sharp-wave ripple activity during slow-wave sleep after learning. *Learning & Memory*, 15(4):222–228.
- Euston, D. R., Tatsuno, M., and McNaughton, B. L. (2007). Fast-forward playback of recent memory sequences in prefrontal cortex during sleep. *Science*, 318(5853):1147–1150.
- Farrant, M. and Nusser, Z. (2005). Variations on an inhibitory theme: phasic and tonic activation of GABA<sub>A</sub> receptors. *Nature Reviews Neuroscience*, 6(3):215–229.
- Feldman, D. E. (2012). The spike-timing dependence of plasticity. *Neuron*, 75(4):556–571.
- Felsen, G., Touryan, J., Han, F., and Dan, Y. (2005). Cortical sensitivity to visual features in natural scenes. *PLoS Biology*, 3(10):e342.
- Feng, T., Silva, D., and Foster, D. J. (2015). Dissociation between the experience-dependent development of hippocampal theta sequences and single-trial phase precession. *Journal of Neuroscience*, 35(12):4890–4902.
- Finnerty, G. and Jefferys, J. (1993). Functional connectivity from CA3 to the ipsilateral and contralateral CA1 in the rat dorsal hippocampus. *Neuroscience*, 56(1):101–108.
- Foer, J. (2011). *Moonwalking with Einstein: The art and science of remembering everything*. Penguin.
- Foster, D. J. and Wilson, M. A. (2006). Reverse replay of behavioural sequences in hippocampal place cells during the awake state. *Nature*, 440(7084):680–683.
- Freemon, F. R., McNew, J. J., and Adey, W. R. (1969). Sleep of unrestrained chimpanzee: cortical and subcortical recordings. *Experimental Neurology*, 25(1):129–137.
- Freemon, F. R. and Walter, R. D. (1970). Electrical activity of human limbic system during sleep. *Comprehensive Psychiatry*, 11(6):544–551.
- Freund, T. F. and Buzsáki, G. (1996). Interneurons of the hippocampus. *Hippocampus*, 6(4):347–470.

## Bibliography

- Fuentealba, P., Begum, R., Capogna, M., Jinno, S., Marton, L. F., Csicsvari, J., Thomson, A., Somogyi, P., and Klausberger, T. (2008a). Ivy cells: a population of nitric-oxide-producing, slow-spiking GABAergic neurons and their involvement in hippocampal network activity. *Neuron*, 57(6):917–929.
- Fuentealba, P., Tomioka, R., Dalezios, Y., Márton, L. F., Studer, M., Rockland, K., Klausberger, T., and Somogyi, P. (2008b). Rhythmically active enkephalin-expressing GABAergic cells in the CA1 area of the hippocampus project to the subiculum and preferentially innervate interneurons. *Journal of Neuroscience*, 28(40):10017–10022.
- Fushiki, A., Zwart, M. F., Kohsaka, H., Fetter, R. D., Cardona, A., and Nose, A. (2016). A circuit mechanism for the propagation of waves of muscle contraction in drosophila. *eLife*, 5:e13253.
- Gassmann, M. and Bettler, B. (2012). Regulation of neuronal GABA<sub>B</sub> receptor functions by subunit composition. *Nature Reviews Neuroscience*, 13(6):380–394.
- Gekel, I. and Neher, E. (2008). Application of an Epac activator enhances neurotransmitter release at excitatory central synapses. *Journal of Neuroscience*, 28(32):7991–8002.
- George, J. M., Jin, H., Woods, W. S., and Clayton, D. F. (1995). Characterization of a novel protein regulated during the critical period for song learning in the zebra finch. *Neuron*, 15(2):361–372.
- Gerstner, W. (1995). Time structure of the activity in neural network models. *Physical Review E*, 51(1):738–758.
- Gerstner, W., Kempter, R., van Hemmen, J. L., and Wagner, H. (1996). A neuronal learning rule for sub-millisecond temporal coding. *Nature*, 383:76–78.
- Gerstner, W. and Kistler, W. M. (2002). *Spiking neuron models: Single neurons, populations, plasticity*. Cambridge university press.
- Girardeau, G., Benchenane, K., Wiener, S. I., Buzsáki, G., and Zugaro, M. B. (2009). Selective suppression of hippocampal ripples impairs spatial memory. *Nature Neuroscience*, 12(10):1222–1223.
- Girardeau, G., Cei, A., and Zugaro, M. (2014). Learning-induced plasticity regulates hippocampal sharp wave-ripple drive. *Journal of Neuroscience*, 34(15):5176–5183.
- Goedeke, S. and Diesmann, M. (2008). The mechanism of synchronization in feed-forward neuronal networks. *New Journal of Physics*, 10(1):015007.
- Goldman, M. S. (2009). Memory without feedback in a neural network. *Neuron*, 61(4):621–634.
- Goodman, D. F. and Brette, R. (2009). The Brian simulator. *Frontiers in Neuroscience*, 3:26.
- Graupner, M. and Brunel, N. (2012). Calcium-based plasticity model explains sensitivity of synaptic changes to spike pattern, rate, and dendritic location. *Proceedings of the National Academy of Sciences*, 109(10):3991–3996.

## Bibliography

- Gulledge, A. T. and Stuart, G. J. (2003). Excitatory actions of GABA in the cortex. *Neuron*, 37(2):299–309.
- Gupta, A. S., van der Meer, M. A., Touretzky, D. S., and Redish, A. D. (2010). Hippocampal replay is not a simple function of experience. *Neuron*, 65(5):695–705.
- Gupta, A. S., van der Meer, M. A., Touretzky, D. S., and Redish, A. D. (2012). Segmentation of spatial experience by hippocampal theta sequences. *Nature Neuroscience*, 15(7):1032–1039.
- Guzman, S. J., Schlögl, A., Frotscher, M., and Jonas, P. (2016). Synaptic mechanisms of pattern completion in the hippocampal CA3 network. *Science*, 353(6304):1117–1123.
- Hafting, T., Fyhn, M., Molden, S., Moser, M.-B., and Moser, E. I. (2005). Microstructure of a spatial map in the entorhinal cortex. *Nature*, 436(7052):801–806.
- Hahn, G., Bujan, A. F., Frégnac, Y., Aertsen, A., and Kumar, A. (2014). Communication through resonance in spiking neuronal networks. *PLoS Computational Biology*, 10(8):e1003811.
- Hahnloser, R. H., Kozhevnikov, A. A., and Fee, M. S. (2002). An ultra-sparse code underlies the generation of neural sequences in a songbird. *Nature*, 419(6902):65–70.
- Hajos, N., Ellender, T. J., Zemankovics, R., Mann, E. O., Exley, R., Cragg, S. J., Freund, T. F., and Paulsen, O. (2009). Maintaining network activity in submerged hippocampal slices: importance of oxygen supply. *European Journal of Neuroscience*, 29(2):319–327.
- Hájós, N., Karlócai, M. R., Németh, B., Ulbert, I., Monyer, H., Szabó, G., Erdélyi, F., Freund, T. F., and Gulyás, A. I. (2013). Input-output features of anatomically identified CA3 neurons during hippocampal sharp wave/ripple oscillation *in vitro*. *Journal of Neuroscience*, 33(28):11677–11691.
- Halff, A. W., Gómez-Varela, D., John, D., and Berg, D. K. (2014). A novel mechanism for nicotinic potentiation of glutamatergic synapses. *Journal of Neuroscience*, 34(6):2051–2064.
- Hamaguchi, K. and Mooney, R. (2012). Recurrent interactions between the input and output of a songbird cortico-basal ganglia pathway are implicated in vocal sequence variability. *Journal of Neuroscience*, 32(34):11671–11687.
- Hamzei-Sichani, F., Kamasawa, N., Janssen, W. G., Yasumura, T., Davidson, K. G., Hof, P. R., Wearne, S. L., Stewart, M. G., Young, S. R., Whittington, M. A., et al. (2007). Gap junctions on hippocampal mossy fiber axons demonstrated by thin-section electron microscopy and freeze-fracture replica immunogold labeling. *Proceedings of the National Academy of Sciences*, 104(30):12548–12553.
- Hanse, E., Seth, H., and Riebe, I. (2013). AMPA-silent synapses in brain development and pathology. *Nature Reviews Neuroscience*, 14(12):839–850.
- Hanuschkin, A., Diesmann, M., and Morrison, A. (2011). A reafferent and feed-forward model of song syntax generation in the bengalese finch. *Journal of Computational Neuroscience*, 31(3):509–532.

## Bibliography

- Hassabis, D., Kumaran, D., Vann, S. D., and Maguire, E. A. (2007). Patients with hippocampal amnesia cannot imagine new experiences. *Proceedings of the National Academy of Sciences*, 104(5):1726–1731.
- Hasselmo, M. E. (1999). Neuromodulation: acetylcholine and memory consolidation. *Trends in Cognitive Sciences*, 3(9):351–359.
- Hasselmo, M. E., Schnell, E., and Barkai, E. (1995). Dynamics of learning and recall at excitatory recurrent synapses and cholinergic modulation in rat hippocampal region CA3. *Journal of Neuroscience*, 15(7):5249–5262.
- Hebb, D. O. (2005 (1949)). *The organization of behavior: A neuropsychological theory*. Psychology Press.
- Hennequin, G., Vogels, T. P., and Gerstner, W. (2012). Non-normal amplification in random balanced neuronal networks. *Physical Review E*, 86(1):011909.
- Hitti, F. L. and Siegelbaum, S. A. (2014). The hippocampal CA2 region is essential for social memory. *Nature*, 508(7494):88–92.
- Hobbes, T. (1994 (1650)). *Human Nature; de Corpore Politico: Or the Fundamental Elements of Policy*. Thoemmes Press.
- Hofer, K. T., Kandrács, Á., Ulbert, I., Pál, I., Szabó, C., Héja, L., and Wittner, L. (2015). The hippocampal CA3 region can generate two distinct types of sharp wave-ripple complexes, *in vitro*. *Hippocampus*, 25(2):169–186.
- Hollnagel, J. O., Maslarova, A., ul Haq, R., and Heinemann, U. (2014). GABA<sub>B</sub> receptor dependent modulation of sharp wave-ripple complexes in the rat hippocampus *in vitro*. *Neuroscience Letters*, 574:15–20.
- Hölscher, C., Anwyl, R., and Rowan, M. J. (1997). Stimulation on the positive phase of hippocampal theta rhythm induces long-term potentiation that can be depotentiated by stimulation on the negative phase in area CA1 *in vivo*. *Journal of Neuroscience*, 17(16):6470–6477.
- Hopfield, J. J. (1982). Neural networks and physical systems with emergent collective computational abilities. *Proceedings of the National Academy of Sciences*, 79(8):2554–2558.
- Houweling, A. R. and Brecht, M. (2007). Behavioural report of single neuron stimulation in somatosensory cortex. *Nature*, 450(7172).
- Hulse, B. K., Moreaux, L. C., Lubenov, E. V., and Siapas, A. G. (2016). Membrane potential dynamics of CA1 pyramidal neurons during hippocampal ripples in awake mice. *Neuron*, 89(4):800–813.
- Hume, D. (1978 (1739)). *A treatise of human nature*. London: John Noon.
- Hume, D. and Hendel, C. W. (1955 (1748)). *An inquiry concerning human understanding*, volume 49. Bobbs-Merrill Indianapolis.
- Huxter, J., Burgess, N., and O’Keefe, J. (2003). Independent rate and temporal coding in hippocampal pyramidal cells. *Nature*, 425(6960):828–832.

## Bibliography

- Jacobs, N. S., Allen, T. A., Nguyen, N., and Fortin, N. J. (2013). Critical role of the hippocampus in memory for elapsed time. *Journal of Neuroscience*, 33(34):13888–13893.
- Jadhav, S. P., Kemere, C., German, P. W., and Frank, L. M. (2012). Awake hippocampal sharp-wave ripples support spatial memory. *Science*, 336(6087):1454–1458.
- Jahnke, S., Memmesheimer, R.-M., and Timme, M. (2013). Propagating synchrony in feed-forward networks. *Frontiers in Computational Neuroscience*, 7:153.
- Jahnke, S., Timme, M., and Memmesheimer, R.-M. (2015). A unified dynamic model for learning, replay, and sharp-wave/ripples. *Journal of Neuroscience*, 35(49):16236–16258.
- James, W. (1884). What is an emotion? *Mind*, (34):188–205.
- Jeffery, K. and Burgess, N. (2006). The boundary vector cell model of place cell firing and spatial memory. *Reviews in the Neurosciences*, 17:71–97.
- Jezek, K., Henriksen, E. J., Treves, A., Moser, E. I., and Moser, M.-B. (2011). Theta-paced flickering between place-cell maps in the hippocampus. *Nature*, 478(7368):246–249.
- Jimenez Rezende, D. and Gerstner, W. (2014). Stochastic variational learning in recurrent spiking networks. *Frontiers in Computational Neuroscience*, 8:38.
- Jones, J., Stubblefield, E. A., Benke, T. A., and Staley, K. J. (2007). Desynchronization of glutamate release prolongs synchronous CA3 network activity. *Journal of Neurophysiology*, 97(5):3812–3818.
- Jung, R. and Kornmüller, A. E. (1938). Eine Methodik der Ableitung iokalisierte Potentialschwankungen aus subcorticalen Hirngebieten. *European Archives of Psychiatry and Clinical Neuroscience*, 109(1):1–30.
- Kammerer, A., Tejero-Cantero, Á., and Leibold, C. (2013). Inhibition enhances memory capacity: optimal feedback, transient replay and oscillations. *Journal of Computational Neuroscience*, 34(1):125–136.
- Kappel, D., Nessler, B., and Maass, W. (2014). STDP installs in winner-take-all circuits an online approximation to hidden Markov model learning. *PLoS Computational Biology*, 10(3):e1003511.
- Karayannis, T., Elfant, D., Huerta-Ocampo, I., Teki, S., Scott, R. S., Rusakov, D. A., Jones, M. V., and Capogna, M. (2010). Slow GABA transient and receptor desensitization shape synaptic responses evoked by hippocampal neurogliaform cells. *Journal of Neuroscience*, 30(29):9898–9909.
- Karlsson, M. P. and Frank, L. M. (2009). Awake replay of remote experiences in the hippocampus. *Nature Neuroscience*, 12(7):913–918.
- Kempter, R., Gerstner, W., and Van Hemmen, J. L. (1999). Hebbian learning and spiking neurons. *Physical Review E*, 59(4):4498.
- Kenet, T., Bibitchkov, D., Tsodyks, M., Grinvald, A., and Arieli, A. (2003). Spontaneously emerging cortical representations of visual attributes. *Nature*, 425(6961):954–956.

## Bibliography

- Kerti-Szigeti, K. and Nusser, Z. (2016). Similar GABA<sub>A</sub> receptor subunit composition in somatic and axon initial segment synapses of hippocampal pyramidal cells. *eLife*, 5:e18426.
- Killian, N. J., Jutras, M. J., and Buffalo, E. A. (2012). A map of visual space in the primate entorhinal cortex. *Nature*, 491(7426):761–764.
- Klampfl, S. and Maass, W. (2013). Emergence of dynamic memory traces in cortical micro-circuit models through STDP. *Journal of Neuroscience*, 33(28):11515–11529.
- Klausberger, T. (2009). GABAergic interneurons targeting dendrites of pyramidal cells in the CA1 area of the hippocampus. *European Journal of Neuroscience*, 30(6):947–957.
- Klausberger, T., Magill, P. J., Márton, L. F., Roberts, J. D. B., Cobden, P. M., Buzsáki, G., and Somogyi, P. (2003). Brain-state-and cell-type-specific firing of hippocampal interneurons *in vivo*. *Nature*, 421(6925):844–848.
- Klausberger, T. and Somogyi, P. (2008). Neuronal diversity and temporal dynamics: the unity of hippocampal circuit operations. *Science*, 321(5885):53–57.
- Klein, S. B., Loftus, J., and Kihlstrom, J. F. (2002). Memory and temporal experience: The effects of episodic memory loss on an amnesic patient's ability to remember the past and imagine the future. *Social Cognition*, 20(5):353.
- Knowles, W. D., Schneiderman, J. H., Wheal, H. V., Stafstrom, C. E., and Schwartzkroin, P. A. (1984). Hyperpolarizing potentials in guinea pig hippocampal CA3 neurons. *Cellular and Molecular Neurobiology*, 4(3):207–230.
- Ko, H., Hofer, S. B., Pichler, B., Buchanan, K. A., Sjöström, P. J., and Mrsic-Flogel, T. D. (2011). Functional specificity of local synaptic connections in neocortical networks. *Nature*, 473(7345):87–91.
- Kobayashi, M., Takei, H., Yamamoto, K., Hatanaka, H., and Koshikawa, N. (2012). Kinetics of GABA<sub>B</sub> autoreceptor-mediated suppression of GABA release in rat insular cortex. *Journal of Neurophysiology*, 107(5):1431–1442.
- Kohus, Z., Káli, S., Rovira-Esteban, L., Schlingloff, D., Papp, O., Freund, T., Hájos, N., and Gulyás, A. (2016). Properties and dynamics of inhibitory synaptic communication within the CA3 microcircuits of pyramidal cells and interneurons expressing parvalbumin or cholecystokinin. *Journal of Physiology*.
- Koniaris, E., Drimala, P., Sotiriou, E., and Papatheodoropoulos, C. (2011). Different effects of zolpidem and diazepam on hippocampal sharp wave—ripple activity *in vitro*. *Neuroscience*, 175:224–234.
- Kosche, G., Vallentin, D., and Long, M. A. (2015). Interplay of inhibition and excitation shapes a premotor neural sequence. *Journal of Neuroscience*, 35(3):1217–1227.
- Kowalski, J., Gan, J., Jonas, P., and Pernía-Andrade, A. J. (2015). Intrinsic membrane properties determine hippocampal differential firing pattern *in vivo* in anesthetized rats. *Hippocampus*, 26:668–682.

## Bibliography

- Kraushaar, U. and Jonas, P. (2000). Efficacy and stability of quantal GABA release at a hippocampal interneuron–principal neuron synapse. *Journal of Neuroscience*, 20(15):5594–5607.
- Kruskal, P. B., Li, L., and MacLean, J. N. (2013). Circuit reactivation dynamically regulates synaptic plasticity in neocortex. *Nature Communications*, 4.
- Kubota, D., Colgin, L. L., Casale, M., Brucher, F. A., and Lynch, G. (2003). Endogenous waves in hippocampal slices. *Journal of Neurophysiology*, 89(1):81–89.
- Kulik, Á., Vida, I., Fukazawa, Y., Guetg, N., Kasugai, Y., Marker, C. L., Rigato, F., Bettler, B., Wickman, K., Frotscher, M., et al. (2006). Compartment-dependent colocalization of Kir3.2-containing  $K^+$  channels and GABA<sub>B</sub> receptors in hippocampal pyramidal cells. *Journal of Neuroscience*, 26(16):4289–4297.
- Kullmann, D. M. (2011). Interneuron networks in the hippocampus. *Current Opinion in Neurobiology*, 21(5):709–716.
- Kullmann, D. M., Ruiz, A., Rusakov, D. M., Scott, R., Semyanov, A., and Walker, M. C. (2005). Presynaptic, extrasynaptic and axonal GABA<sub>A</sub> receptors in the CNS: where and why? *Progress in Biophysics and Molecular Biology*, 87(1):33–46.
- Kumar, A., Rotter, S., and Aertsen, A. (2008). Conditions for propagating synchronous spiking and asynchronous firing rates in a cortical network model. *Journal of Neuroscience*, 28(20):5268–5280.
- Kumar, A., Rotter, S., and Aertsen, A. (2010). Spiking activity propagation in neuronal networks: reconciling different perspectives on neural coding. *Nature Reviews Neuroscience*, 11(9):615–627.
- Lang, M., Moradi-Chameh, H., Zahid, T., Gane, J., Wu, C., Valiante, T., and Zhang, L. (2014). Regulating hippocampal hyperexcitability through GABA<sub>B</sub> receptors. *Physiological Reports*, 2(4):e00278.
- Lanza, M., Fassio, A., Gemignani, A., Bonanno, G., and Raiteri, M. (1993). CGP 52432: a novel potent and selective GABA<sub>B</sub> autoreceptor antagonist in rat cerebral cortex. *European Journal of Pharmacology*, 237(2-3):191–195.
- Lashley, K. S. (1951). The problem of serial order in behavior. In *Cerebral mechanisms in behavior*, pages 112–136.
- Lazar, A., Pipa, G., and Triesch, J. (2009). SORN: a self-organizing recurrent neural network. *Frontiers in Computational Neuroscience*, 3:23.
- Le Duigou, C., Simonnet, J., Teleńczuk, M. T., Fricker, D., and Miles, R. (2014). Recurrent synapses and circuits in the CA3 region of the hippocampus: an associative network. *Frontiers in Cellular Neuroscience*, 7:262.
- Lee, A. K. and Wilson, M. A. (2002). Memory of sequential experience in the hippocampus during slow wave sleep. *Neuron*, 36(6):1183–1194.

## Bibliography

- Lei, S. and McBain, C. J. (2003). GABA<sub>B</sub> receptor modulation of excitatory and inhibitory synaptic transmission onto rat CA3 hippocampal interneurons. *Journal of Physiology*, 546(2):439–453.
- Leibold, C. and Kempter, R. (2006). Memory capacity for sequences in a recurrent network with biological constraints. *Neural Computation*, 18(4):904–941.
- Leibold, C. and Kempter, R. (2008). Sparseness constrains the prolongation of memory lifetime via synaptic metaplasticity. *Cerebral Cortex*, 18(1):67–77.
- Leung, L. S. and Peloquin, P. (2006). GABA<sub>B</sub> receptors inhibit backpropagating dendritic spikes in hippocampal CA1 pyramidal cells *in vivo*. *Hippocampus*, 16(4):388–407.
- Lévi, S., Logan, S. M., Tovar, K. R., and Craig, A. M. (2004). Gephyrin is critical for glycine receptor clustering but not for the formation of functional GABAergic synapses in hippocampal neurons. *Journal of Neuroscience*, 24(1):207–217.
- Levy, D. H. N. and Ruppin, I. M. E. (2000). Distributed synchrony of spiking neurons in a Hebbian cell assembly. In *Advances in Neural Information Processing Systems 12: Proceedings of the 1999 Conference*, volume 12, page 129. MIT Press.
- Li, M. and Greenside, H. (2006). Stable propagation of a burst through a one-dimensional homogeneous excitatory chain model of songbird nucleus HVC. *Physical Review E*, 74(1):011918.
- Li, P. and Slaughter, M. (2007). Glycine receptor subunit composition alters the action of GABA antagonists. *Visual Neuroscience*, 24(04):513–521.
- Li, X.-G., Somogyi, P., Ylinen, A., and Buzsaki, G. (1994). The hippocampal CA3 network: an *in vivo* intracellular labeling study. *Journal of Comparative Neurology*, 339(2):181–208.
- Lisman, J. and Spruston, N. (2005). Postsynaptic depolarization requirements for LTP and LTD: a critique of spike timing-dependent plasticity. *Nature Neuroscience*, 8(7):839–841.
- Litwin-Kumar, A. and Doiron, B. (2012). Slow dynamics and high variability in balanced cortical networks with clustered connections. *Nature Neuroscience*, 15(11):1498–1505.
- Litwin-Kumar, A. and Doiron, B. (2014). Formation and maintenance of neuronal assemblies through synaptic plasticity. *Nature Communications*, 5:5319.
- Liu, Q.-Y., Schaffner, A. E., Chang, Y. H., Maric, D., and Barker, J. L. (2000). Persistent activation of GABA<sub>A</sub> receptor/Cl<sup>-</sup> channels by astrocyte-derived GABA in cultured embryonic rat hippocampal neurons. *Journal of Neurophysiology*, 84(3):1392–1403.
- Locke, J. (1948 (1690)). An essay concerning human understanding.
- Lømo, T. (1966). Frequency potentiation of excitatory synaptic activity in dentate area of hippocampal formation. In *Acta Physiologica Scandinavica*, page 128.
- Long, M. A., Jin, D. Z., and Fee, M. S. (2010). Support for a synaptic chain model of neuronal sequence generation. *Nature*, 468(7322):394–399.

## Bibliography

- López-Bendito, G., Shigemoto, R., Kulik, A., Vida, I., Fairén, A., and Luján, R. (2004). Distribution of metabotropic GABA receptor subunits GABA<sub>B1a/b</sub> and GABA<sub>B2</sub> in the rat hippocampus during prenatal and postnatal development. *Hippocampus*, 14(7):836–848.
- Louie, K. and Wilson, M. A. (2001). Temporally structured replay of awake hippocampal ensemble activity during rapid eye movement sleep. *Neuron*, 29(1):145–156.
- Lowel, S. and Singer, W. (1992). Selection of intrinsic horizontal connections in the visual cortex by correlated neuronal activity. *Science*, 255(5041):209.
- Luczak, A., Barthó, P., and Harris, K. D. (2009). Spontaneous events outline the realm of possible sensory responses in neocortical populations. *Neuron*, 62(3):413–425.
- Luczak, A., Bartho, P., and Harris, K. D. (2013). Gating of sensory input by spontaneous cortical activity. *Journal of Neuroscience*, 33(4):1684–1695.
- Luczak, A. and MacLean, J. N. (2012). Default activity patterns at the neocortical microcircuit level. *Frontiers in Integrative Neuroscience*, 6:30.
- Maccaferri, G. and Lacaille, J.-C. (2003). Interneuron diversity series: Hippocampal interneuron classifications—making things as simple as possible, not simpler. *Trends in Neurosciences*, 26(10):564–571.
- MacLean, J. N., Watson, B. O., Aaron, G. B., and Yuste, R. (2005). Internal dynamics determine the cortical response to thalamic stimulation. *Neuron*, 48(5):811–823.
- Maguire, E. A., Gadian, D. G., Johnsrude, I. S., Good, C. D., Ashburner, J., Frackowiak, R. S., and Frith, C. D. (2000). Navigation-related structural change in the hippocampi of taxi drivers. *Proceedings of the National Academy of Sciences*, 97(8):4398–4403.
- Maier, N., Güldenagel, M., Söhl, G., Siegmund, H., Willecke, K., and Draguhn, A. (2002). Reduction of high-frequency network oscillations (ripples) and pathological network discharges in hippocampal slices from connexin 36-deficient mice. *Journal of Physiology*, 541(2):521–528.
- Maier, N., Morris, G., Johenning, F. W., and Schmitz, D. (2009). An approach for reliably investigating hippocampal sharp wave-ripples *in vitro*. *PLoS One*, 4(9):e6925.
- Maier, N., Morris, G., Schuchmann, S., Korotkova, T., Ponomarenko, A., Böhm, C., Wozny, C., and Schmitz, D. (2012). Cannabinoids disrupt hippocampal sharp wave-ripples via inhibition of glutamate release. *Hippocampus*, 22(6):1350–1362.
- Maier, N., Nimmrich, V., and Draguhn, A. (2003). Cellular and network mechanisms underlying spontaneous sharp wave–ripple complexes in mouse hippocampal slices. *Journal of Physiology*, 550(3):873–887.
- Maier, N., Tejero-Cantero, Á., Dorrn, A. L., Winterer, J., Beed, P. S., Morris, G., Kempfer, R., Poulet, J. F., Leibold, C., and Schmitz, D. (2011). Coherent phasic excitation during hippocampal ripples. *Neuron*, 72(1):137–152.
- Malenka, R. C. and Bear, M. F. (2004). LTP and LTD: an embarrassment of riches. *Neuron*, 44(1):5–21.

## Bibliography

- Malerba, P., Krishnan, G. P., Fellous, J.-M., and Bazhenov, M. (2016). Hippocampal CA1 ripples as inhibitory transients. *PLoS Computational Biology*, 12(4):e1004880.
- Manns, J. R. and Eichenbaum, H. (2006). Evolution of declarative memory. *Hippocampus*, 16(9):795–808.
- Manns, J. R. and Eichenbaum, H. (2009). A cognitive map for object memory in the hippocampus. *Learning & Memory*, 16(10):616–624.
- Mao, B.-Q., Hamzei-Sichani, F., Aronov, D., Froemke, R. C., and Yuste, R. (2001). Dynamics of spontaneous activity in neocortical slices. *Neuron*, 32(5):883–898.
- Markram, H., Lübke, J., Frotscher, M., and Sakmann, B. (1997). Regulation of synaptic efficacy by coincidence of postsynaptic APs and EPSPs. *Science*, 275(5297):213–215.
- Marr, D. (1971). Simple memory: A theory for archicortex. *Philosophical Transactions of the Royal Society of London B: Biological Sciences*, 262(841):23–81.
- Marrosu, F., Portas, C., Mascia, M. S., Casu, M. A., Fà, M., Giagheddu, M., Imperato, A., and Gessa, G. L. (1995). Microdialysis measurement of cortical and hippocampal acetylcholine release during sleep-wake cycle in freely moving cats. *Brain Research*, 671(2):329–332.
- Marshall, L., Helgadóttir, H., Mölle, M., and Born, J. (2006). Boosting slow oscillations during sleep potentiates memory. *Nature*, 444(7119):610–613.
- Martin, S., Grimwood, P., and Morris, R. (2000). Synaptic plasticity and memory: an evaluation of the hypothesis. *Annual Review of Neuroscience*, 23(1):649–711.
- Mehring, C., Hehl, U., Kubo, M., Diesmann, M., and Aertsen, A. (2003). Activity dynamics and propagation of synchronous spiking in locally connected random networks. *Biological Cybernetics*, 88(5):395–408.
- Memmesheimer, R.-M. (2010). Quantitative prediction of intermittent high-frequency oscillations in neural networks with supralinear dendritic interactions. *Proceedings of the National Academy of Sciences*, 107(24):11092–11097.
- Miles, R. and Wong, R. (1986). Excitatory synaptic interactions between CA3 neurones in the guinea-pig hippocampus. *Journal of Physiology*, 373:397.
- Mishra, R. K., Kim, S., Guzman, S. J., and Jonas, P. (2016). Symmetric spike timing-dependent plasticity at CA3–CA3 synapses optimizes storage and recall in autoassociative networks. *Nature Communications*, 7:11552.
- Mizuseki, K. and Buzsáki, G. (2013). Preconfigured, skewed distribution of firing rates in the hippocampus and entorhinal cortex. *Cell Reports*, 4(5):1010–1021.
- Moldakarimov, S., Bazhenov, M., and Sejnowski, T. J. (2015). Feedback stabilizes propagation of synchronous spiking in cortical neural networks. *Proceedings of the National Academy of Sciences*, 112(8):2545–2550.
- Monasson, R. and Rosay, S. (2014). Crosstalk and transitions between multiple spatial maps in an attractor neural network model of the hippocampus: Collective motion of the activity. *Physical Review E*, 89(3):032803.

## Bibliography

- Morrison, A., Aertsen, A., and Diesmann, M. (2007). Spike-timing-dependent plasticity in balanced random networks. *Neural Computation*, 19(6):1437–1467.
- Moscovitch, M., Rosenbaum, R. S., Gilboa, A., Addis, D. R., Westmacott, R., Grady, C., McAndrews, M. P., Levine, B., Black, S., Winocur, G., et al. (2005). Functional neuroanatomy of remote episodic, semantic and spatial memory: a unified account based on multiple trace theory. *Journal of Anatomy*, 207(1):35–66.
- Mostafa, H. and Indiveri, G. (2014). Sequential activity in asymmetrically coupled winner-take-all circuits. *Neural Computation*, 26:1973–2004.
- Murphy, B. K. and Miller, K. D. (2009). Balanced amplification: a new mechanism of selective amplification of neural activity patterns. *Neuron*, 61(4):635–648.
- Nakashiba, T., Buhl, D. L., McHugh, T. J., and Tonegawa, S. (2009). Hippocampal CA3 output is crucial for ripple-associated reactivation and consolidation of memory. *Neuron*, 62(6):781–787.
- Nakashiba, T., Young, J. Z., McHugh, T. J., Buhl, D. L., and Tonegawa, S. (2008). Transgenic inhibition of synaptic transmission reveals role of CA3 output in hippocampal learning. *Science*, 319(5867):1260–1264.
- Nayeem, N., Green, T., Martin, I., and Barnard, E. (1994). Quaternary structure of the native GABA<sub>A</sub> receptor determined by electron microscopic image analysis. *Journal of Neurochemistry*, 62(2):815–818.
- Newman, E. A. (2001). Propagation of intercellular calcium waves in retinal astrocytes and Müller cells. *Journal of Neuroscience*, 21(7):2215–2223.
- Niessing, J. and Friedrich, R. W. (2010). Olfactory pattern classification by discrete neuronal network states. *Nature*, 465(7294):47–52.
- Nimmrich, V., Maier, N., Schmitz, D., and Draguhn, A. (2005). Induced sharp wave-ripple complexes in the absence of synaptic inhibition in mouse hippocampal slices. *Journal of Physiology*, 563(3):663–670.
- Oja, E. (1982). Simplified neuron model as a principal component analyzer. *Journal of Mathematical Biology*, 15(3):267–273.
- O’Keefe, J. and Dostrovsky, J. (1971). The hippocampus as a spatial map. Preliminary evidence from unit activity in the freely-moving rat. *Brain Research*, 34(1):171–175.
- O’Keefe, J. and Recce, M. L. (1993). Phase relationship between hippocampal place units and the EEG theta rhythm. *Hippocampus*, 3(3):317–330.
- Okun, M. and Lampl, I. (2008). Instantaneous correlation of excitation and inhibition during ongoing and sensory-evoked activities. *Nature Neuroscience*, 11(5):535–537.
- Ólafsdóttir, H. F., Carpenter, F., and Barry, C. (2016). Coordinated grid and place cell replay during rest. *Nature Neuroscience*, 19:792–794.
- Omura, Y., Carvalho, M. M., Inokuchi, K., and Fukai, T. (2015). A lognormal recurrent network model for burst generation during hippocampal sharp waves. *Journal of Neuroscience*, 35(43):14585–14601.

## Bibliography

- O'Neill, J., Boccaro, C., Stella, F., Schoenenberger, P., and Csicsvari, J. (2017). Superficial layers of the medial entorhinal cortex replay independently of the hippocampus. *Science*, 355(6321):184–188.
- O'Neill, J., Senior, T., and Csicsvari, J. (2006). Place-selective firing of CA1 pyramidal cells during sharp wave/ripple network patterns in exploratory behavior. *Neuron*, 49(1):143–155.
- Oschmann, F., Mergenthaler, K., Jungnickel, E., and Obermayer, K. (2017). Spatial separation of two different pathways accounting for the generation of calcium signals in astrocytes. *PLoS Computational Biology*, 13(2):e1005377.
- Papatheodoropoulos, C., Sotiriou, E., Kotzadimitriou, D., and Drimala, P. (2007). At clinically relevant concentrations the anaesthetic/amnesic thiopental but not the anticonvulsant phenobarbital interferes with hippocampal sharp wave-ripple complexes. *BMC Neuroscience*, 8(1):60.
- Parpura, V., Basarsky, T. A., Liu, F., Jeftinija, K., Jeftinija, S., and Haydon, P. G. (1994). Glutamate-mediated astrocyte–neuron signalling. *Nature*, 369:744–747.
- Pavlov, I. (1897). Lectures on the work of the principal digestive glands. *St. Petersburg: Kushnereff*.
- Perin, R., Berger, T. K., and Markram, H. (2011). A synaptic organizing principle for cortical neuronal groups. *Proceedings of the National Academy of Sciences*, 108(13):5419–5424.
- Pfister, J.-P. and Gerstner, W. (2006). Triplets of spikes in a model of spike-timing-dependent plasticity. *Journal of Neuroscience*, 26(38):9673–9682.
- Platkiewicz, J. and Brette, R. (2011). Impact of fast sodium channel inactivation on spike threshold dynamics and synaptic integration. *PLoS Computational Biology*, 7(5):e1001129.
- Poe, G. R., Walsh, C. M., and Bjorness, T. E. (2010). Cognitive neuroscience of sleep. *Progress in Brain Research*, 185:1.
- Poole, B., Markowitz, J. E., and Gardner, T. J. (2012). The song must go on: resilience of the songbird vocal motor pathway. *PLoS One*, 7(6):e38173.
- Pulvermüller, F. (2010). Brain embodiment of syntax and grammar: Discrete combinatorial mechanisms spelt out in neuronal circuits. *Brain and Language*, 112(3):167–179.
- Quiroga, R. Q., Reddy, L., Kreiman, G., Koch, C., and Fried, I. (2005). Invariant visual representation by single neurons in the human brain. *Nature*, 435(7045):1102–1107.
- Ramón y Cajal, S. (1894). The croonian lecture: La fine structure des centres nerveux. *Proceedings of the Royal Society of London*, 55(331-335):444–468.
- Ramón y Cajal, S. and Azoulay, L. (1955 (1911)). *Histologie du système nerveux de l'homme & des vertébrés*. Consejo superior de investigaciones científicas, Instituto Ramon Y Cajal.
- Rapp, P. R. and Gallagher, M. (1996). Preserved neuron number in the hippocampus of aged rats with spatial learning deficits. *Proceedings of the National Academy of Sciences*, 93(18):9926–9930.

## Bibliography

- Rasch, B., Büchel, C., Gais, S., and Born, J. (2007). Odor cues during slow-wave sleep prompt declarative memory consolidation. *Science*, 315(5817):1426–1429.
- Reichinnek, S., Künsting, T., Draguhn, A., and Both, M. (2010). Field potential signature of distinct multicellular activity patterns in the mouse hippocampus. *Journal of Neuroscience*, 30(46):15441–15449.
- Renart, A., Moreno-Bote, R., Wang, X.-J., and Parga, N. (2007). Mean-driven and fluctuation-driven persistent activity in recurrent networks. *Neural Computation*, 19(1):1–46.
- Ricciardi, L. M. (2013 (1977)). *Diffusion processes and related topics in biology*, volume 14. Springer Science & Business Media.
- Robbe, D. and Buzsáki, G. (2009). Alteration of theta timescale dynamics of hippocampal place cells by a cannabinoid is associated with memory impairment. *Journal of Neuroscience*, 29(40):12597–12605.
- Rolls, E. T. and Tovee, M. J. (1995). Sparseness of the neuronal representation of stimuli in the primate temporal visual cortex. *Journal of Neurophysiology*, 73(2):713–726.
- Romani, S. and Tsodyks, M. (2015). Short-term plasticity based network model of place cells dynamics. *Hippocampus*, 25(1):94–105.
- Romano, S. A., Pietri, T., Pérez-Schuster, V., Jouary, A., Haudrechy, M., and Sumbre, G. (2015). Spontaneous neuronal network dynamics reveal circuit’s functional adaptations for behavior. *Neuron*, 85(5):1070–1085.
- Roudi, Y. and Latham, P. E. (2007). A balanced memory network. *PLoS Computational Biology*, 3(9):e141.
- Rutishauser, U., Mamelak, A. N., and Schuman, E. M. (2006). Single-trial learning of novel stimuli by individual neurons of the human hippocampus-amygdala complex. *Neuron*, 49(6):805–813.
- Sadeh, S., Clopath, C., and Rotter, S. (2015). Emergence of functional specificity in balanced networks with synaptic plasticity. *PLoS Computational Biology*, 11(6):e1004307.
- Sadovsky, A. J. and MacLean, J. N. (2013). Scaling of topologically similar functional modules defines mouse primary auditory and somatosensory microcircuitry. *Journal of Neuroscience*, 33(35):14048–14060.
- Sarel, A., Finkelstein, A., Las, L., and Ulanovsky, N. (2017). Vectorial representation of spatial goals in the hippocampus of bats. *Science*, 355(6321):176–180.
- Sasaki, T., Matsuki, N., and Ikegaya, Y. (2014). Interneuron firing precedes sequential activation of neuronal ensembles in hippocampal slices. *European Journal of Neuroscience*, 39(12):2027–2036.
- Scanziani, M. (2000). GABA spillover activates postsynaptic GABA<sub>B</sub> receptors to control rhythmic hippocampal activity. *Neuron*, 25(3):673–681.

## Bibliography

- Scarpetta, S. and de Candia, A. (2014). Alternation of up and down states at a dynamical phase-transition of a neural network with spatiotemporal attractors. *Frontiers in Systems Neuroscience*, 8:88.
- Schlingloff, D., Káli, S., Freund, T. F., Hájos, N., and Gulyás, A. I. (2014). Mechanisms of sharp wave initiation and ripple generation. *Journal of Neuroscience*, 34(34):11385–11398.
- Schmitz, D., Schuchmann, S., Fisahn, A., Draguhn, A., Buhl, E. H., Petrasch-Parwez, E., Dermietzel, R., Heinemann, U., and Traub, R. D. (2001). Axo-axonal coupling: a novel mechanism for ultrafast neuronal communication. *Neuron*, 31(5):831–840.
- Schönberger, J., Draguhn, A., and Both, M. (2014). Lamina-specific contribution of glutamatergic and GABAergic potentials to hippocampal sharp wave-ripple complexes. *Frontiers in Neural Circuits*, 8:103.
- Schwenk, J., Metz, M., Zolles, G., Turecek, R., Bildl, W., Tarusawa, E., Kulik, A., Unger, A., Gassmann, M., Schulte, U., et al. (2010). GABA<sub>B</sub> receptors are heteromultimers with a family of auxiliary subunits. *The Febs Journal*, 277:85–86.
- Scoville, W. B. and Milner, B. (1957). Loss of recent memory after bilateral hippocampal lesions. *Journal of Neurology, Neurosurgery & Psychiatry*, 20(1):11–21.
- Segev, R., Baruchi, I., Hulata, E., and Ben-Jacob, E. (2004). Hidden neuronal correlations in cultured networks. *Physical Review Letters*, 92(11):118102.
- Semon, R. W. (1921 (1904)). *The mneme*. G. Allen & Unwin Limited.
- Semyanov, A., Walker, M. C., Kullmann, D. M., and Silver, R. A. (2004). Tonically active GABA<sub>A</sub> receptors: modulating gain and maintaining the tone. *Trends in Neurosciences*, 27(5):262–269.
- Shein-Idelson, M., Ondracek, J. M., Liaw, H.-P., Reiter, S., and Laurent, G. (2016). Slow waves, sharp waves, ripples, and REM in sleeping dragons. *Science*, 352(6285):590–595.
- Shimono, M. and Beggs, J. M. (2015). Functional clusters, hubs, and communities in the cortical microconnectome. *Cerebral Cortex*, 25(10):3743–3757.
- Sieghart, W. and Sperk, G. (2002). Subunit composition, distribution and function of GABA<sub>A</sub> receptor subtypes. *Current Topics in Medicinal Chemistry*, 2(8):795–816.
- Sik, A., Tamamaki, N., and Freund, T. (1993). Complete axon arborization of a single CA3 pyramidal cell in the rat hippocampus, and its relationship with postsynaptic parvalbumin-containing interneurons. *European Journal of Neuroscience*, 5(12):1719–1728.
- Šimić, G., Kostović, I., Winblad, B., and Bogdanović, N. (1997). Volume and number of neurons of the human hippocampal formation in normal aging and Alzheimer's disease. *Journal of Comparative Neurology*, 379(4):482–494.
- Sirota, A., Csicsvari, J., Buhl, D., and Buzsáki, G. (2003). Communication between neocortex and hippocampus during sleep in rodents. *Proceedings of the National Academy of Sciences*, 100(4):2065–2069.

## Bibliography

- Sivilotti, L. and Nistri, A. (1991). GABA receptor mechanisms in the central nervous system. *Progress in Neurobiology*, 36(1):35–92.
- Skaggs, W. E. and McNaughton, B. L. (1996). Theta phase precession in hippocampal. *Hippocampus*, 6:149–172.
- Softky, W. R. and Koch, C. (1993). The highly irregular firing of cortical cells is inconsistent with temporal integration of random EPSPs. *Journal of Neuroscience*, 13(1):334–350.
- Somogyi, P., Katona, L., Klausberger, T., Lasztóczki, B., and Viney, T. J. (2014). Temporal redistribution of inhibition over neuronal subcellular domains underlies state-dependent rhythmic change of excitability in the hippocampus. *Philosophical Transactions of the Royal Society B*, 369(1635):20120518.
- Song, S., Sjöström, P. J., Reigl, M., Nelson, S., and Chklovskii, D. B. (2005). Highly non-random features of synaptic connectivity in local cortical circuits. *PLoS Biology*, 3(3):e68.
- Spalding, K. L., Bergmann, O., Alkass, K., Bernard, S., Salehpour, M., Huttner, H. B., Boström, E., Westerlund, I., Vial, C., Buchholz, B. A., et al. (2013). Dynamics of hippocampal neurogenesis in adult humans. *Cell*, 153(6):1219–1227.
- Squire, L. R. (1992). Memory and the hippocampus: a synthesis from findings with rats, monkeys, and humans. *Psychological Review*, 99(2):195.
- Stark, E., Roux, L., Eichler, R., and Buzsáki, G. (2015). Local generation of multineuronal spike sequences in the hippocampal CA1 region. *Proceedings of the National Academy of Sciences*, 112(33):10521–10526.
- Stark, E., Roux, L., Eichler, R., Senzai, Y., Royer, S., and Buzsáki, G. (2014). Pyramidal cell-interneuron interactions underlie hippocampal ripple oscillations. *Neuron*, 83(2):467–480.
- Steidl, E.-M., Neveu, E., Bertrand, D., and Buisson, B. (2006). The adult rat hippocampal slice revisited with multi-electrode arrays. *Brain Research*, 1096(1):70–84.
- Stemmler, M., Mathis, A., and Herz, A. V. (2015). Connecting multiple spatial scales to decode the population activity of grid cells. *Science Advances*, 1(11):e1500816.
- Stewart, D. (1855). *The Collected Works: Philosophical essays*, volume 5. Constable.
- Stumpf, C. (1965). Drug action on the electrical activity of the hippocampus. *International Review of Neurobiology*, 8:77–138.
- Szabadics, J., Varga, C., Molnár, G., Oláh, S., Barzó, P., and Tamás, G. (2006). Excitatory effect of GABAergic axo-axonic cells in cortical microcircuits. *Science*, 311(5758):233–235.
- Takahashi, N., Sasaki, T., Matsumoto, W., Matsuki, N., and Ikegaya, Y. (2010). Circuit topology for synchronizing neurons in spontaneously active networks. *Proceedings of the National Academy of Sciences*, 107(22):10244–10249.
- Takeuchi, T., Duszkiewicz, A. J., and Morris, R. G. (2014). The synaptic plasticity and memory hypothesis: encoding, storage and persistence. *Philosophical Transactions of the Royal Society B*, 369(1633):20130288.

## Bibliography

- Tanaka, K. Z., Pevzner, A., Hamidi, A. B., Nakazawa, Y., Graham, J., and Wiltgen, B. J. (2014). Cortical representations are reinstated by the hippocampus during memory retrieval. *Neuron*, 84(2):347–354.
- Tang, Q., Burgalossi, A., Ebbesen, C. L., Ray, S., Naumann, R., Schmidt, H., Spicher, D., and Brecht, M. (2014). Pyramidal and stellate cell specificity of grid and border representations in layer 2 of medial entorhinal cortex. *Neuron*, 84(6):1191–1197.
- Taube, J. S., Muller, R. U., and Ranck, J. B. (1990a). Head-direction cells recorded from the postsubiculum in freely moving rats. I. Description and quantitative analysis. *Journal of Neuroscience*, 10(2):420–435.
- Taube, J. S., Muller, R. U., and Ranck, J. B. (1990b). Head-direction cells recorded from the postsubiculum in freely moving rats. II. Effects of environmental manipulations. *Journal of Neuroscience*, 10(2):436–447.
- Taxidis, J., Coombes, S., Mason, R., and Owen, M. R. (2012). Modeling sharp wave-ripple complexes through a CA3–CA1 network model with chemical synapses. *Hippocampus*, 22(5):995–1017.
- Taylor, M. (1973). The problem of stimulus structure in the behavioural theory of perception. *South African Journal of Psychology*, 3:23–45.
- Thomas, S. A. (2015). Neuromodulatory signaling in hippocampus-dependent memory retrieval. *Hippocampus*, 25(4):415–431.
- Titchener, E. B. (1905). *Experimental psychology: A manual of laboratory practice*, volume 2. Macmillan.
- Titchener, E. B. (1909). *Lectures on the experimental psychology of the thought-processes*. Macmillan.
- Traub, R. D., Schmitz, D., Maier, N., Whittington, M. A., and Draguhn, A. (2012). Axonal properties determine somatic firing in a model of *in vitro* CA1 hippocampal sharp wave/ripples and persistent gamma oscillations. *European Journal of Neuroscience*, 36(5):2650–2660.
- Trengove, C., van Leeuwen, C., and Diesmann, M. (2013). High-capacity embedding of synfire chains in a cortical network model. *Journal of Computational Neuroscience*, 34(2):185–209.
- Trussell, L. O., Zhang, S., and Ramant, I. M. (1993). Desensitization of AMPA receptors upon multiquantal neurotransmitter release. *Neuron*, 10(6):1185–1196.
- Tsodyks, M. V. and Markram, H. (1997). The neural code between neocortical pyramidal neurons depends on neurotransmitter release probability. *Proceedings of the National Academy of Sciences*, 94(2):719–723.
- Ueno, S., Bracamontes, J., Zorumski, C., Weiss, D. S., and Steinbach, J. H. (1997). Bicuculline and gabazine are allosteric inhibitors of channel opening of the GABA<sub>A</sub> receptor. *Journal of Neuroscience*, 17(2):625–634.

## Bibliography

- Unknown, A. (80BC). Ad C. Herennium de ratione dicendi (Rhetorica ad Herennium), book 3.
- van den Pol, A. N. and Gorcs, T. (1988). Glycine and glycine receptor immunoreactivity in brain and spinal cord. *Journal of Neuroscience*, 8(2):472–492.
- van Vreeswijk, C. and Sompolinsky, H. (1996). Chaos in neuronal networks with balanced excitatory and inhibitory activity. *Science*, 274(5293):1724–1724.
- van Vreeswijk, C. and Sompolinsky, H. (1998). Chaotic balanced state in a model of cortical circuits. *Neural Computation*, 10(6):1321–1371.
- Vanderwolf, C. H. (1969). Hippocampal electrical activity and voluntary movement in the rat. *Electroencephalography and Clinical Neurophysiology*, 26(4):407–418.
- Varga, C., Golshani, P., and Soltesz, I. (2012). Frequency-invariant temporal ordering of interneuronal discharges during hippocampal oscillations in awake mice. *Proceedings of the National Academy of Sciences*, 109(40):E2726–E2734.
- Viney, T. J., Lasztoczi, B., Katona, L., Crump, M. G., Tukker, J. J., Klausberger, T., and Somogyi, P. (2013). Network state-dependent inhibition of identified hippocampal CA3 axo-axonic cells *in vivo*. *Nature Neuroscience*, 16(12):1802–1811.
- Vladimirov, N., Tu, Y., and Traub, R. D. (2013). Synaptic gating at axonal branches, and sharp-wave ripples with replay: a simulation study. *European Journal of Neuroscience*, 38(10):3435–3447.
- Vogels, T. P., Froemke, R. C., Doyon, N., Gilson, M., Haas, J. S., Liu, R., Maffei, A., Miller, P., Wierenga, C., Woodin, M. A., et al. (2013). Inhibitory synaptic plasticity: spike timing-dependence and putative network function. *Frontiers in Neural Circuits*, 7:119.
- Vogels, T. P., Sprekeler, H., Zenke, F., Clopath, C., and Gerstner, W. (2011). Inhibitory plasticity balances excitation and inhibition in sensory pathways and memory networks. *Science*, 334(6062):1569–1573.
- Waddington, A., Appleby, P. A., De Kamps, M., and Cohen, N. (2012). Triphasic spike-timing-dependent plasticity organizes networks to produce robust sequences of neural activity. *Frontiers in Computational Neuroscience*, 6:88.
- Wallace, D. J. and Kerr, J. N. (2010). Chasing the cell assembly. *Current Opinion in Neurobiology*, 20(3):296–305.
- Wang, F., Smith, N. A., Xu, Q., Fujita, T., Baba, A., Matsuda, T., Takano, T., Bekar, L., and Nedergaard, M. (2012). Astrocytes modulate neural network activity by  $\text{Ca}^{2+}$ -dependent uptake of extracellular  $\text{K}^+$ . *Science Signaling*, 5(218):ra26.
- Wang, P. and Slaughter, M. M. (2005). Effects of GABA receptor antagonists on retinal glycine receptors and on homomeric glycine receptor alpha subunits. *Journal of Neurophysiology*, 93(6):3120–3126.
- Wang, Y., Neubauer, F. B., Lüscher, H.-R., and Thurley, K. (2010). GABA<sub>B</sub> receptor-dependent modulation of network activity in the rat prefrontal cortex *in vitro*. *European Journal of Neuroscience*, 31(9):1582–1594.

## Bibliography

- Washburn, M. F. (1916). *Movement and mental imagery: Outlines of a motor theory of the complexer mental processes*. Houghton Mifflin.
- Watt, H. J. (1904). *Experimentelle Beiträge zu einer Theorie des Denkens*. W. Engelmann.
- West, M., Slomianka, L., and Gundersen, H. J. G. (1991). Unbiased stereological estimation of the total number of neurons in the subdivisions of the rat hippocampus using the optical fractionator. *The Anatomical Record*, 231(4):482–497.
- Wetherington, J. P. and Lambert, N. A. (2002). GABA<sub>B</sub> receptor activation desensitizes postsynaptic GABA<sub>B</sub> and A1 adenosine responses in rat hippocampal neurones. *Journal of Physiology*, 544(2):459–467.
- Whiting, P. J. (2003). GABA<sub>A</sub> receptor subtypes in the brain: a paradigm for CNS drug discovery? *Drug Discovery Today*, 8(10):445–450.
- Wills, T. J., Lever, C., Cacucci, F., Burgess, N., and O’Keefe, J. (2005). Attractor dynamics in the hippocampal representation of the local environment. *Science*, 308(5723):873–876.
- Wilson, M. and McNaughton, B. (1993). Dynamics of the hippocampal ensemble code for space. *Science*, 261(5124):1055–1058.
- Wilson, M. A., McNaughton, B. L., et al. (1994). Reactivation of hippocampal ensemble memories during sleep. *Science*, 265(5172):676–679.
- Wittenberg, G. M. and Wang, S. S.-H. (2006). Malleability of spike-timing-dependent plasticity at the CA3–CA1 synapse. *Journal of Neuroscience*, 26(24):6610–6617.
- Wood, E. R., Dudchenko, P. A., and Eichenbaum, H. (1999). The global record of memory in hippocampal neuronal activity. *Nature*, 397(6720):613–616.
- Xue, M., Atallah, B. V., and Scanziani, M. (2014). Equalizing excitation-inhibition ratios across visual cortical neurons. *Nature*, 511(7511):596–600.
- Yates, F. A. (1992 (1966)). *The art of memory*, volume 64. Random House.
- Yeung, J. Y., Canning, K. J., Zhu, G., Pennefather, P., MacDonald, J. F., and Orser, B. A. (2003). Tonically activated GABA<sub>A</sub> receptors in hippocampal neurons are high-affinity, low-conductance sensors for extracellular GABA. *Molecular Pharmacology*, 63(1):2–8.
- Ylinen, A., Bragin, A., Nádasdy, Z., Jandó, G., Szabo, I., Sik, A., and Buzsáki, G. (1995). Sharp wave-associated high-frequency oscillation (200 Hz) in the intact hippocampus: network and intracellular mechanisms. *Journal of Neuroscience*, 15(1):30–46.
- Yoshii, N., Shimokochi, M., Miyamoto, K., and Ito, M. (1966). Studies on the neural basis of behavior by continuous frequency analysis of EEG. *Progress in Brain Research*, 21:217–250.
- Zenke, F., Agnes, E. J., and Gerstner, W. (2015). Diverse synaptic plasticity mechanisms orchestrated to form and retrieve memories in spiking neural networks. *Nature Communications*, 6.

## Bibliography

- Zhang, L. I., Tao, H. W., Holt, C. E., Harris, W. A., and Poo, M.-m. (1998). A critical window for cooperation and competition among developing retinotectal synapses. *Nature*, 395(6697):37–44.
- Zhang, Y. V., Ormerod, K. G., and Littleton, J. T. (2017). Astrocyte  $\text{Ca}^{2+}$  influx negatively regulates neuronal activity. *eNeuro*, 16:0340.



# Acknowledgements

I would like to take the opportunity to thank to all the people that in one way or another helped getting through the development of this thesis. First and foremost, I would like to express my gratitude to my supervisor, Richard Kempfer. He has shown me how to ask questions in science and how to attack the problems with the arsenal of simplest methods first. Apart from the outstanding scientific supervision that Richard provided, his patience and methodology have been a model how to approach and solve problems outside of the academic life. I would like to specially thank Henning Sprekeler, who initiated the project on assembly sequences and supported me in making it done. Special thanks to Nikolaus Maier for providing me with data and for the helpful discussions on the origin of SWRs.

Many thanks to the people that provided feedback on various parts of this thesis: Richard Kempfer, Henning Sprekeler, Nikolaus Maier, Adam Wilkins, Roberta Evangelista, Pia Rose, Eric Reifenstein, Nadia Varley, José Donoso, and André Holzbecher.

I would like to thank my officemates over the years for all the positive vibes, meaningful discussions, and not so meaningful but fun distractions: Paula Kuokkanen, Jorge Jaramillo, José Donoso, Thomas McColgan, Martina Michalikova, André Holzbecher, Leonidas Eleftheriou. I also thank to all the ITB-Neuro members for their support, feedback, and for the discussions on various topics in the science field. You, people generate a unique and friendly atmosphere!

Finally, big thanks to my closest friends for the all the implicit support: Dobri, Svetlio, Pesho, Tosho, Bibi, Stani, Ogi, Sasho, Florian, Dmitry, Henning, Alex, and Martina. The trips with you have been brutal events that left irreversible traces in my memory. Last but not least, a deep gratitude to my family members in Bulgaria, Russia, and Germany for all the support. A special thank to Ping and Tiona for the motivation, for the patience, and for making life even more interesting.



# **Selbständigkeitserklärung**

Ich erkläre, dass ich die vorliegende Arbeit selbständig und nur unter Verwendung der angegebenen Literatur und Hilfsmittel angefertigt habe.

Berlin, September 12, 2017

Nikolay Chenkov